Neutrino Event Rates in Neutrino Oscillation Experiments

Dissertation Submitted For The Award Of The Degree Of

Master Of Philosophy

Submitted By

Farhana Zaidi

Supervisor

Dr. Md. Sajjad Athar

Associate Professor

Department Of Physics

Aligarh Muslim University

Aligarh, India

2013

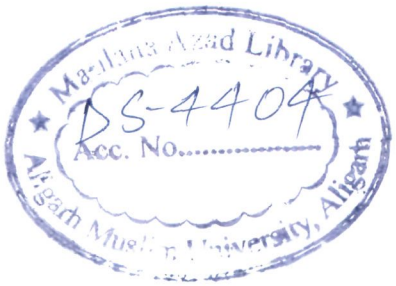

PHYSICS DEPARTMENT
ALIGARH MUSLIM UNIVERSITY
ALIGARH - 202002 (INDIA)

PH.: 91-571-2700984
PH. & FAX: 91-571-2701001

Dated: April 8, 2013

CERTIFICATE

Certified that the work reported in this Dissertation entitled, **"Neutrino Event Rates in Neutrino Oscillation Experiments"**, is the original work of Miss Farhana Zaidi, done under my supervision.

Md. Sajjad Athar
(Md. Sajjad Athar)
Associate Professor

Acknowledgment

"Oh Allah! Nothing is easy except what You have made easy. If You wish, You can make the difficult easy."

I am highly thankful to Almighty Allah to always help me and blessed me .

First of all I want to express my deep gratitude to my supervisor **Dr. Md. Sajjad Athar** *who always guide me and encourage me to present my M.Phil. work in such form. His hard working attitude is always a source of inspiration to me. I am highly oblidgue to him.*

I am thankful to the Chairman, Department of Physics, **Prof. Rahim Ullah Khan** *for providing all the required facilities for my research work.*

I also want to express my gratitude to my seniors **Miss Shikha Chauhan, Miss Huma Haider** *and* **Mr. Rafi Alam** *for their help and guidance. I also wish to say thank to all my friends particularly* **Zaheen Haider, Asra Shakeel** *and* **Anuj Chandra** *for their help.*

It's really pleasant to express my gratitude to my parents for their support. As well as I want to say a sincere thank to my brothers and my sister for their moral support.

Farhana Zaidi.

Farhana Zaidi

Dedicated

To

My Parents

Contents

List of Figures

List of Tables

Chapter 1

Introduction

In 1930 W. Pauli proposed a hypothetical particle in order to explain the continuous nature of beta spectrum as well as to save the angular momentum conservation law. He suggested that the missing energy in the beta decay $X \rightarrow Y + e^-$ might be carried by some unseen weakly interacting, neutral and massless particle and he called it neutron. After the discovery of today's neutron(member of nucleon doublet) by J. Chadwick in 1932, E. Fermi rechristened it as *neutrino* and gave his celebrated theory of weak interaction which was constructed in analogy with the Dirac's formulation of quantum electrodynamics.

In the Standard Model(SM) of particle physics, there are six charged leptons($e^{\pm}, \mu^{\pm}, \tau^{\pm}$) and six neutral leptons($\nu_e, \bar{\nu}_e, \nu_\mu, \bar{\nu}_\mu, \nu_\tau, \bar{\nu}_\tau$). It was $\bar{\nu}_e$ which was first detected by F. Reines and C. L. Cowan in 1956 at Savannah River Plant in South Carolina. Since then much emphasis has been put to understand the nature of this elusive particle. Photons and neutrinos are the most abundant elementary particles in the universe. So, to know the mysteries of the universe, we must also understand the properties of neutrinos. Neutrinos can penetrate the entire planet without interacting even with a single grain. In Table-1.1, we have summarized the present understanding of the neutrinos [1]. Number of flavors of neutrinos from the standard model fit to LEP data is N=2.984±0.008 [1].

There are various sources of neutrinos which are coming continuously from all directions. Below we have listed some of the major sources of neutrinos [2, 3]:

Solar neutrinos : Nuclear fusion reaction is taking place inside the core of the Sun. The

Flavors	Mass	Magnetic moment(μ_B)
ν_e	<2(eV)	$<0.32\times10^{-10}$
ν_μ	<0.19(MeV)	$<6.8\times10^{-10}$
ν_τ	<18.2(MeV)	$<3.9\times10^{-7}$

Table 1.1: Upper limits of neutrino masses and their magnetic moments.

Sun is powered by the two groups of thermonuclear reactions known as the pp chain and CNO cycle. The basic reaction is given by

$$4p + 2e^- \rightarrow^4 H_e + 2\nu_e + 26.731MeV \tag{1.1}$$

In such processes the emerged neutrinos have energy which ranges from keV to few tens of MeV. Solar neutrinos were first detected in 1970 in the Homestake experiment. Since then solar neutrinos have been observed by many terrestrial detectors like Kamiokande, Super-Kamiokande, GALLEX/GNO, SAGE, etc.

Atmospheric neutrinos : Atmospheric neutrinos are produced in the decay of secondary cosmic ray particles (mainly pions and kaons) which in turn are produced during the interaction of primary cosmic ray particles(mainly protons and alpha particles) with the Earth's atmosphere. The basic reaction is given by

$$\begin{aligned} &\pi^+ \rightarrow \mu^+ + \nu_\mu \; ; \qquad \mu^+ \rightarrow e^+ + \nu_e + \bar{\nu}_\mu \\ &\pi^- \rightarrow \mu^- + \bar{\nu}_\mu \; ; \qquad \mu^- \rightarrow e^- + \bar{\nu}_e + \nu_\mu. \end{aligned} \tag{1.2}$$

Energy of these neutrinos ranges from few tens of MeV to 100 GeV. The neutrinos of energy above 1GeV are mainly produced in the decay of

$$\begin{aligned} K^\pm &\rightarrow \mu^\pm + \nu_\mu(\bar{\nu}_\mu) \\ K_L &\rightarrow \pi^\pm + e^\mp + \nu_e(\bar{\nu}_e). \end{aligned} \tag{1.3}$$

Supernova neutrinos : When the mass of the white dwarf reaches the Chandrasekhar limit($M_C \simeq 1.4M_\odot$)[1], the star becomes unstable. The thermonuclear reactions proceed further and star becomes hotter until it expands into a red giant. At the end of its life it collapse to a neutron star and radiates almost all its binding energy in the form of neutrinos. And most of these neutrinos have energies from a few hundreds of keV to several tens of MeV. Supernova neutrinos can be detected by all the present solar neutrino detectors. Neutrinos from SN 1987A were observed by Kamiokande-II, IMB, BST and Mont Blanc detectors.

Geo-neutrinos : $\bar{\nu}_e$ are emitted in the beta decay of radionuclides occurring in the Earth. Geoneutrinos carry information about the spatial distribution of radionuclides and their abundances inside the Earth. Main source of geoneutrinos are ^{40}K, ^{232}Th, ^{238}U. In 2005 it was first detected by KamLAND experiment at Kamioka observatory in Japan. These neutrinos have energy of the order of tens of MeV.

[1] $M_\odot$ is solar mass.

$\sin^2(2\theta_{12})$	0.857 ± 0.024
Δm^2_{12}	$(7.50 \pm 0.20) \times 10^{-5}\ eV^2$
$\sin^2(2\theta_{23})$	> 0.95
Δm^2_{32}	$(2.32^{+0.12}_{-0.08}) \times 10^{-3}\ eV^2$
$\sin^2(2\theta_{13})$	0.098 ± 0.013

Table 1.2: Neutrino oscillation parameters.

Relic neutrinos : Cosmic neutrinos are the relic of Big Bang and these are known as relic neutrinos. Just one second after the Big Bang, neutrinos decoupled from the matter. The temperature of relic neutrinos at that time was of the order of a few MeV. These neutrinos took part in the Big Bang nucleosynthesis in the first minute of the Universe. At present it is estimated that the temperature of relic neutrinos is roughly 1.95K and their density is about $330/\text{cm}^3$.

Reactor neutrinos : Human made fission reactors are the major source of $\bar{\nu}_e$ produced in the beta decay process of neutron rich nuclei. Each fission produces average energy of about 200 MeV with six $\bar{\nu}_e$. There are many reactor neutrino experiments for example, KamLAND, Chooz, Palo Verde, Daya Bay etc.

Accelerator neutrinos : Particle accelerators are a big source of neutrinos. There are various methods of production of neutrino beam and according to that accelerator experiments can be classified as

1. Pion decay in flight
2. Muon decay at rest

Neutrinos from accelerator are produced through the decay of pions and kaons which results from the high energy proton beam when it strikes a target.

Neutrinos from Beta Beams [4, 5] as well as SNS (Spallation Neutron Source) [6] neutrinos have also been discussed in the literature. The idea of Beta Beam was first proposed by P. Zucchelli in 2002. In Beta Beam facility one can produce a pure neutrino or antineutrino beam from the beta unstable radioactive ions circulating in a storage ring. Advantage of Beta Beam is that it produces only electron flavor neutrino so there is no need for charge identification in the detector. It is expected that Beta Beam facility will improve our ability to check the CP violation in lepton sector, neutrino mass hierarchy and the value of third mixing angle θ_{13}. At SNS facility, neutrinos are produced in the interactions of the proton beam in the target which besides producing neutrons also produces $\pi-$mesons which get stopped inside the dense target material and their subsequent decay chain produce neutrinos. In the last few years it has been discovered that neutrinos are not massless as they change flavor. This phenomenon is known as neutrino oscillations and it was first proposed by Pontecorvo in 1957. Theoretically, the evidence of tiny neutrino

Experiment	Channel	Physics potential
T2KK	$\nu_\mu \rightarrow \nu_{\mu,e}$	Improve $sin^2 2\theta_{13}$
MINERνA	$\nu_\mu \rightarrow \nu_{\mu,e}$	To measure neutrino nucleus cross sections with various nuclear targets
MiniBooNE	$\nu_\mu \rightarrow \nu_{\mu,e}$	To confirm or refute LSND results
MEMPHYS	$\nu_\mu \rightarrow \nu_{\mu,e}$	Improve $sin^2 2\theta_{13}$, CP violating δ phase
MODULAr	$\nu_\mu \rightarrow \nu_{\mu,e}$	Improve $sin^2 2\theta_{13}$, CP violating δ phase
WBB	$\nu_\mu \rightarrow \nu_{\mu,e}$	Improve $sin^2 2\theta_{13}$, CP violating δ phase
MINOS	$\nu_\mu \rightarrow \nu_{\mu,e}$	Compare ν_μ and $\bar{\nu}_\mu$ Osc.: CPT test Improve $sin^2 2\theta_{13} \sim$ factor of 2 over CHOOZ
ICARUS	$\nu_\mu \rightarrow \nu_{e,\mu,\tau}$	$\|\delta_{32}\|$, $sin^2\theta_{23}$, $sin^2 2\theta_{13}$
OPERA	$\nu_\mu \rightarrow \nu_{e,\mu,\tau}$	$\|\delta_{32}\|$, $sin^2\theta_{23}$, $sin^2 2\theta_{13}$
T2K	$\nu_\mu \rightarrow \nu_{e,\mu}$	Improve $sin^2 2\theta_{13} \sim$ factor of 6 over CHOOZ CP Violation, Proton decay (phase II)
NOνA	$\nu_\mu \rightarrow \nu_{e,\mu}$	Improve $sin^2 2\theta_{13} \sim$ factor of 6 over CHOOZ Sign δ_{32}, CP violation
Super-Kamiokande-III	$\nu_\mu \rightarrow \nu_{e,\mu}$	Improve $sin^2 2\theta_{13} \sim$ factor of 2.3 over CHOOZ
UNO	$\nu_\mu \rightarrow \nu_{e,\mu,\tau}$	Sign δ_{32}, $sin^2\theta_{13}$ to below 0.005 $\nu_\mu \rightarrow \nu_e$ appearance : δ_{21}, θ_{12}
Hyper-K	$\nu_\mu \rightarrow \nu_{e,\mu,\tau}$	$sin^2\theta_{13}$ sensitivity below 10^{-3}, Sign δ_{32}, δ_{CP}
RENO	$\bar{\nu}_e$	To set a limit on θ_{13}
Daya Bay	$\bar{\nu}_e$	To measure the mixing angle θ_{13}, CP violation
Double Chooz	$\bar{\nu}_e$	To set a limit on θ_{13}
IceCube	ν_e, ν_μ, ν_τ	To constrain θ_{23}, Mass hierarchy
INO	$\nu_\mu \rightarrow \nu_\mu$	L/E dip, CPT test

Table 1.3: List of Neutrino oscillation experiments.

masses represents one of the indications of physics beyond the Standard Model(SM). The production eigenstates and the propagation eigenstates are different and they are related by a mixing matrix. The atmospheric neutrinos have provided the first model-independent indication of oscillations of ν_μ's through the Super-Kamiokande experiment and this oscillation phenomenon has been confirmed by many experiments like SNO, MINOS, etc.

In case of oscillations with two neutrino flavors the relation between the neutrino states is described by one mixing angle and one mass difference. The flavor eigenstates are linear

Nuclei	Detector	Experiment
^{12}C	Scintillator, Mineral Oil	NOνA, MINERνA, MiniBooNE
^{16}O	Water Cerenkov	T2K, Super-Kamiokande-III, UNO, Hyper-K, K2K, MEMPHYS
^{40}Ar	Liquid Argon TPC	ICARUS
^{56}Fe	Iron Calorimeter	MINOS, MINERνA, INO
^{208}Pb	Emulsion	OPERA, MINERνA

Table 1.4: Nuclear targets used in the different detectors.

superposition of mass eigenstates

$$\begin{pmatrix} \nu_e \\ \nu_\mu \end{pmatrix} = \begin{pmatrix} \cos\theta & \sin\theta \\ -\sin\theta & \cos\theta \end{pmatrix} \begin{pmatrix} \nu_1 \\ \nu_2 \end{pmatrix}$$

The transition probability corresponding to two-flavor neutrinos is given by

$$P(\nu_e \rightarrow \nu_\mu) = \sin^2 2\theta \times \sin^2\left(\frac{\Delta m^2 L}{4E}\right) = 1 - P(\nu_e \rightarrow \nu_e) \tag{1.4}$$

Above expression tells us that oscillations will occur only if both θ and $\Delta m^2 = m_2^2 - m_1^2$ are non-vanishing. While in the case of three flavor neutrino oscillations

$$|\nu_\alpha\rangle = \sum_i U_{\alpha i} |\nu_i\rangle \ , \quad \alpha = e, \mu, \tau, \quad i = 1, 2, 3. \tag{1.5}$$

Where U is the Pontecorvo-Maki-Nakagawa-Sakata unitary mixing matrix commonly known as PMNS unitary matrix which is given by

$$U = \begin{pmatrix} C_{12}C_{13} & S_{12}C_{13} & S_{13}e^{-i\delta} \\ -C_{23}S_{12} - S_{23}S_{13}C_{12}e^{i\delta} & C_{23}C_{12} - S_{23}S_{13}S_{12}e^{i\delta} & S_{23}C_{13} \\ S_{23}S_{12} - C_{23}S_{13}C_{12}e^{i\delta} & -S_{23}C_{12} - C_{23}S_{13}S_{12}e^{i\delta} & C_{23}C_{13} \end{pmatrix},$$

where $C_{ij} = \cos\theta_{ij}$, $S_{ij} = \sin\theta_{ij}$ and δ is the CP violating phase. The present limits on the neutrino oscillation parameters are tabulated in Table-1.2 [1]. These values represent a combined analysis of several neutrino oscillation experiments observing reactor, accelerator and solar neutrinos. Still there are many unanswered questions regarding neutrinos and their properties like,

1. What are the absolute value of masses of neutrino?
2. Is there CP violation in the leptonic sector?
3. Whether neutrinos obey normal mass hierarchy or inverted mass hierarchy?

4. What is the sign of Δm^2_{31}?

5. What is the precise value of third mixing angle θ_{13}?

Recently, many neutrino oscillation experiments are going on and many more are planned in order to determine precisely the neutrino oscillation parameters. In Table-1.3, we have listed some of them.

Most of these oscillation experiments are planned in the few GeV energy region to which neutrino oscillation parameters are sensitive. For example, the average neutrino energy of MiniBooNE experiment is about 750 MeV, for K2K it is 1.3 GeV, for T2K 600 MeV and for NOνA experiment it is 2 GeV. Some of the neutrino energy spectra are shown in Fig.-1.1, Fig.-1.2, and Fig.-1.3 for the MiniBooNE, Super-Kamiokande, and T2K experiments respectively. In this energy region, the contribution to the cross section comes from the various processes like quasielastic, inelastic, and deep inelastic process. Furthermore, the experiments are using various nuclear targets as given in Table-1.4. Therefore, the nucleons with which the scattering is taking place are not free but are bound inside a nucleus. For example in the T2K experiment mainly charged leptons are produced through the quasielastic scattering process, however there is some contribution from the inelastic channel also. While in the NOνA experiment it is expected that all three channels viz. quasielastic scattering, inelastic scattering as well as deep inelastic scattering would play an important role. These may be understood by looking at the famous Lipari curve[7](Fig.-1.4), where the cross section is plotted as a function of neutrino energy. Here the sensitivity of the average neutrino energy spectrum of the different neutrino experiments are also shown. As all these experiments are using nuclear targets, where nucleons are not sitting at rest like it has momentum and have to obey Pauli exclusion principle that the initial nucleon momentum should be below the Fermi momentum of the nucleon in the nucleus and after the interaction the momentum of outgoing nucleon should be above the Fermi momentum of the nucleon in the nucleus. Besides these there are several nuclear effects which one should take into account while evaluating the neutrino nucleus cross section for the various channels. In the neutrino event generators like NUANCE [8], NEUGEN [9], NEUT [10], etc., those are being used for predicting neutrino event rate, for the neutrino-nucleus cross section common phenomenological inputs are the model of Llewellyn Smith [11] for quasielastic reaction, Rein and Sehgal model[12] for the inelastic reaction and Bodek and Yang [13] model for the deep inelastic reaction.

It has been discussed in literature that these accounted effects are not sufficient and there are more to it. For example, in the quasielastic scattering, besides Fermi motion and Pauli blocking one should also take into account the nucleon correlations as these nucleons are strongly interacting particles and the coupling strengths may/will get modified.

Figure 1.1: ν and $\bar{\nu}$ flux at the MiniBooNE detector.

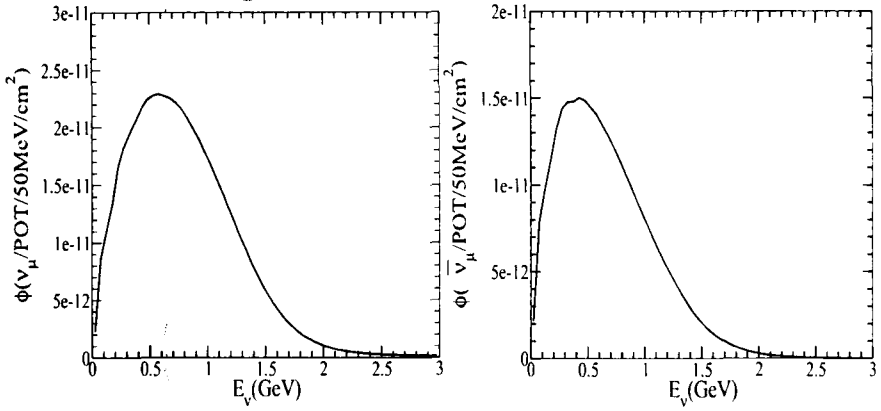

Figure 1.2: The atmospheric neutrino flux.

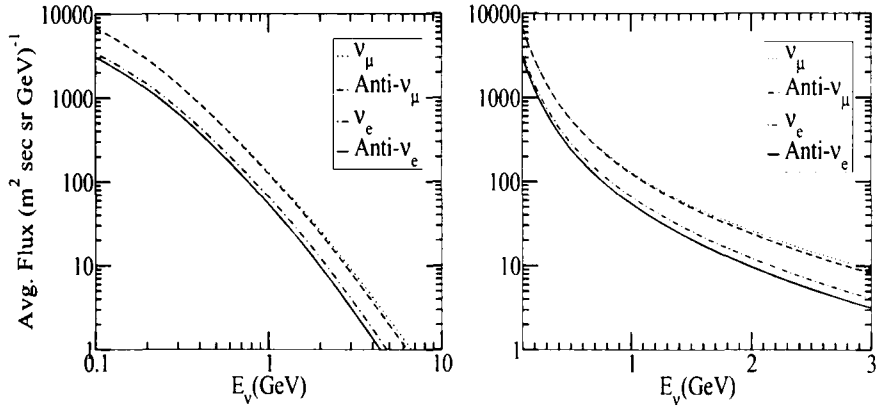

Figure 1.3: The T2K flux.

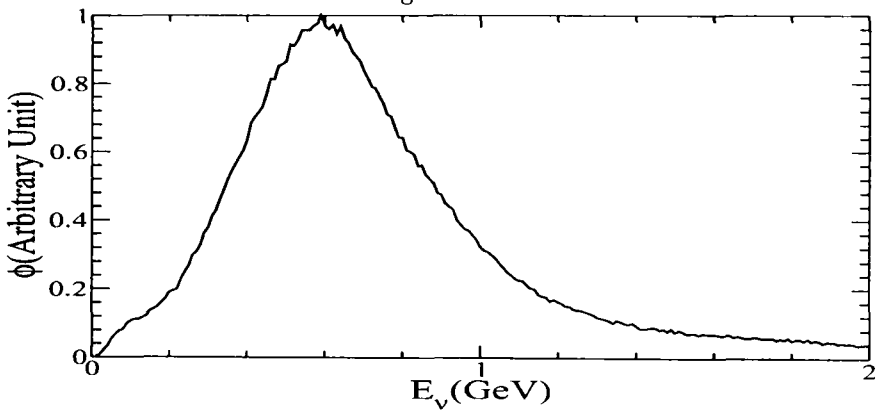

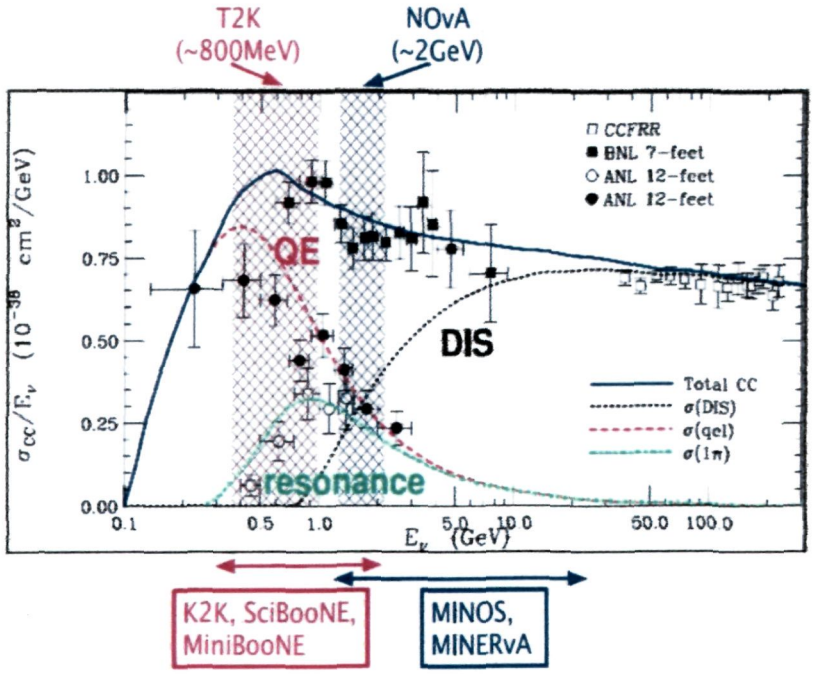

Figure 1.4: Contribution to the total scattering cross section.

Similarly, for the one pion production there will be various resonances like $P_{33}(1232)$, $S_{11}(1535)$, $D_{13}(1520)$, $S_{11}(1650)$ etc.(where subscript represents the isospin and total angular momentum of resonance state, for example, P_{33} means I=3/2, J=$3/2^+$) which may contribute to the one pion production besides the background term the contribution from nucleons s and u channel and others, and furthermore one pion production mainly gets contribution from the $P_{33}(1232)$ resonance whose width and mass get modified in the nuclear medium. Moreover, the produced pions may get rescattered or absorbed while coming out of the nucleus. Likewise in the deep inelastic process there is shadowing, anti-shadowing, EMC effect and Fermi motion which modulates the cross section. Therefore, proper understanding of neutrino nucleus cross section is a must. The earlier Monte Carlo generators like NUANCE [8], NEUGEN [9], NEUT [10] etc. were mainly developed by the experimentalists, who relied on the inputs taken from the older experiments performed either with hydrogen, deuterium targets or very heavy targets like Freon or Freon propane. The energy range in these experiments were also quite high (E_ν >3 GeV) and an extrapolation were performed to apply it to low and intermediate energies neutrinos as well as considering the same nuclear effect in all the different target materials.

In the era of precise neutrino oscillation physics, it has been realised that besides performing new experiments in the different energy region, there is a strong need for the understanding of theoretical cross sections which goes as an input in the Monte Carlo while calculating the event rates. Recently series of neutrino conferences(NUINT and NuFact) which are being regularly organised to have a common platform for the experimentalists as well theorists to discuss the neutrino nucleus reactions in the few GeV energy region. Some of the dedicated experiments have planned like SciBooNE and MINERνA whose aim is to measure neutrino nucleus reaction cross sections. SciBooNE experiment [14] is designed to measure neutrino cross sections on carbon near 1 GeV energy region. While the MINERνA experiment[15] at Fermi lab is using neutrinos in the energy region of 1-20 GeV and the measurement of scattering cross section is planned with several target materials like hydrogen, deuterium, carbon, oxygen, argon, iron and lead.

Although lots of efforts are being made on both theoretically as well as experimentally to understand neutrino nucleus-reaction cross sections but still there is uncertainty in the cross sections of about 20-30%. This has also to do with not having a precise knowledge of the neutrino energies. As nobody can see a neutrino and measure its energy and momentum in the incoming beam the energy of incoming neutrino is evaluated based on the kinematics of particles obtained in the final state depending on the detector acceptance and measurement accuracy. Therefore, it has been emphasized that reconstructed neutrino energy and true neutrino energy may be different and true neutrino energy is really a difficult task to calculate as medium effects make the kinematics calculation quite difficult.

To avoid the complexity of nuclear medium effects in neutrino nucleus cross sections, many experiments are going on or planned, with the concept of the same detector at the near site of the accelerator and at farther distance, like at T2K or NOνA. However, due to oscillations there will be different neutrino energy spectra for near and far detectors and convoluted effects would not be cancelled out. It is important to understand these convoluted effects in order to compare the measured neutrino-nucleon cross sections with theoretical models.

In the present work we are using GENIE Monte Carlo version 2.7.1 [16] to calculate the total and differential scattering cross sections of various possible processes for both charged and neutral current case. GENIE [16] is being designed by a group consisting of many theoretical as well as experimental neutrino physicists. This is a C++ code. This version provides cross section for neutrino-nucleus interaction process for a wide energy range of neutrinos from $\sim$100 MeV to few hundreds of GeV. GENIE has been adopted by the scientific community working at MINOS, MINERνA, NOνA, T2K, INO, LBNE etc.

The Aligarh group [17]-[41] in the last one and half decade has studied nuclear medium effects in neutrino-nucleus cross sections. The charged and neutral current quasielastic scattering cross section has been obtained in several nuclei by taking Fermi motion, Pauli blocking, nucleon correlations, Coulomb's effect on the outgoing charged lepton, etc., into account. For the one pion production process the cross section has been mainly evaluated

in the Δ-dominance model, by taking medium modification of Δ properties in the nuclear medium and the final state interactions of pions. The coherent charged(neutral) pion production has also been studied and which is a benchmark calculation for the studies of coherent pion production process in the few GeV energy region.

Recently this group has also studied one kaon production, associated particle production, eta production, etc. Furthermore, this group has recently studied medium effects on the structure functions to calculate deep inelastic neutrino-nucleus reaction cross sections.

In this work, we have compared the results obtained by the GENIE Monte Carlo code [16] and the results obtained by the Aligarh group [20]-[41]. In chapter 2, we have studied charged current and neutral current quasielastic processes. We have calculated the Q^2-distribution and lepton energy distribution for charged current quasielastic process in iron at 1 GeV. Furthermore, we have done the calculation for total scattering cross section for charged and neutral current quasielastic processes from the models used in GENIE Monte Carlo code [16] and compared the obtained results with the results of Aligarh group [23].

In chapter 3, we study the single pion production from the incoherent and coherent scattering processes. We have presented the results for the Q^2-distribution and pion kinetic energy distribution for charged current neutrino/antineutrino induced single pion production process in iron by using GENIE Monte Carlo code [16]. We have also shown the results of total scattering cross section for charged and neutral current processes obtained from the model[12] used in GENIE Monte Carlo code [16]. Furthermore, for coherent scattering process we show the results of Q^2 distribution in case of charged and neutral current single pion production at 1GeV. For charged current coherent process we have also shown the total scattering cross section by using GENIE Monte Carlo code [16].

In chapter 4, we have studied the neutrino/antineutrino induced associated particle production for free as well as bound nucleon using GENIE Monte Carlo code [16]. We have calculated the total scattering cross section for charged current and neutral current KΛ and KΣ production processes by using GENIE Monte Carlo code [16].

In chapter 5, we study the neutrino induced deep inelastic process for nucleons bound inside the nucleus. We have shown the results of charged current differential scattering cross section obtained from the numerical calculation performed by Aligarh group [38]. We have also calculated the total scattering cross section for charged current deep inelastic process by using GENIE [16] and NUANCE [8] Monte Carlo and then compared with the numerical results obtained by the Aligarh group.

Finally, in chapter 6 we have presented the summary and conclusion of our work.

Chapter 2

Elastic and Quasielastic Scattering

2.1 Introduction

In this chapter we describe charged current quasielastic(CCQE) and neutral current(NC) elastic processes depending upon whether a W or a Z boson is exchanged from a free nucleon or a bound nucleon inside the nucleus. Here we do a comparative study between the cross section obtained by GENIE Monte Carlo code [16] and the cross section obtained using the local Fermi gas model with and without random phase approximation(RPA) developed by Aligarh group [23].

For the quasielastic process a neutrino/antineutrino interacts with a neutron /proton through charged current interaction. The reaction for these processes are given below:

$$\left.\begin{array}{l} \nu_l(k) + n(p) \rightarrow l^-(k') + p(p'), \\ \bar{\nu}_l(k) + p(p) \rightarrow l^+(k') + n(p'), \\ where\ l = \mu, e, \tau \end{array}\right\} \tag{2.1}$$

Here k and k' are the four momenta of incoming neutrino and the corresponding lepton in the final state, and p and p' are respectively the momenta of incoming and outgoing nucleon. This process can be understood with the help of Feynman diagram depicted in Fig.-2.1(a), where a neutrino/antineutrino is a source of W^+/W^- boson which gets absorbed by a neutron/proton target.

In the elastic scattering process initial and final state particles remains the same. This process for a neutrino/antineutrino reaction taking place on a nucleon (neutron/proton)

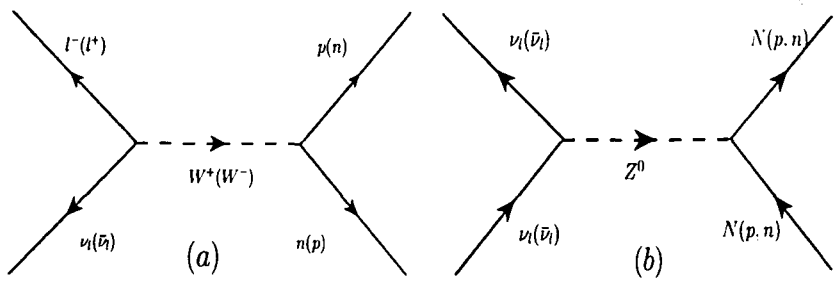

Figure 2.1: Feynman diagram corresponding to the charged current quasiclastic and neutral current elastic processes.

target is given by:

$$\left.\begin{array}{l} \nu_l(k) + n(p) \rightarrow \nu_l(k') + n(p') \\ \nu_l(k) + p(p) \rightarrow \nu_l(k') + p(p') \\ \bar{\nu}_l(k) + n(p) \rightarrow \bar{\nu}_l(k') + n(p') \\ \bar{\nu}_l(k) + p(p) \rightarrow \bar{\nu}_l(k') + p(p'), \end{array}\right\} \tag{2.2}$$

where k and k' are the four momenta of incoming and outgoing neutrino while p and p' are the four momenta of incoming and outgoing nucleon. Feynman diagram for the neutral current elastic process is shown in Fig.-2.1(b).

2.2 Formalism

The invariant matrix element for the charged current quasielastic reaction given in Eq.(2.1) is obtained by using the Feynman rules

$$\mathcal{M} = \frac{G_F}{\sqrt{2}} \cos\theta_C \; l_\mu \; J^\mu, \tag{2.3}$$

where

$$\frac{G_F}{\sqrt{2}} = \frac{g^2}{8M_W^2}. \tag{2.4}$$

$G_F (= 1.16639 \times 10^{-5} GeV^{-2})$ is the Fermi coupling constant and θ_C is the Cabibbo angle. The vertex for the leptonic part is described by

$$-\frac{ig_{\mu\nu}}{2\sqrt{2}}\gamma^\mu(1-\gamma^5) \tag{2.5}$$

and the vertex for the hadronic part is given by

$$-\frac{ig_{\mu\nu} - \frac{q_\mu q_\nu}{M_W^2}}{q^2 - M_W^2}. \tag{2.6}$$

l_μ is the weak leptonic current given by,

$$l_\mu = \bar{u}(k')\gamma_\mu(1 \mp \gamma_5)u(k), \tag{2.7}$$

where the minus sign is for neutrino and the plus sign is for antineutrino. The hadronic current J_μ is given by,

$$\begin{aligned} J_\mu &= \bar{u}(p')\left[F_1^V(q^2)\gamma_\mu + F_2^V(q^2)i\sigma_{\mu\nu}\frac{q^\nu}{2M} + F_A^V(q^2)\gamma_\mu\gamma_5\right. \\ &+ \left. F_P^V(q^2)q_\mu\gamma_5\right]u(p), \end{aligned} \tag{2.8}$$

where $q^2 = (k - k')^2$ is the four momentum transfer square and M is the nucleon mass. In Eq.(2.8), the vector part V^μ and the axial vector part A^μ are

$$V^\mu = F_1^V(q^2)\gamma_\mu + F_2^V(q^2)i\sigma_{\mu\nu}\frac{q^\nu}{2M} \tag{2.9}$$

and

$$A^\mu = -(F_A^V(q^2)\gamma_\mu - F_P^V(q^2)q_\mu), \tag{2.10}$$

where $F_{1,2}^V$ are the isovector vector form factors that are determined from electron scattering experiments and F_A^V, F_P^V are respectively axial vector and pseudoscalar form factors. The form factors generally are taken to be of dipole form. The isovector form factors are written as [23] :

$$\begin{aligned} F_1^V(q^2) &= F_1^p(q^2) - F_1^n(q^2) \\ F_2^V(q^2) &= F_2^p(q^2) - F_2^n(q^2) \end{aligned} \tag{2.11}$$

$F_1^{p,n}$ and $F_2^{p,n}$ are standard Dirac and Pauli form factors of nucleon respectively those are redefined in terms of experimentally determined electromagnetic Sach's form factors,

$$F_1^{p,n} = \frac{G_E^{p,n}(q^2) - \frac{q^2}{4M^2}G_M^{p,n}(q^2)}{1 - \frac{q^2}{4M^2}} \tag{2.12}$$

$$F_2^{p,n} = \frac{G_M^{p,n}(q^2) - G_E^{p,n}(q^2)}{1 - \frac{q^2}{4M^2}}, \tag{2.13}$$

Coefficients	$G_E^p(Q^2)$	$G_M^p(Q^2)$	$G_E^n(Q^2)$	$G_M^n(Q^2)$
a_0	1	1	0	1
a_1	-0.0578±0.166	0.150±0.312E-1	1.25±0.368	1.81±0.402
a_2	0	0	1.30±1.99	0
b_1	11.1±0.217	11.1±0.103	-9.86±6.46	14.1±0.597
b_2	13.6±1.39	19.6±0.281	305±28.6	20.7±2.55
b_3	33.0±8.95	7.54±0.967	-758±77.5	68.7±14.1
b_4	0	0	802±156	0

Table 2.1: The coefficients of the functional form fit Eq.(2.19) for the electromagnetic Sach's form factors in BBBA-05 parametrization [42].

where $G_E^{p,n}$ and $G_M^{p,n}$ are electric and magnetic Sach's form factors for proton and neutron that gives the information about charge distribution and current distribution, respectively and are determined in the charged lepton scattering experiments. The expressions for the electromagnetic Sach's form factors are given by [23] :

$$G_E^p(q^2) = \frac{1}{(1 - q^2/M_v^2)^2} = G_D(q^2) \tag{2.14}$$

$$G_M^p(q^2) = (1 + \mu_p)G_E^p(q^2) \tag{2.15}$$

$$G_M^n(q^2) = \mu_n G_E^p(q^2) \tag{2.16}$$

$$G_E^n(q^2) = (\frac{q^2}{4M^2})\mu_n G_E^p(q^2)\xi_n \tag{2.17}$$

$$\xi_n = \frac{1}{(1 - \lambda_n \frac{q^2}{4M^2})} \tag{2.18}$$

where $\mu_p = 1.7927\mu_N$, $\mu_n = -1.913\mu_N$, $M_v = 0.84GeV$, $\lambda_n = 5.6$, μ_N is the nucleon magnetic moment.
μ_p and μ_n stand for the proton and neutron anomalous magnetic moment respectively. M_v is the axial vector mass. Recently, several other parametrization for the electric and magnetic form factors have been discussed in literature. For example there is Bradford et al. [42] (BBBA2005) parametrization given by

$$G_{E,M}^{p,n}(Q^2) = \frac{\sum_{k=0}^{n} a_k \tau^k}{1 + \sum_{k=1} b_k \tau^k}. \tag{2.19}$$

where $\tau = \frac{Q^2}{4M^2}$ and the coefficients are tabulated in Table-2.1.
The isovector axial vector form factor [23] is defined as

$$F_A^V(Q^2) = \frac{F_A(0)}{\left(1 - \frac{q^2}{4M_A^2}\right)^2} \tag{2.20}$$

where the axial dipole mass $M_A = 1.05$ GeV that is determined experimentally and axial charge $F_A(0) = 1.258$ which is determined in β decay experiments. The pseudoscalar form factor $F_P^V(q^2)$ is dominated by the pion pole and is defined by using the Golberger-Treiman relation at $Q^2 = -q^2 \approx 0$ when partial conservation of axial vector current (PCAC) is assumed:

$$F_P^V(q^2) = \frac{2MF_A^V(q^2)}{(m_\pi^2 - q^2)}, \tag{2.21}$$

where m_π is the pion mass and M stands for the nucleon mass.

The general expression of the differential scattering cross section for ν_μ induced charged current quasielastic lepton production process given in Eq.(2.1) is written as

$$\begin{aligned} d\sigma &= \left(\frac{G_F^2 \cos^2\theta_C}{2}\right) \frac{(2\pi)^4 \delta^4(k + p - p' - k')}{4\sqrt{(k\cdot k')^2 - m_\nu^2 M_n^2}} \frac{d^3\vec{k'}}{(2\pi)^3 2E_l} \\ &\times \frac{d^3\vec{p'}}{(2\pi)^3 2E_p} L_{\mu\nu}^{(\nu)} J^{\mu\nu}, \end{aligned} \tag{2.22}$$

Here the leptonic tensor $L_{\mu\nu}^{(\nu)} = \sum l_\mu l_\nu^\dagger$ and the hadronic tensor $J^{\mu\nu} = \sum J^\mu J^{\nu\dagger}$. The matrix element square is given by taking average over initial spin states and sum over final spin states using Eq.(2.3),

$$|\mathcal{M}|^2 = \frac{G_F^2}{2} \cos^2\theta_C \; L_{\mu\nu}^{(\nu)} \; J^{\mu\nu} \tag{2.23}$$

In the laboratory frame the expression for the total scattering cross section is given by,

$$\sigma_0(E_l, |\vec{k'}|) = \frac{|\vec{k'}|^2}{4\pi E_l E_\nu} \frac{M_n M_p}{E_n E_p} \bar{\Sigma}\Sigma |\mathcal{M}|^2 \delta(q_0 + E_n - E_p), \tag{2.24}$$

where E_ν, E_l, E_n and E_p are the energies of neutrino, corresponding lepton in final state, neutron and proton respectively. M_n and M_p are respectively neutron and proton masses. $q_0 = E_\nu - E_l$ is the energy transfer.

For neutral current elastic scattering process Eq.(2.2) the matrix element is written as

$$\mathcal{M} = \frac{G_F}{\sqrt{2}} \; l_\mu \; J^\mu, \tag{2.25}$$

where l_μ is the leptonic current given by

$$l_\mu = \bar{u}(k')\gamma_\mu(1 - \gamma_5)u(k) \tag{2.26}$$

and the hadronic current J_μ is given by

$$J_\mu = \bar{u}(p')\left[\left(\gamma_\mu - \frac{q_\mu \not{q}}{q^2}\right)\tilde{F}_1^N + \frac{i\sigma_{\mu\nu}q^\nu \tilde{F}_2^N}{2M_N} + \gamma_\mu\gamma_5\tilde{F}_A^N + \frac{q_\mu\gamma_5\tilde{F}_P^N}{M_N}\right]u(p), \tag{2.27}$$

where $\tilde{F}_{1,2}^N$ is vector form factor, $\tilde{F}_A^N$ and $\tilde{F}_P^N$ are respectively axial and pseudoscalar form factors. These form factors are written in terms of Dirac and Pauli form factors of the nucleon and a strange component $F_{1,2}^s$, in the following way [26]:

$$\tilde{F}_{1,2}^p = (\frac{1}{2} - 2sin^2\theta_W)F_{1,2}^p - \frac{1}{2}F_{1,2}^n - \frac{1}{2}F_{1,2}^s \tag{2.28}$$

$$\tilde{F}_{1,2}^n = (\frac{1}{2} - 2sin^2\theta_W)F_{1,2}^n - \frac{1}{2}F_{1,2}^p - \frac{1}{2}F_{1,2}^s\ , \tag{2.29}$$

where θ_W is the weak mixing angle. Axial form factors $\tilde{F}_{p,n}^A$ are given by [26]

$$\tilde{F}_{p,n}^A = \pm\frac{1}{2}F_A - \frac{1}{2}F_A^s \tag{2.30}$$

$$F_A^s(q^2) = \frac{\Delta s}{(1 + \frac{q^2}{M_A^2})^2} \tag{2.31}$$

Here symbols have the same meaning as for the vector part and Δs denotes the strange sea quark contribution to the nucleon spin. The representative values of Δs are 0 and -0.15 [43]. The neutral current cross section is more sensitive to strange axial form factor than to the strange vector form factors. This effect become more significant for scattering on protons because the dominance of axial vector in $\nu p \rightarrow \nu p$ makes this reaction more sensitive to strange axial form factor than the reaction $\nu n \rightarrow \nu n$.

As most of the neutrino experiments are being performed using nuclear targets, therefore, nuclear medium effects such as Pauli blocking, Fermi motion, binding energy correction etc. should be accounted for. In this work, we have studied nucleons bound inside iron(^{56}Fe) nuclear target. Iron is presently planned to be used in the proposed India-based Neutrino Observatory(INO). In order to taken into account these medium effects several methods has been developed like Fermi gas model([11], [44]), local Fermi gas model [23], shell model [45, 46] continuum random phase approximation (CRPA) [47, 48], etc. In this study we summarize the expression of cross section used in various methods. First we discuss in brief the general Fermi gas model. It is a statistical model of the nucleus. This model pictures the nucleus as a degenerate gas of protons and neutrons because all the

particles lie in the lowest possible state in a manner consistent with the Pauli exclusion principle. According to the Heisenberg uncertainty principle

$$dp_x.dx \geq h \tag{2.32}$$

In a fully degenerate system of fermions (i.e. lowest energy state is fully occupied), there is a single particle in 6-dimensional volume

$$\begin{aligned} dV_{ps} &= (dx.dp_x).(dy.dp_y).(dz.dp_z) = h^3 \\ dV_{ps} &= (dx.dy.dz)(dp_x.dp_y.dp_z) = dV.dp^3 \end{aligned} \tag{2.33}$$

Minimum number of nucleons(dN) that can be contained in a certain volume of phase space is obtained by

$$dN = \frac{dV_{ps}}{h^3} = \frac{dV.dp^3}{h^3} = \frac{dV.4\pi p^2 dp}{(2\pi\hbar)^3} \tag{2.34}$$

To explain Fermi gas model for the nucleus let us consider the following-

$$\begin{aligned} &V(x) = 0; \quad 0 < x < L, \quad V(x) = \infty; \quad x \geq L \\ &V(y) = 0; \quad 0 < y < L, \quad V(y) = \infty; \quad y \geq L \\ &V(z) = 0; \quad 0 < z < L, \quad V(z) = \infty; \quad z \geq L \end{aligned} \tag{2.35}$$

Total potential energy is given by

$$V = V(x) + V(y) + V(z) \tag{2.36}$$

Using the time independent Schrodinger equation

$$\left(-\frac{\hbar^2}{2M}\nabla^2 + V\right)\psi = E\psi, \tag{2.37}$$

where wave function $\psi = \psi(x).\psi(y).\psi(z)$ and energy $E = E_x + E_y + E_z$, for an infinite square well.

$$\psi(x) = \sqrt{\frac{2}{L}} sin\left(\frac{n_x}{L}\right); \quad E_x = \frac{p_x^2}{2M} = \frac{(\hbar\pi)^2}{2ML^2}n_x^2 \tag{2.38}$$

So, the total energy eigenvalue is given by

$$E = \frac{(\hbar\pi)^2}{2ML^2}(n_x^2 + n_y^2 + n_z^2) \tag{2.39}$$

and the total momentum

$$p = \frac{\hbar\pi}{L}\sqrt{n_x^2 + n_y^2 + n_z^2} \tag{2.40}$$

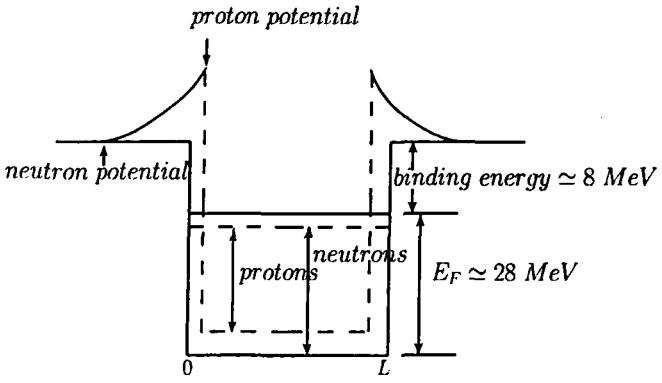

Figure 2.2: Potential well for neutrons and protons in a heavy nucleus, showing the Fermi level.

Hence

$$dp^3 = \left(\frac{\hbar\pi}{L}\right)^3 \tag{2.41}$$

All the low levels filled up to a maximum are called Fermi levels and the corresponding energy and momentum are respectively denoted by E_F and p_F. The number of momentum states within the momentum-sphere up to Fermi level is given by

$$N = \frac{1}{8} \times \frac{4}{3} \times \frac{\pi p_F^3}{dp^3} \tag{2.42}$$

In the above expression a factor of 1/8 of sphere comes because $n_x, n_y, n_z > 0$. Using relation $p_F = \sqrt{2ME_F}$ and Eq.(2.41) in Eq.(2.42), we get

$$\begin{aligned} N &= 2 \times \frac{1}{8} \times \frac{4}{3} \times \frac{\pi(2ME_F)^{3/2}}{(\frac{\hbar\pi}{L})^3} \\ N &= \frac{V}{3} \times \pi \left(\frac{2ME_F}{\pi^2\hbar^2}\right)^{3/2}, \end{aligned} \tag{2.43}$$

where factor of 2 comes due to two spin states and $L^3 = V$. From the above expression Fermi energy E_F is given by

$$E_F = \frac{(\pi\hbar)^2}{2M} \left(\frac{3N}{\pi V}\right)^{2/3} \tag{2.44}$$

and the Fermi momentum p_F is given by

$$p_F = \sqrt{2ME_F} = (2M)^{1/2}\frac{(\pi\hbar)^2}{2M}\left(\frac{3N}{\pi V}\right)^{2/3} = \hbar(3\pi^2)^{1/3}\left(\frac{N}{V}\right)^{1/3}, \tag{2.45}$$

where N=Z for protons, N=(A-Z) for neutrons and $V = \frac{4}{3}\pi R^3$ and $R = R_0 A^{1/3}$. The behaviour of the potential described here has been shown in Fig.-2.2.

2.2.1 Llewellyn Smith model

In the Llewellyn Smith model [11], per nucleon cross section is taken equal to the cross section for free nucleon Eq.(2.24) multiplied by a factor of $(1 - \frac{D}{N})$, where

$$\begin{aligned} D &= Z \quad for \quad 2x < u - v \\ &= \frac{1}{2}A\left\{1 - \frac{3x}{4}(u^2 + v^2) + \frac{x^3}{2} - \frac{3}{32x}(u^2 - v^2)^2\right\} \\ &\quad for\ u - v < x < u + v \\ &= 0 \quad for \quad x > u + v \\ A &= N + Z \end{aligned} \tag{2.46}$$

with $x = \frac{|\vec{q}|}{2k_F}$, $u = (\frac{2N}{A})^{1/3}$, $v = (\frac{2Z}{A})^{1/3}$ and N, Z are number of neutrons and protons of the initial nucleus respectively, k_F is the Fermi momentum and the three momentum transfer $|\vec{q}| = \sqrt{(q^2 + m^2)/4M^2 - q^2}$. In this energy range neutrino-nucleus reactions has been calculated in the closure approximation with harmonic-oscillator potentials for closed-shell nuclei.

2.2.2 Smith Moniz model

In this model the expression of differential cross section for the charged current quasielastic process Eq.(2.22) in which a charged lepton of mass m_l is detected at an angle θ with respect to the incident neutrino ν_l is given by

$$d^2\sigma = \frac{G^2}{2}\frac{1}{(2\pi)^2}\frac{1}{2|\vec{k}.p|}\frac{d\vec{k}'}{2\epsilon_2}\eta_{\mu\nu}W_{\mu\nu} \tag{2.47}$$

where

$$\eta_{\mu\nu} = Tr\{\gamma_\mu(1 + \gamma_5)\ \not{k}\gamma_\nu(1 + \gamma_5)\ \not{k}'\} \tag{2.48}$$

and

$$W_{\mu\nu} = (2\pi)^3\Omega\bar{\Sigma}_i\Sigma_f\delta^{(4)}(p - p' - q)\langle p|j_\nu^{(-)}(0)|p'\rangle\langle p'|j_\mu^{(+)}(0)|p\rangle E. \tag{2.49}$$

$J_\mu^{(\pm)}(0) = V_\mu^{(\pm)}(0) + A_\mu^{(\pm)}(0)$ is the nuclear weak current, Ω is the quantization volume, E is the energy of the target, m is the proton mass and G is the weak coupling constant.

Under Lorentz and time reversal invariance $W_{\mu\nu}$ can be defined as

$$W_{\mu\nu} = W_1\delta_{\mu\nu} + \frac{W_2}{m_T^2}p_\mu p_\nu + \frac{W_\alpha}{m_T^2}q_\mu q_\nu + \frac{W_\beta}{m_T^2}(p_\mu q_\nu + p_\nu q_\mu) + \frac{W_8}{m_T^2}\epsilon_{\mu\nu\sigma\tau}p_\sigma q_\tau \tag{2.50}$$

where m_T is the target mass, W_j are the form factors which depend only upon the scalars q^2 and $q \cdot p$. Using the definition $cos\chi = k_2/\epsilon_2 cos\theta$, the cross section in the lab frame is given by

$$\begin{aligned}\left(\frac{d^2\sigma}{dk'd\Omega_2}\right)_\nu &= \frac{G^2k'^2cos^2(\frac{1}{2}\chi)}{2\pi^2m_T}\left\{W_2 + [2W_1 + \frac{m_l^2}{m_T^2}W_\alpha]tan^2(\frac{1}{2}\chi)\right. \\ &+ (W_\beta + W_8)m_l^2/(m_T\epsilon_2 cos^2(\frac{1}{2}\chi)) - 2W_8/m_T tan(\frac{1}{2}\chi) \\ &\times \left. sec(\frac{1}{2}\chi)[q^2cos^2(\frac{1}{2}\chi) + |\vec{q}|^2sin^2(\frac{1}{2}\chi) + m_l^2]^{\frac{1}{2}}\right\}\end{aligned} \tag{2.51}$$

For antineutrino reactions the sign of the form factor W_8 is reversed. In the lab frame $W_{\mu\nu}$ can be expressed in terms of the single nucleon matrix elements:

$$(W_{\mu\nu})_{lab} = \int d\vec{k}\mathcal{F}(\vec{k},\vec{q},\omega)T_{\mu\nu} \tag{2.52}$$

where

$$\mathcal{F}(\vec{k},\vec{q},\omega) = \frac{m_T\Omega}{(2\pi)^3}\frac{\delta(\epsilon_k - \epsilon k - q + \omega)n_i(k)(1 - n_f(|\vec{k} - \vec{q}|))}{\epsilon_k\epsilon_{k-q}} \tag{2.53}$$

and

$$\begin{aligned}T_{\mu\nu} &= \epsilon_k\epsilon_{k-q}\Omega^2\Sigma_{\lambda\lambda'}\langle\vec{k} - \vec{q}\lambda'|j_\mu^{(+)}(0)|k\lambda\rangle\langle k\lambda|j_\nu^{(-)}(0)|\vec{k} - \vec{q}\lambda'\rangle \\ &\equiv T_1\delta_{\mu\nu} + T_2/m^2k_\mu k_\nu + T_\alpha/m^2q_\mu q_\nu \\ &+ T_\beta/m^2(k_\mu q_\nu + k_\nu q_\mu) + T_8/m^2\epsilon_{\mu\nu\sigma\tau}k_\sigma q_\tau\end{aligned} \tag{2.54}$$

here single particle form factors T_j depend only upon q^2, $n_i(k)$ is the neutron/proton momentum distribution for incident neutrinos/antineutrinos, $n_f(k)$ is the proton/neutron momentum distribution for outgoing neutrinos /antineutrinos. For quasielastic scattering the Pauli exclusion factor $(1 - n_f(|\vec{k} - \vec{q}|))$ is included and for a pure Fermi gas model $n_i(k) = \theta(k_{F_i} - |k|)$. This factor ensures that the recoil nucleon lies outside the Fermi sea. Using the Lorentz transformation properties of $W_{\mu\nu}$ and $T_{\mu\nu}$, W_j's can be determined in terms of T_j's. In lab frame Eq.(2.50) becomes

$$\begin{aligned}W_{\mu\nu} &= W_1\delta_{\mu\nu} - W_2\delta_{\mu4}\delta_{\nu4} + W_\alpha/m_T^2\ q_\mu q_\nu + iW_\beta/m_T\ (\delta_{\mu4}q_\nu + \delta_{\nu4}q_\mu) \\ &- iW_8/m_T\ \epsilon_{\mu\nu\sigma4}q_\sigma\end{aligned} \tag{2.55}$$

Now substitute Eq.(2.54) in Eq.(2.52) and compare it with Eq.(2.55). After performing the angular integration, W_i's can be given as

$$\left.\begin{array}{l} W_1 = a_1 T_1 + \frac{1}{2}(a_2 - a_3)T_2, \\ W_2 = [a_4 + 2\omega/|\vec{q}|a_5 + \omega^2/|\vec{q}|^2 a_3 + \frac{1}{2}q^2/|\vec{q}|^2(a_2 - a_3)]T_2, \\ W_\alpha = m_T^2/|\vec{q}|^2(\frac{3}{2}a_3 - \frac{1}{2}a_2)T_2 + m_T^2/m^2 a_1 T_\alpha + 2m_T^2/(m|\vec{q}|)a_6 T_\beta, \\ W_\beta = m_T/m(a_7 + \omega/|\vec{q}|a_6)T_\beta, \\ W_8 = m_T/m(a_7 + \omega/|\vec{|}a_6)T_8 \end{array}\right\} \quad (2.56)$$

where

$$a_1 = \int d\vec{k}\mathcal{F}(\vec{k},\vec{q},\omega), \quad a_5 = \int d\vec{k}\mathcal{F}(\vec{k},\vec{q},\omega)\frac{\epsilon_k k\ cos\tau}{m^2},$$

$$a_2 = \int d\vec{k}\mathcal{F}(\vec{k},\vec{q},\omega)\frac{k^2}{m^2}, \quad a_6 = \int d\vec{k}\mathcal{F}(\vec{k},\vec{q},\omega)\frac{k\ cos\tau}{m},$$

$$a_3 = \int d\vec{k}\mathcal{F}(\vec{k},\vec{q},\omega)\frac{k^2\ cos^2\tau}{m^2}, \quad a_7 = \int d\vec{k}\mathcal{F}(\vec{k},\vec{q},\omega)\frac{\epsilon_k}{m},$$

$$a_4 = \int d\vec{k}\mathcal{F}(\vec{k},\vec{q},\omega)\frac{\epsilon_k}{m^2}.$$

a_j's contains all the information in the single particle momentum distributions and energies. For quasielastic scattering the matrix element is given by

$$\begin{aligned} \langle\vec{k}'\lambda'|j_\mu^{(\pm)}(0)|\vec{k}\lambda\rangle &= i\left(\frac{m^2}{\epsilon_k\epsilon_{k'}\Omega^2}\right)^{\frac{1}{2}}\bar{u}(\vec{k}'\lambda')\{F_1\gamma_\mu + F_2\,\sigma_{\mu\alpha}q_\alpha - iF_s q_\mu\tau_z \\ &+ F_A\gamma_5\gamma_\mu - iF_P\gamma_5 q_\mu + F_T\gamma_5\sigma_{\mu\alpha}q_\alpha\tau_z\}\tau_\pm u(\vec{k}\lambda) \end{aligned} \quad (2.57)$$

Using this form of matrix element in Eq.(2.54), T_j's can be written as

$$\left.\begin{array}{l} T_1 = \frac{1}{2}q^2(F_1 + 2mF_2)^2 + (2m^2 + \frac{1}{2}q^2)F_A^2, \\ T_2 = 2m^2(F_1^2 + q^2F_2^2 + F_A^2 + q^2F_T^2), \\ T_\alpha = -m^2/q^2 T_1 + \frac{1}{4}T_2 + m^2F_S[-2mF_1 + q^2F_2 + (2m^2 + \frac{1}{2}q^2)F_S] \\ \quad +m^2(2mF_A - q^2F_P)[-F_T + 1/(2q^2)(2mF_A - q^2F_P)] \\ T_\beta = -\frac{1}{2}T_2 + m^2F_S[2mF_1 - q^2F_2] + m^2F_T[2mF_A - q^2F_P], \\ T_8 = 2m^2F_A(F_1 + 2mF_2). \end{array}\right\} \quad (2.58)$$

2.2.3 Local Fermi gas model

In the local density approximation [23] evaluation of the cross section is done as a function of local Fermi momentum $p_F(r)$ and integrated over whole nucleus. Various medium effects are taken into account inside the nucleus like Pauli blocking and Fermi motion via the

imaginary part of the Lindhard function using relativistic kinematics for particle-hole excitations in the nuclear medium. We have to take care of Coulomb force acting on the outgoing lepton which modulates the momenta and energy of the leptons coming out of the nucleus, and its effect is significant for leptons of low momentum and for a heavier nuclear target. By using random phase approximation weak transition strengths are renormalised through the interaction of p-h excitations as they propagate in the nuclear medium using N-N potential explained by pion and rho exchanges. Neutrino scatters from a neutron or proton moving inside a finite nucleus with local density $\rho_n(r)$ *or* $\rho_p(r)$ in a medium with the corresponding Fermi momenta distribution. In this approximation, the local Fermi momenta of nucleons is given by

$$p_{Fn} = \left[3\pi^2\rho_n(r)\right]^{1/3}; \quad p_{Fp} = \left[3\pi^2\rho_p(r)\right]^{1/3} \tag{2.59}$$

The expression for the scattering cross section in the local density approximation is given by

$$\sigma(E_l, \theta_l) = \int \rho_n(r)\, d^3\vec{r}\, \sigma_0(E_l, \theta_l), \tag{2.60}$$

where E_l is the energy of lepton, θ_l is scattering angle of lepton and $\sigma_0(E_l, \theta_l)$ is the double differential of charged current free neutrino-nucleon scattering in the laboratory frame

$$\sigma_0(E_l, \theta_l) = \frac{1}{4\pi^2}\frac{|\vec{p}_l|^2}{E_\nu E_l}\frac{M_n M_p}{E_n E_p}\bar{\sum}\sum|\mathcal{M}|^2\,\delta[q_0 + E_n - E_p] \tag{2.61}$$

where $q_0 = (E_\nu - E_l)$ is the energy transfer and $\bar{\sum}\sum|\mathcal{M}|^2$ is matrix element square averaged over initial spin states and summed over final spin states. Volume occupied by each nucleon is $2\pi\hbar$ in symmetric nuclear matter. Since each nucleon may have two spin orientation so each unit cell will occupy two nucleons in configuration space. So, number of nucleons in a certain volume($\hbar = 1$ in natural units) may be written as

$$N = 2V\int_0^{p_F}\frac{d^3p}{(2\pi)^3}, \quad \text{or} \quad \rho(r) = \frac{N}{V} = 2\int\frac{d^3p}{(2\pi)^3}\, n_n(\vec{p}, \vec{r}) \tag{2.62}$$

where $n_n(\vec{p}, \vec{r})$ is the local neutron occupation number. $n_n(\vec{p}, \vec{r})$=1 for $p \leq p_{F_n}$ and is equal to zero for $p > p_{F_n}$, where p_{F_n} is local Fermi momentum of neutron.
Hence,

$$\begin{aligned}\sigma_0(E_l, \theta_l) &= 2\int d^3r\,\frac{d^3p}{(2\pi)^3}\, n_n(\vec{p}, \vec{r})\,\sigma_0(E_l, \theta_l) \\ &= 2\int d^3r\,\frac{d^3p}{(2\pi)^3}\, n_n(\vec{p}, \vec{r})\,\frac{1}{4\pi^2}\,\frac{|\vec{p}_l|^2}{E_\nu E_l}\,\frac{M_n M_p}{E_n E_p}\,\bar{\Sigma}\Sigma|\mathcal{M}|^2 \\ &\times\ \delta\left(q_0 + E_n - E_p\right)\end{aligned} \tag{2.63}$$

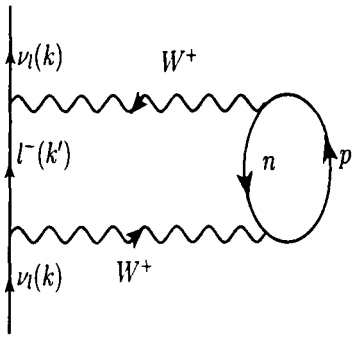

Figure 2.3: Diagrammatic representation of the neutrino self energy diagram corresponding to the ph-excitation leading to $\nu_l + p \rightarrow l^- + n$ in nuclei.

Since nucleons are no longer free as they are moving in the Fermi sea of nucleons in initial and final nuclei, therefore, the energies of nucleons(E_n and E_p) in the delta function now become the function of their momenta $E_n(|p_n|)$ and $E_p(|q + p_n|)$, where p_n is the momentum of target neutron inside the nucleus. Also these nucleons have to satisfy the Pauli principle such that the initial momentum of the neutron should be lesser than the Fermi momentum of the neutron inside the nucleus $p_n < p_{Fn}$ and similarly the outgoing proton momentum should be greater than the Fermi momentum of the proton inside the nucleus $p'_p > p_{Fp}$, where $p'_p = |q + p_n|$ and p_{Fn} and p_{Fp} are local Fermi momentum of neutrons and protons at the interaction point inside the nucleus. This constraint is the Pauli blocking condition that is considered while performing the integration over initial nucleon momentum in Eq.(2.60) with the replacement of the factor

$$\int d^3r \, \frac{d^3p}{(2\pi)^3} \, n_n(\vec{p},\vec{r}) \, \frac{M_n M_p}{E_n E_p} \, \delta(q_0 + E_n - E_p) \tag{2.64}$$

occurring in Eq.(2.63) by $-(1/\pi)Im\ U_N(q_0,\vec{q})$, where $U_N(q_0,\vec{q})$ is the Lindhard function corresponding to the particle hole(ph) excitations induced by weak interaction process through W-boson exchange shown in Fig.-2.3. This has been discussed in detail in references [50]- [54].

Nucleon Correlations

In the nucleus the strength of the electroweak coupling may change from their free nucleon values due to the presence of strongly interacting nucleons. Conservation of Vector Current (CVC) forbids any change in the charge coupling while magnetic and axial vector couplings are likely to change from their free nucleon values. These changes are calculated by

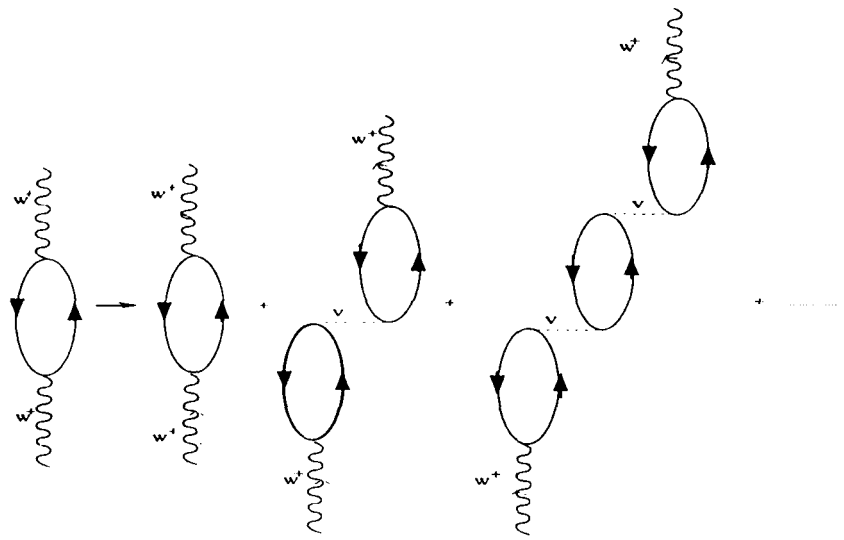

Figure 2.4: Irreducible diagrams responsible for the polarization (RPA) effects in the 1p1h contribution to the W-self energy.

considering the interaction of ph excitations in the nuclear medium in Random Phase Approximation (RPA).

The diagram shown in Fig.-2.4 simulates the effect of the strongly interacting nuclear medium at the weak vertex. The ph-ph interaction is shown by the wavy line in Fig.-2.4 and is described by the π and ρ exchanges. The details of RPA approach are described in [23]. Furthermore, the effect of the Δ degrees of freedom in the nuclear medium is included in the calculation of the RPA response by considering the effect of ph-Δh and Δh-Δh excitations. Therefore, these correlations may be shown by a modified figure depicted in Fig.-2.5.

The decomposition of the potential in longitudinal and transverse parts helps in summing the geometric series, for example, the contribution of Fig.-2.5 is given by

$$\begin{aligned}\bar{U}(q) &= [U(q) + U(q)V_{ij}(q)\sigma_i\sigma_j U(q) + U(q)V_{ik}(q)\sigma_i\sigma_k U(q) \\ &\quad \times V_{kj}(q)\sigma_k\sigma_j U(q) + ..]\vec{\tau}\cdot\vec{\tau}, \end{aligned} \tag{2.65}$$

where $V_{ij} = V_t(\delta_{ij} - \hat{q}_i\hat{q}_j) + V_l\hat{q}_i\hat{q}_j$. Here $V(q)$ is the ph-ph interaction mediated by π and ρ exchanges. V_l and V_t are the strength of the nucleon-nucleon potential in longitudinal and transverse channels, calculated with π and ρ exchanges. These are further modulated by the Landau Migdal parameter g' to take into account the short range correlation effects.

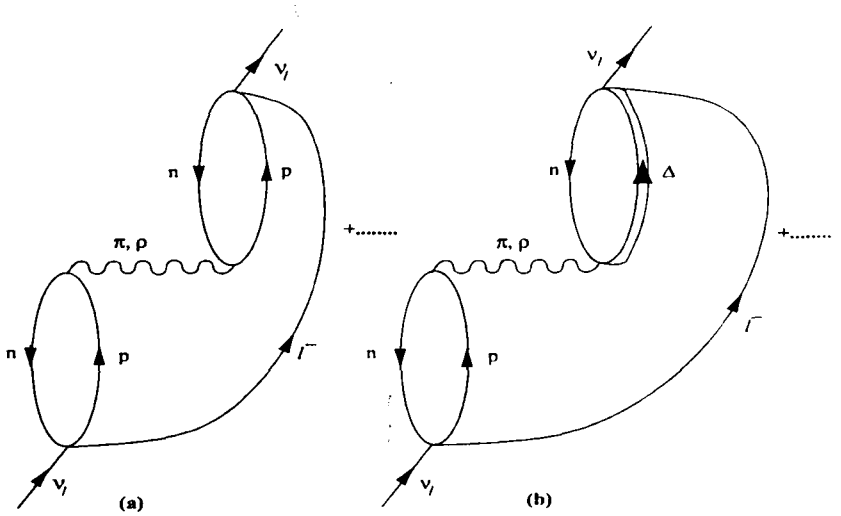

Figure 2.5: Many body Feynman diagrams (in the limit $M_W \rightarrow \infty$) accounting for the medium polarization effects contributing to the process $\nu_l + n \rightarrow l^- + p$ transitions.

Longitudinal and transverse part of the potentials are given by:

$$V_l(q) = \frac{f_\pi^2}{m_\pi^2}\left[\frac{|\vec{q}|^2}{q_0^2 - \vec{q}^2 - m_\pi^2}\left(\frac{\Lambda_\pi^2 - m_\pi^2}{\Lambda_\pi^2 - q^2}\right)^2 + g'\right] \tag{2.66}$$

$$V_t(q) = \frac{f_\pi^2}{m_\pi^2}\left[\frac{|\vec{q}|^2 c_\rho}{q_0^2 - \vec{q}^2 - m_\pi^2}\left(\frac{\Lambda_\rho^2 - m_\rho^2}{\Lambda_\rho^2 - q^2}\right)^2 + g'\right] \tag{2.67}$$

with g'=0.6-0.7, and

$$c_\rho = \left[\frac{f_\rho^2}{m_\rho^2}\right] / \left[\frac{f_\pi^2}{m_\pi^2}\right] \approx 2. \tag{2.68}$$

One may write the longitudinal part of Eq.(2.65) as

$$\begin{aligned}
\bar{U}(q) &= [U(q) + U(q)V_l\hat{q}_i\hat{q}_j\sigma_i\sigma_j U(q) + U(q)V_l\hat{q}_i\hat{q}_k\sigma_i\sigma_k U(q)V_l\hat{q}_k\hat{q}_j \\
&\quad \times\sigma_k\sigma_j U(q) + ...]\ \vec{\tau}\cdot\vec{\tau} \\
&= [U(q) + U(q)V_l U(q) + U(q)V_l U(q)V_l U(q) + ...]\ \hat{q}_i\hat{q}_j\ \sigma_i\sigma_j\ \vec{\tau}\cdot\vec{\tau} \\
&= U(q)[1 + V_l U(q) + (V_l U(q))^2 + ...]\ \hat{q}_i\hat{q}_j\ \sigma_i\sigma_j\ \vec{\tau}\cdot\vec{\tau} \\
&= \left[\frac{U(q)}{1 - U(q)V_l}\right]\ \hat{q}_i\hat{q}_j\ \sigma_i\sigma_j\ \vec{\tau}\cdot\vec{\tau}
\end{aligned} \tag{2.69}$$

Similarly, the transverse part is given by

$$\bar{U}(q) = \left[\frac{U(q)}{1 - U(q)V_t}\right] (\delta_{ij} - \hat{q}_i\hat{q}_j)\, \sigma_i\sigma_j\, \vec{\tau}\cdot\vec{\tau} \tag{2.70}$$

Therefore, we can write Eq.(2.65) as:

$$\bar{U}(q) = \left[\left(\frac{U(q)}{1 - U(q)V_t}\right) (\delta_{ij} - \hat{q}_i\hat{q}_j) + \left(\frac{U(q)}{1 - U(q)V_l}\right) \hat{q}_i\hat{q}_j\right] \vec{\sigma_i}\, \vec{\sigma_j}\vec{\tau}\cdot\vec{\tau} \tag{2.71}$$

where $U_N \rightarrow U = U_N + U_\Delta$, with U_N and U_Δ as the Lindhard function for particle-hole(ph) and Δh excitations, respectively, in the medium.

The RPA response of this term after summing the higher order diagrams like Fig.-2.5 is modified and is given by J^{ij}_{RPA}

$$J^{ij} \rightarrow J^{ij}_{RPA} = F_A^2(q^2)\mathrm{Im}U \left[\frac{\hat{q}_i\hat{q}_j}{|1 - UV_l|^2} + \frac{\delta_{ij} - \hat{q}_i\hat{q}_j}{|1 - UV_t|^2}\right] \tag{2.72}$$

where V_l and V_t are the longitudinal and transverse part of the nucleon-nucleon potential calculated with π and ρ exchanges. Similarly there are modifications in the magnetic coupling and pseudoscalar couplings and the interference terms. These together modifies the expression of the hadronic tensor given in Eq.(2.72). Hence, when we include RPA the expression of total scattering cross section becomes

$$\begin{aligned}\sigma(E_\nu) &= -2G_F^2\cos^2\theta_c \int_{r_{min}}^{r_{max}} r^2 dr \int_{k'_{min}}^{k'_{max}} k' dk' \int_{Q^2_{min}}^{Q^2_{max}} dQ^2 \frac{1}{E_\nu^2 E_l} \\ &\times\ L^{(\nu)}_{\mu\nu} J^{\mu\nu}_{RPA} Im U_N[E_\nu - E_l - Q_r - V_c(r), \vec{q}].\end{aligned} \tag{2.73}$$

2.3 Comparative Study

In this work, we have performed a comparative study between the results of the cross section obtained by using a local Fermi gas model [23] and the results of the cross section obtained by the GENIE Monte Carlo code [16]. In this Monte Carlo, Llewellyn-Smith model [11] is taken for quasielastic scattering process. The model by Ahrens et al. [49] is incorporated by GENIE Monte Carlo code [16] for neutral current elastic processes and the axial form factors are taken to be of dipole form. In GENIE Monte Carlo code [16], BBBA2005 [42] parametrization is used. The axial vector mass is taken as 1.05 GeV for charged current quasiclastic and neutral current elastic processes. The value of the axial dipole mass M_A is in debate since last 2-3 years as the results from the recent accelerator experiments like K2K, MiniBooNE and MINOS suggest a higher values of M_A while the NOMAD experiment still agrees with the global value of $M_A(1.03 \pm 0.02 GeV)$. The Fermi gas model used in GENIE Monte Carlo code [16] takes into account Pauli blocking, Fermi motion and binding energy correction but it does not consider nuclear correlations. In

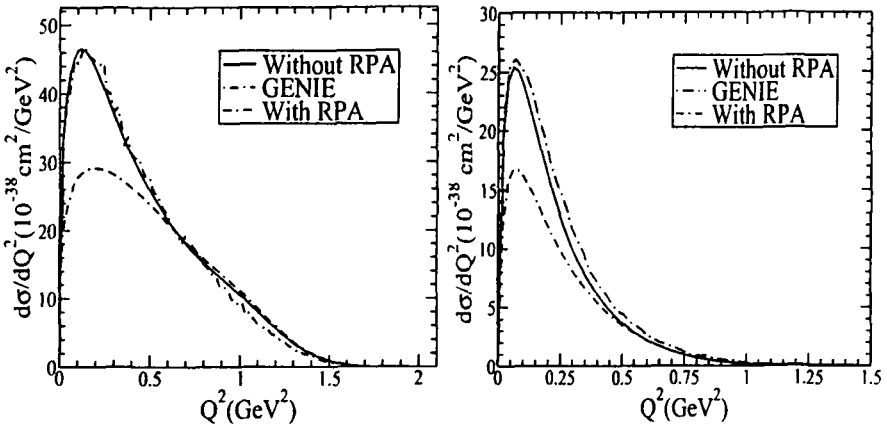

Figure 2.6: $d\sigma/dQ^2$ vs Q^2 for CCQE process in $\nu_\mu - ^{56}Fe$ reaction(left-panel) and $\bar{\nu}_\mu - ^{56}Fe$(right-panel) at $E_\nu = 1$GeV.

GENIE Monte Carlo code [16] values of Fermi momentum k_F that has been taken is 0.221 GeV/c for ^{12}C, 0.225 GeV/c for ^{16}O, 0.251 GeV/c for protons in ^{56}Fe, and 0.256 GeV/c for neutrons in ^{56}Fe.

2.4 Results and Conclusions

In this section, we present the results for the total scattering cross section(σ), Q^2 distribution and lepton energy distribution for neutrino/antineutrino induced processes in bound as well as for free nucleon. For neutral current elastic and charged current quasielastic processes the results are obtained with the vector dipole mass $M_V = 0.84$ GeV and the axial dipole mass $M_A = 1.05$ GeV.

2.4.1 Differential Scattering Cross Section

In Fig.-2.6, we have presented the results for Q^2-distribution for CCQE processes given in Eq.(2.1). Here we have compared the results obtained by GENIE Monte Carlo code [16] and local Fermi gas model [23] with and without random phase approximation(RPA) at neutrino energy $E_\nu = 1$ GeV.

In Fig.-2.6, the results obtained by using Llewellyn Smith Fermi gas model [11] in GENIE Monte Carlo code [16] is shown by dashed-dotted line and solid line is the result obtained by local Fermi gas model [23] without RPA effect. We find that these results are in good agreement. When we incorporate RPA effect then there is further reduction of 36% at $Q^2 = 0.05$ GeV^2, around 38% at $Q^2 = 0.12$ GeV^2 and 7% at $Q^2 = 0.5$ GeV^2. In

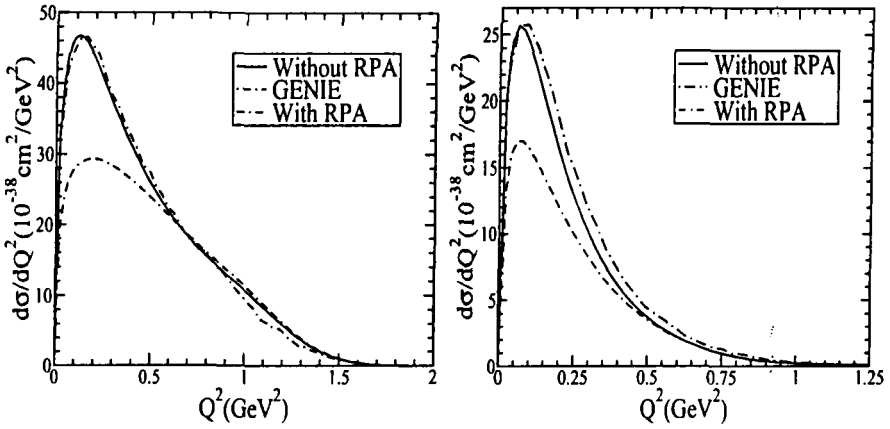

Figure 2.7: $d\sigma/dQ^2$ vs Q^2 for CCQE process in $\nu_e - ^{56}Fe$ reaction(left-panel) and in $\bar{\nu}_e - ^{56}Fe$ reaction(right-panel) at $E_\nu = 1$GeV.

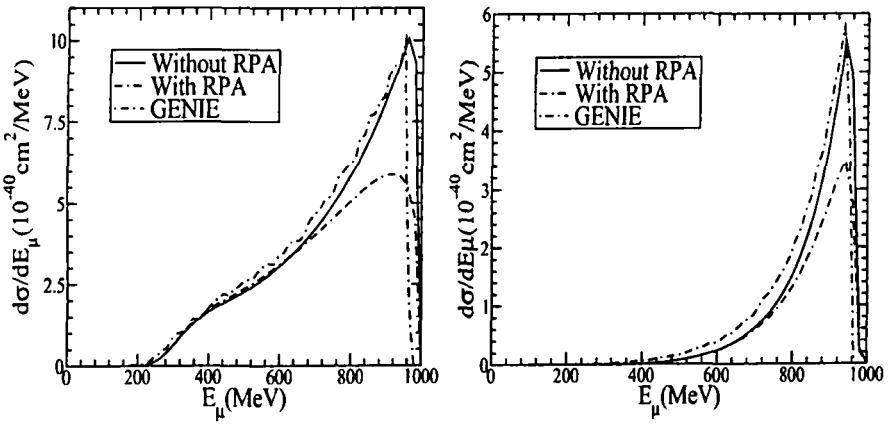

Figure 2.8: $d\sigma/dE_\mu$ vs E_μ for CCQE process in $\nu_\mu - ^{56}Fe$ reaction(left-panel) and in $\bar{\nu}_\mu - ^{56}Fe$ reaction(right-panel) at $E_\nu = 1$GeV.

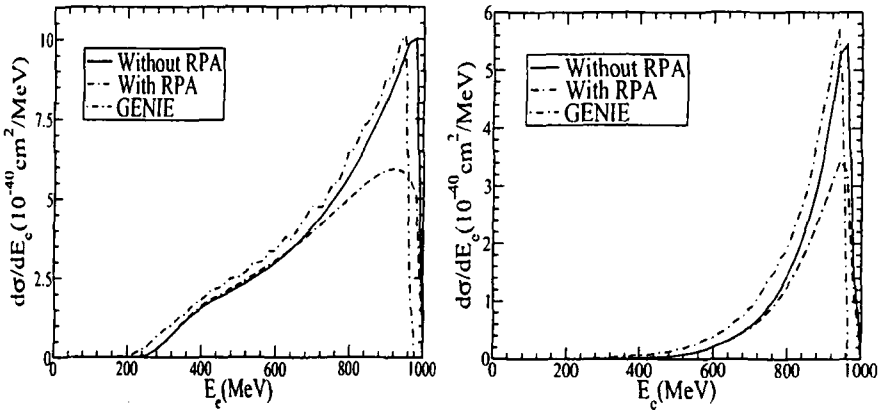

Figure 2.9: $d\sigma/dE_e$ vs E_e for CCQE process in $\nu_e - {}^{56}Fe$ reaction(left-panel) and in $\bar{\nu}_e - {}^{56}Fe$ reaction(right-panel) at E_ν = 1GeV.

this figure we have also shown the Q^2 distribution for $\bar{\nu}_\mu$ induced process at E_ν = 1 GeV. With the inclusion of RPA the reduction is 35% at Q^2 = 0.068 GeV^2(peak value), 30% at Q^2 = 0.02 GeV^2 and 23% at Q^2 = 0.5 GeV^2 as compared to the results obtained by using GENIE Monte Carlo code [16]. Similarly, we do this for ν_e and $\bar{\nu}_e$ induced processes and the reduction is 29% at Q^2 = 0.03 GeV^2, 38% at Q^2 = 0.12 GeV^2 and 4% at Q^2 = 0.5 GeV^2 for the first one and 28% at Q^2 = 0.02 GeV^2, 34% at Q^2 = 0.065 GeV^2 and 14% at Q^2 = 0.5 GeV^2 for the later and the results are shown in Fig.-2.7.

In Fig.-2.8, we have shown the lepton energy(E_l) distribution of CCQE lepton production process for neutrino(left panel) and antineutrino(right panel) respectively. The difference in the results of lepton energy(E_l) distribution obtained by using Llewellyn Smith Fermi gas model in GENIE Monte Carlo code [16] and from local Fermi gas model [23] with RPA effect is 44% for ν_μ at E_l =960 MeV(peak value) and 4% at E_l = 700 MeV and for $\bar{\nu}_\mu$ this difference is around 40% at E_l =940 MeV and 28% at E_l =700 MeV. While for ν_e and $\bar{\nu}_e$(Fig.-2.9) this difference is 42% at E_l = 940 MeV(peak value), 20% at E_l =700 MeV and 42% E_l = 937 MeV(peak value), 34% at E_l =700 MeV, respectively.

2.4.2 Total Scattering Cross Section

For the charged current quasielastic $\nu_\mu(\bar{\nu}_\mu)$ induced lepton production process in ^{56}Fe the results are shown in Fig.-2.10 calculated using the local Fermi gas model [23] and by using the GENIE Monte Carlo code [16]. We find that the results obtained by GENIE Monte Carlo [16] and by local Fermi gas model without RPA are in good agreement. When we include random phase approximation in local Fermi gas model [23] then there is a further

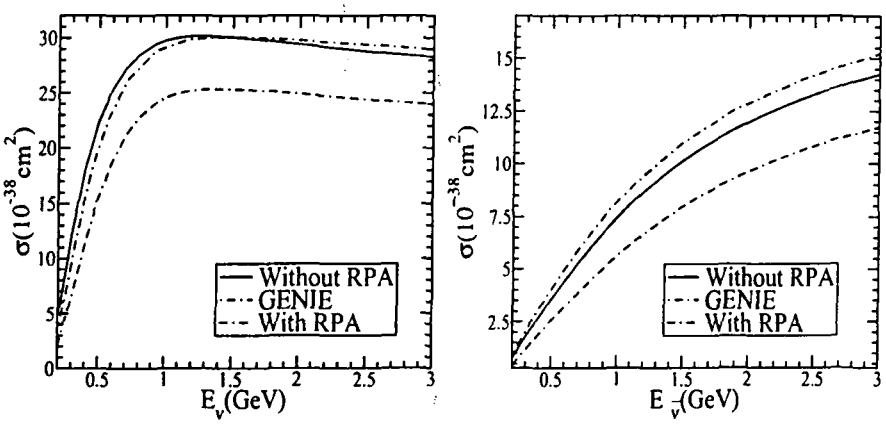

Figure 2.10: σ vs E_ν for CCQE ν_μ induced reaction(left-panel) in ^{56}Fe and for CCQE $\bar{\nu}_\mu$ induced reaction(right-panel) in ^{56}Fe.

reduction of around 17% at E_ν = 1.0 GeV and 15% at E_ν = 3.0 GeV for ν_μ and in the case of antineutrino ($\bar{\nu}_\mu$) induced lepton production process reduction is around 31% at E_ν =1.0 GeV and 23% at E_ν =3.0 GeV.

Similar calculations have been done for electron type neutrino (ν_e) and antineutrino ($\bar{\nu}_e$) induced lepton production processes and the results are shown in Fig.-2.11. The results obtained by using GENIE Monte Carlo [16] is shown by dashed-dotted line and the results obtained from local Fermi gas model [23] with RPA effect is shown by double dashed-dotted line. The reduction in the cross section for $\nu_e/\bar{\nu}_e$ induced processes is same as in the case of $\nu_\mu/\bar{\nu}_\mu$ while including RPA effects.

We have also obtained the results for ν_l and $\bar{\nu}_l$ induced charged current quasielastic process on free nucleon target. From the Fig.-2.12 it is clear that the results obtained by using GENIE Monte Carlo [16] and from the local Fermi gas model [23] without random phase approximation are in good agreement.

In Fig.-2.13, we have presented the results for the total cross section σ for neutral current elastic scattering process induced by ν_μ and $\bar{\nu}_\mu$ in free proton obtained from the GENIE Monte Carlo code [16] and local Fermi gas model [23], which are in good agreement. For neutral current elastic scattering process, BBBA2005 parametrization [42] is used in GENIE Monte Carlo code [16] as well as in local Fermi gas model [23] and the expressions for vector and axial form factors given in Eq.(2.28), Eq.(2.30) and Eq.(2.31) are used.

In Fig.-2.14, the results of total scattering cross section are also shown for $\nu/\bar{\nu}$ induced neutral current elastic scattering processes in ^{56}Fe with and without random phase approximation. When we include RPA effect there is a further reduction of 30% at E_ν=1.5 GeV in the cross section for $\nu_\mu p \rightarrow \nu_\mu p$ inside ^{56}Fe calculated by using the model de-

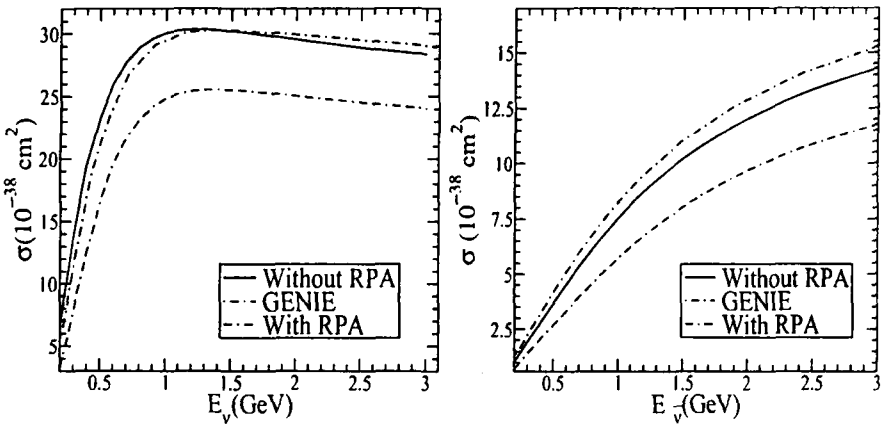

Figure 2.11: σ vs E_ν for CCQE ν_e induced reaction(left-panel) in ^{56}Fe and for CCQE $\bar{\nu}_e$ induced reaction(right-panel) in ^{56}Fe.

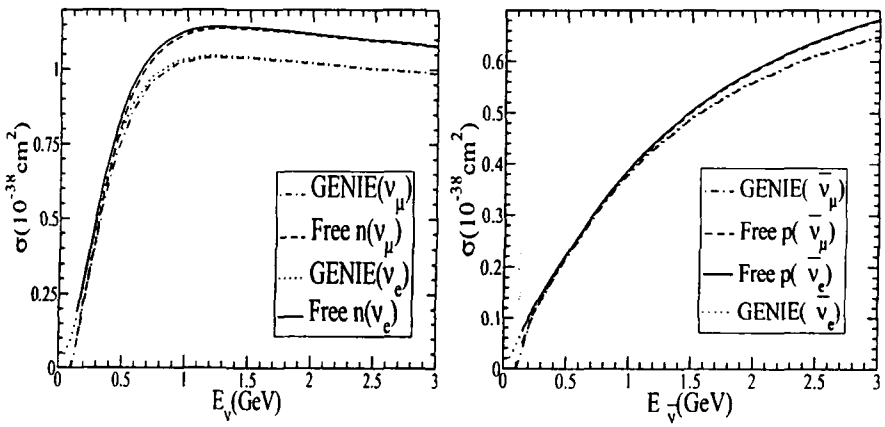

Figure 2.12: σ vs E_ν for CCQE ν_l induced reaction(left-panel) on free neutron and for CCQE $\bar{\nu}_l$ induced reaction(right-panel) on free proton.

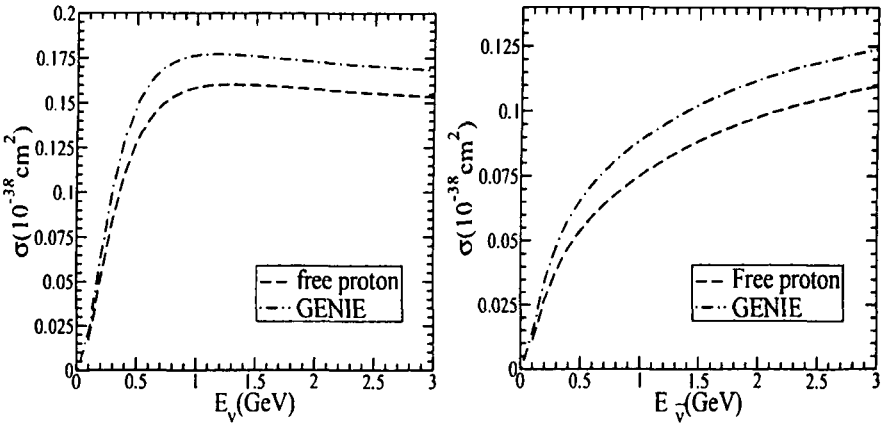

Figure 2.13: σ vs E_ν for ν_μ induced NC elastic reaction(left-panel) and for $\bar{\nu}_\mu$ induced NC elastic reaction(right-panel) in free proton.

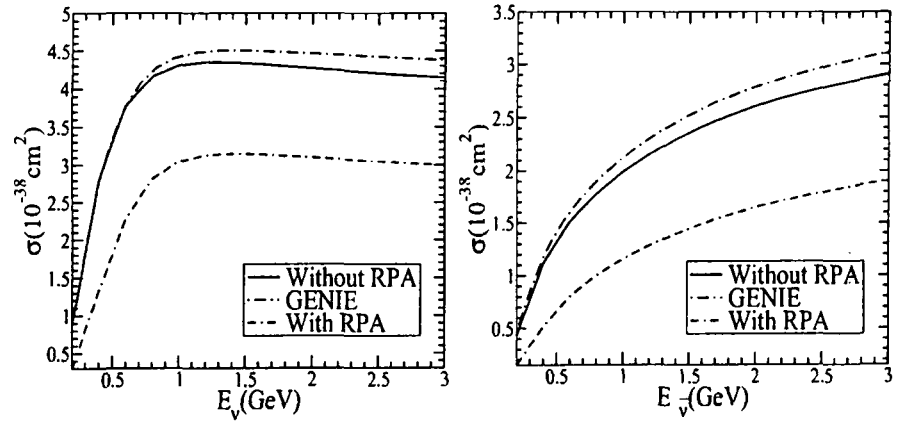

Figure 2.14: σ vs E_ν for ν_μ induced NC elastic reaction(left-panel) and for $\bar{\nu}_\mu$ induced NC elastic reaction(right-panel) for p in ^{56}Fe.

scribed by Ahrens et al. [49] incorporated in GENIE Monte Carlo code [16] and from the local Fermi gas model [23].

In this study we observe that by considering nucleon correlations using random phase approximation, scattering cross section gets suppressed and this reduction in the cross section is significant, therefore, nuclear correlations should be taken into account in the Monte Carlo generators.

Chapter 3

Inelastic Pion Production

3.1 Introduction

In this chapter, we present the scattering of neutrino/antineutrino induced processes from a free nucleon or a nucleon bound inside a nucleus, where a pion is produced. In the intermediate energy region for the neutrino induced single pion production process the pions are produced through Born diagrams(Fig.-3.1) as well as through resonant channels where a Δ or N^* is produced, and which decays to a pion and a nucleon. If the energy of the neutrino is high then two pions or multi pions may also get produced. In the energy region of MiniBooNE, T2K, and the atmospheric neutrino experiments, it is the one pion production which is the most dominant one among the several possible inelastic reactions. It has been theoretically estimated that the maximum contribution to the one pion production comes from the Δ resonance channel. The neutrino and antineutrino induced channels for the charged current induced single pion production on free nucleons where Δ is in the intermediate state, are:

$$\begin{aligned} &\nu_l\, p \to l^-\, \Delta^{++} \to l^-\, p\, \pi^+, \quad \bar{\nu}_l\, p \to l^+\, \Delta^0 \to l^+\, p\, \pi^- \\ &\nu_l\, n \to l^-\, \Delta^{+} \to l^-\, n\, \pi^+, \quad \bar{\nu}_l\, p \to l^+\, \Delta^0 \to l^+\, n\, \pi^0 \\ &\nu_l\, n \to l^-\, \Delta^{+} \to l^-\, p\, \pi^0, \quad \bar{\nu}_l\, n \to l^+\, \Delta^- \to l^+\, n\, \pi^- \end{aligned} \tag{3.1}$$

Similarly, the different channels for producing pions in the neutral current $\nu/\bar{\nu}$ induced reactions on free nucleons are:

$$\begin{aligned} &\nu_l\, p \to \nu_l\, \Delta^{+} \to \nu_l\, p\, \pi^0, \quad \bar{\nu}_l\, p \to \bar{\nu}_l\, \Delta^{+} \to \bar{\nu}_l\, p\, \pi^0 \\ &\nu_l\, p \to \nu_l\, \Delta^{+} \to \nu_l\, n\, \pi^+, \quad \bar{\nu}_l\, p \to \bar{\nu}_l\, \Delta^{+} \to \bar{\nu}_l\, n\, \pi^+ \\ &\nu_l\, n \to \nu_l\, \Delta^{0} \to \nu_l\, n\, \pi^0, \quad \bar{\nu}_l\, n \to \bar{\nu}_l\, \Delta^{0} \to \bar{\nu}_l\, n\, \pi^0 \\ &\nu_l\, n \to \nu_l\, \Delta^{0} \to \nu_l\, p\, \pi^-, \quad \bar{\nu}_l\, n \to \bar{\nu}_l\, \Delta^{0} \to \bar{\nu}_l\, p\, \pi^-, \end{aligned} \tag{3.2}$$

where l= e, μ, τ. When the neutrino/antineutrino scattering with the nucleons bound inside the nucleus takes place, there are two possible processes, known as incoherent and

coherent pion production processes. In the case of incoherent process the nucleus goes into the excited state and may change its identity. In the case of coherent pion production process, the nucleus remains in the ground state and all the energy transferred to the nucleus is taken by the outgoing pion. During these processes inside the nucleus the outgoing pion may interact with the spectator nucleons sitting inside the nucleus and may get rescattered or absorbed while coming out of the nucleus. In subsection 3.2.1, we describe the effective Lagrangians for hadronic interactions contributing to the weak processes and then we write the matrix element for single pion production from free nucleons for different resonant and non-resonant channels. In the intermediate energy region of about 1 GeV, the dominant contribution to the single pion production process from nucleons comes from the Δ resonance due to very strong P wave pion nucleon coupling leading to Δ-resonance and higher resonances has sufficiently small contribution. That is why, in the resonant production of pions we emphasize only on Δ resonance. The Δ resonance produced inside the nuclear medium can decay either through $\Delta N \rightarrow NN\pi$ or non-mesonic decay through $\Delta N \rightarrow NN$, which is not possible in the case of free nucleons. It has been found that the propagation of Δ in the nuclear medium affects the propagation of pions through the nucleus as well as modifies the transition amplitude.

The neutrino induced weak pion production processes from nucleons and nuclei at intermediate energies are important in order to understand the hadronic structure. The pion production processes are useful to determine the nucleon form factors, pion dynamics in the nuclear matter and to calculate the coupling strength of pion to the nucleon. The weak pion production along with the electro-pion production from nucleon in the delta resonance region is used to determine the electroweak N-Δ transition form factors.

3.2 Incoherent Scattering

Incoherent pion production processes may be represented by the following reactions:

$$\begin{aligned} \nu_l + A &\rightarrow l^- + \pi + A' \\ \bar{\nu}_l + A &\rightarrow l^+ + \pi + A' \\ \nu_l + A &\rightarrow \nu_l + \pi + A' \\ \bar{\nu}_l + A &\rightarrow \bar{\nu}_l + \pi + A', \end{aligned} \tag{3.3}$$

where l =e, μ , τ, A and A' are initial and final nuclei. Here A' may be different from A depending upon the charge of pion. This process can be easily understood with the help of Feynman diagrams, that are shown in Fig.-3.1.

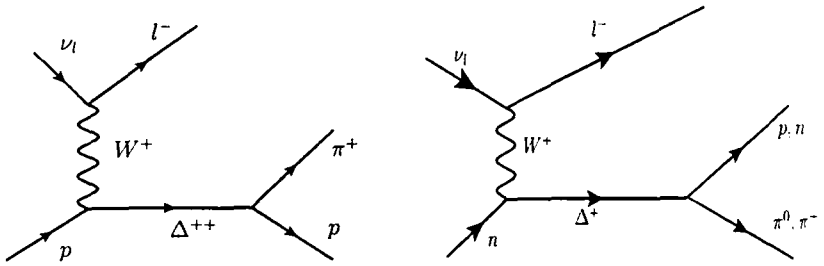

Figure 3.1: Feynman diagram corresponding to the charged current single pion production from a nucleon target.

3.2.1 Formalism

In section we write the effective Lagrangians for different hadronic interactions of charged and neutral current induced processes mediated by the $W^{\pm}$ and Z^0 intermediate vector bosons.

Charged Current Interaction

The Lagrangians for various charged current processes are written as ([55], [56]):

$$\mathcal{L}_{\pi NN} = \frac{f_{\pi NN}}{m_\pi}\ \bar{\Psi}\gamma_\mu\gamma_5\tau\Psi.\partial^\mu\Phi_\pi \tag{3.4}$$

$$\mathcal{L}_{\pi N\Delta} = i\ \frac{f_{\pi N\Delta}}{m_\pi}\ \bar{\Psi}^\mu_\Delta(\partial_\mu\Phi_\pi)\mathbf{T}\Psi\ +\ \text{hermitian conjugate} \tag{3.5}$$

$$\mathcal{L}^V_{WNN} = \frac{g}{2\sqrt{2}}\ \bar{\Psi}\left[F_1^V\gamma_\mu W^\mu + F_2^V\frac{\sigma_{\mu\nu}}{2M}\partial^\nu W^\mu\right]\frac{\tau_3}{2}\Phi \tag{3.6}$$

$$\mathcal{L}^A_{WNN} = -\frac{g}{2\sqrt{2}}\ \bar{\Psi}\left[F_A^V\gamma_\mu W^\mu + i\frac{F_P^V}{2M}\partial_\mu W^\mu\right]\frac{\tau_3}{2}\gamma_5\Psi \tag{3.7}$$

$$\mathcal{L}^V_{WNN\pi} = \frac{g}{2\sqrt{2}}\ \frac{f_{\pi NN}}{m_\pi}\ \bar{\Psi}\ \left(\vec{\tau}\times\vec{\phi}_\pi\right)_3\gamma_\mu\gamma_5\Psi\ W^\mu\ F_\pi(Q^2) \tag{3.8}$$

$$\begin{aligned}\mathcal{L}^A_{WNN\pi} \ =\ & \frac{g}{2\sqrt{2}}\ \frac{f_{\pi NN}}{m_\pi}\ \bar{\Psi}\left(\vec{\tau}\times\vec{\phi}_\pi\right)_3 \\ & \left[F_1^V\gamma_\mu + F_2^V\frac{\sigma_{\mu\nu}}{2M}\partial^\nu\right]\Psi\ W^\mu\ F_\pi(Q^2)\end{aligned} \tag{3.9}$$

$$\mathcal{L}^V_{W\pi\pi} = \frac{g}{2\sqrt{2}}\ \left\{\vec{\phi}_\pi\times\left(\partial_\mu\vec{\phi}_\pi\right)\right\}_3\ W^\mu\ F_\pi(Q^2) \tag{3.10}$$

Neutral Current Interaction

The Lagrangian for the neutral current(NC) induced single pion production processes are written as ([56], [57])

$$\begin{aligned}\mathcal{L}^V_{ZNN} &= \bar{\Psi}\frac{1}{2}\left[\left(\xi_V^{I=0}F_1^S + \xi_V^{I=1}\tau_3 F_1^V\right)\gamma_\mu + \left(\xi_V^{I=0}\kappa_s F_2^S + \xi_V^{I=1}\kappa_v\tau_3 F_2^V\right)\right. \\ &\times \left.\frac{\sigma_{\mu\nu}}{2M}\partial^\nu\right] Z^\mu\Psi \qquad (3.11)\end{aligned}$$

$$\mathcal{L}^V_{Z\pi\pi} = \xi_V^{I=1}\left\{\vec{\phi}_\pi \times \left(\partial_\mu\vec{\phi}_\pi\right)\right\}_3 Z^\mu\, F_\pi(Q^2) \qquad (3.12)$$

$$\mathcal{L}^V_{ZNN\pi} = \frac{f_{\pi NN}}{m_\pi}\times\xi_V^{I=1}\bar{\Psi}\left(\vec{\tau}\times\vec{\phi}_\pi\right)_3\gamma_\mu\gamma_5\Psi Z^\mu\, F_\pi(Q^2) \qquad (3.13)$$

$$\begin{aligned}\mathcal{L}^A_{ZNN} &= \bar{\Psi}\frac{1}{2}\left[\left(\xi_A^{I=0}F_A^S + \xi_A^{I=1}\tau_3 F_A^V\right)\gamma_\mu + \left(\xi_A^{I=0}F_P^S + \xi_A^{I=1}\tau_3 F_P^V\right)\right. \\ &\times \left.\frac{i\partial_\mu}{2M}\right] Z^\mu\Psi \\ &= \bar{\Psi}\left[F_A^V(Q^2)\gamma_\mu + F_P^V\frac{i\partial_\mu}{2M}\right]\frac{\tau_3}{2}Z^\mu\Psi\,\xi_A^{I=1} \qquad (3.14)\end{aligned}$$

$$\begin{aligned}\mathcal{L}^A_{ZNN\pi} &= \frac{f_{\pi NN}}{m_\pi}\times\xi_A^{I=1}\,\bar{\Psi}\left(\vec{\tau}\times\vec{\phi}_\pi\right)_3\left[F_1^V\gamma_\mu W^\mu\right. \\ &- \left.\kappa_v F_2^V\frac{\sigma_{\mu\nu}}{2M}\partial^\nu Z^\mu\right]\Psi\, F_\pi(Q^2)\,, \qquad (3.15)\end{aligned}$$

where $\kappa_{(s,v)} = (\kappa_p \pm \kappa_n)$ and g is the coupling constants for the weak-isospin group SU(2). The form factors F_1, F_2, F_π, F_A and F_p are the functions of four momentum transfer square($Q^2 = -q^2$). In the standard model (SM) of particle physics, the isospin factors $\xi_{V,A}^{I=0,1}$ are written as [56]:

$$\begin{aligned}\xi_V^{I=1} &= \frac{1}{2\sin\theta_W\cos\theta_W}\,(1-2\sin^2\theta_W), \\ \xi_V^{I=0} &= -\frac{1}{2\sin\theta_W\cos\theta_W}\,2\sin^2\theta_W, \\ \xi_A^{I=1} &= -\frac{1}{2\sin\theta_W\cos\theta_W}, \\ \xi_A^{I=0} &= 0, \qquad (3.16)\end{aligned}$$

where θ_W is the Weinberg angle.

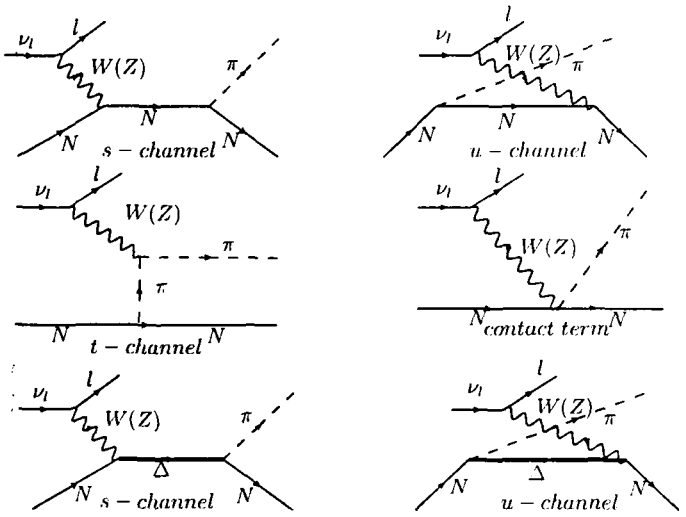

Figure 3.2: Feynman diagrams considered for weak pion production.

Matrix Element

The Lagrangian for the charged current neutrino induced incoherent processes is written as

$$\mathcal{L}_{int}^{weak} = -\frac{g}{2\sqrt{2}} J_\mu^{CC}(x)\, W_\mu^\dagger(x) + \text{hermitian conjugate}, \tag{3.17}$$

where $J_\mu^{CC}(x)$ is the charged current for weak interaction which couples to the intermediate W-boson fields $W_\mu^\pm$. The weak current $J_\mu^{CC}(x)$ contains leptonic as well as hadronic part which is given by

$$J_\mu^{CC}(x) = l_\mu(x) + J_\mu(x), \tag{3.18}$$

$l_\mu(x)$ is the leptonic current given by

$$l_\mu(x) = \bar{\psi}_l(k')\gamma_\mu(1-\gamma^5)\psi_{\nu_l}(k) \tag{3.19}$$

and $J_\mu(x) = \cos\theta_C\ (J_\mu^V(x) + J_\mu^A(x))$ is the hadronic current which is written in terms of vector and axial vector parts and θ_C is the Cabibbo angle. At low momentum transfer ($q^2 << M_W^2$) for neutrino induced charged current processes the invariant matrix element is given by

$$\mathcal{M} = \frac{G_F}{\sqrt{2}} J^{\mu\dagger}(x)\, l_\mu(x) + \text{hermitian conjugate}, \tag{3.20}$$

where G_F(=1.16639 $\times 10^{-5}$ GeV^{-2}) is the Fermi coupling constant, M_W is the mass of W-boson, and G_F is related to the W-boson mass by the relation $g^2/8\ M_W^2 = G_F/\sqrt{2}$.

Generally, for hadronic current the matrix element is calculated by using the nucleon and meson exchanges and the resonance excitation diagrams. In the intermediate energy region, for single pion production maximum contribution to the cross section comes from the Δ resonance. In the following subsections we write down the interaction Lagrangian for charged and neutral current interactions for nonresonant and resonance terms corresponding to the processes given in Eqs. 3.1 and 3.2. Feynman diagrams corresponding to these processes is shown in Fig.-3.2

Non-Resonant Terms

Here we write the matrix element for the charged current processes shown in Feynman diagram(Fig.-3.2) for various Born terms like nucleon direct(s), crossed(u), pion pole(t) and contact term [55], [56]

$$\begin{aligned}
\mathcal{M}_s^N &= \frac{f_{\pi NN}}{m_\pi}\frac{G_F}{\sqrt{2}}\cos\theta_C\ \bar{u}(\vec{p'})\gamma_5\ \not{k}_\pi \left(\frac{\not{p}+\not{q}+M}{s-M^2}\right)\times \\
&\left[\left(F_1^V(Q^2)\gamma_\mu + \frac{F_2^V(Q^2)}{2M}\sigma_{\mu\nu}\partial^\nu\right)\right. \\
&\left. -\left(F_A^V(Q^2)\gamma_\mu + i\frac{F_P^V(Q^2)}{2M}\partial_\mu\right)\right]\ u(\vec{p})\ l^\mu
\end{aligned}$$

$$\begin{aligned}
\mathcal{M}_u^N &= \frac{f_{\pi NN}}{m_\pi}\frac{G_F}{\sqrt{2}}\cos\theta_C\ \bar{u}(\vec{p'})\left[\left(F_1^V(Q^2)\gamma_\mu + \frac{F_2^V(Q^2)}{2M}\sigma_{\mu\nu}\partial^\nu\right)\right. \\
&\left. -\left(F_A^V(Q^2)\gamma_\mu + i\frac{F_P^V(Q^2)}{2M}\partial_\mu\right)\right]\times \\
&\left(\frac{\not{p}-\not{k}_\pi+M}{u-M^2}\right)\gamma_5\ \not{k}_\pi\ u(\vec{p})\ l^\mu
\end{aligned}$$

$$\begin{aligned}
\mathcal{M}_t^\pi &= \frac{f_{\pi NN}}{m_\pi}\frac{G_F}{\sqrt{2}}\cos\theta_C\ 2MF_\pi(Q^2)\left(\frac{2k_\pi - q}{t-m_\pi^2}\right)\times \\
&\left[\bar{u}(\vec{p'})\gamma_5 u(\vec{p})\right]\ l^\mu
\end{aligned}$$

$$\begin{aligned}
\mathcal{M}_c &= \frac{f_{\pi NN}}{m_\pi}\frac{G_F}{\sqrt{2}}\cos\theta_C\ \bar{u}(\vec{p'})\left[F_\pi(Q^2)\gamma_\mu\gamma_5\right. \\
&\left. -\left(F_1^V(Q^2)\gamma_\mu + i\frac{F_2^V(Q^2)}{2M}\sigma_{\mu\nu}\partial^\nu\right)\right]\ u(\vec{p})\ l^\mu
\end{aligned} \tag{3.21}$$

For neutral current processes corresponding to the Feynman diagrams(Fig.-3.2), the matrix element for nucleon nucleon direct(s), crossed(u), pion pole(t) and contact(c) term is written as ([56], [57])

$$\begin{aligned}
\mathcal{M}_s^N &= \frac{f_{\pi NN}}{m_\pi}\frac{G_F}{\sqrt{2}}\,\bar{u}(\vec{p'})\,\gamma_5\,\not{k}_\pi\left(\frac{\not{p}+\not{q}+M}{s-M^2}\right)\times \\
&\quad \left[\xi_V^{I=1}\left(I_s^D\gamma_\mu + iI_s^P\frac{\sigma_{\mu\nu}}{2M}q^\nu\right)+\xi_A^{I=1}\left(I_s^A\gamma_\mu - I_s^I\frac{q_\mu}{2M}\right)\right]\,u(\vec{p})\,l^\mu \\
\mathcal{M}_u^N &= \frac{f_{\pi NN}}{m_\pi}\frac{G_F}{\sqrt{2}}\,\bar{u}(\vec{p'})\,\left[\xi_V^{I=1}\left(I_s^D\gamma_\mu + iI_s^P\frac{\sigma_{\mu\nu}}{2M}q^\nu\right)\right. \\
&\quad \left.+\xi_A^{I=1}\left(I_s^A\gamma_\mu - I_s^I\frac{q_\mu}{2M}\right)\right]\gamma_5\,\not{k}_\pi\left(\frac{\not{p}+\not{q}+M}{s-M^2}\right)\,u(\vec{p})\,l'' \\
\mathcal{M}_t^\pi &= \frac{f_{\pi NN}}{m_\pi}\frac{G_F}{\sqrt{2}}\,\xi_V^{I=1}\,2MI_tF_\pi(Q^2)\left(\frac{2k_\pi - q}{t-m_\pi^2}\right)\left[\bar{u}(\vec{p'})\gamma_5 u(\vec{p})\right]l^\mu \\
\mathcal{M}_c &= \frac{f_{\pi NN}}{m_\pi}\frac{G_F}{\sqrt{2}}\,I_t\,\bar{u}(\vec{p'})\,\left[\xi_V^{I=1}F_\pi(Q^2)\gamma_\mu\gamma_5\right. \\
&\quad \left.-\xi_A^{I=1}\left(F_1^V\gamma_\mu + i\frac{F_2^V}{2M}\sigma_{\mu\nu}q^\nu\right)\right]\,u(\vec{p})\,l^\mu,
\end{aligned} \tag{3.22}$$

where expressions for the isospin matrix elements used in the above equation are given by [56]

$$\begin{aligned}
I_{(s,u)}^D &= \frac{1}{2}\left[\frac{\xi_V^{I=0}}{\xi_V^{I=1}}F_1^SI^0 + F_1^V(I^+ \pm I^-)\right], \\
I_{(s,u)}^P &= \frac{1}{2}\left[\frac{\xi_V^{I=0}}{\xi_V^{I=1}}F_2^SI^0 + F_2^V(I^+ \pm I^-)\right], \\
I_{(s,u)}^A &= \frac{1}{2}\left[\frac{\xi_A^{I=0}}{\xi_A^{I=1}}F_A^SI^0 + F_A^V(I^+ \pm I^-)\right], \\
I_{(s,u)}^I &= \frac{1}{2}\left[\frac{\xi_A^{I=0}}{\xi_A^{I=1}}F_P^SI^0 + F_P^V(I^+ \pm I^-)\right], \\
I_t &= I^-
\end{aligned} \tag{3.23}$$

with

$$I^0 = \chi_f^\dagger\tau_\pi\chi_i, \quad I^+ = \chi_f^\dagger\frac{1}{2}\{\tau_\pi,\tau_3\}\,\chi_i, \quad I^- = \chi_f^\dagger\frac{1}{2}[\tau_\pi,\tau_3]\,\chi_i, \tag{3.24}$$

where $\chi_i(\chi_f)$ is the initial(final) nucleon isospin function and τ_3 is the Pauli isospin matrix.

Resonant Terms

For the incoherent one pion production processes in the intermediate energy region, excitation of low mass resonances contributes to the cross section. The $\Delta(1232)$ resonance

has the dominant contribution to the cross section as well as in some channels isospin 1/2 resonance also have a non-negligible contribution. The $\Delta(1232)$ resonance has been observed in the pion-nucleon scattering. The Aligarh group [25] has performed the calculations for the one pion production processes in the Δ dominance model. They used the standard Rarita-Schwinger formalism [22], [55], [58], [59], [60], [61] for the charged current neutrino-nucleon Δ production processes. The basic reactions for the charged current neutrino-nucelon Δ production are given by

$$\nu_l(k) + p(p) \rightarrow l^-(k') + \Delta^{++}(P) \tag{3.25}$$

$$\nu_l(k) + n(p) \rightarrow l^-(k') + \Delta^{+}(P) \tag{3.26}$$

The matrix element for Δ production process given in Eq.(3.25) is written as

$$\langle l^- \ \Delta^{++}|\mathcal{M}|\nu_l \ p\rangle = \frac{G_F}{\sqrt{2}} \cos\theta_C \ l_\mu \ \langle \Delta^{++}|V^\mu - A^\mu|p\rangle, \tag{3.27}$$

where l_μ is the invariant matrix element of the weak leptonic current given by Eq.(3.19). The matrix elements $\langle \Delta^{++}|V^\mu|p\rangle$ corresponds to the N-Δ transition matrix elements of the vector V^μ transition hadronic current and $\langle \Delta^{++}|A^\mu|p\rangle$ corresponds axial vector A^μ transition hadronic current between N and Δ states for the charged current interaction. From the conservation of vector current(CVC) we know that the matrix elements of the weak hadronic vector current are related by isospin Clebsch-Gordon coefficients to the matrix elements of the isospin I=1 electromagnetic current measured in electroproduction of pions. The isospin I=0 component of the electromagnetic current has no contribution in the electroproduction of the Δ resonance, therefore, relationship becomes simply [11], [58], [62]

$$\langle \ \Delta^{++} \ | \ V^\alpha \ | \ p \ \rangle = \sqrt{3} \ \langle \ \Delta^{+} \ | \ V^\alpha_{em} \ | \ p \ \rangle \tag{3.28}$$

For the neutrino-proton induced Δ^{++} production process the matrix element of the hadronic transition currents in the s-channel is written as ([11], [22], [27], [31], [55], [57], [58], [60], [61], [63]-[66]):

$$\langle \Delta^{++}|V^\mu|p\rangle = \sqrt{3}\bar{\psi}_\alpha(P) \left[\left(\frac{C_3^V(q^2)}{M}(g^{\alpha\mu} \not{q} - q^\alpha \gamma^\mu) + \frac{C_4^V(q^2)}{M^2}(g^{\alpha\mu} q\cdot P - q^\alpha P^\mu) + \frac{C_5^V(q^2)}{M^2}(g^{\alpha\mu} q\cdot p - q^\alpha p^\mu) + \frac{C_6^V(q^2)}{M^2} q^\alpha q^\mu \right) \gamma_5 \right] u(p), \tag{3.29}$$

and

$$\langle \Delta^{++}|A^\mu|p\rangle = \sqrt{3}\bar{\psi}_\alpha(P) \left[\left(\frac{C_3^A(q^2)}{M}(g^{\alpha\mu} \not{q} - q^\alpha \gamma^\mu) + \frac{C_4^A(q^2)}{M^2} \times (g^{\alpha\mu} q\cdot P - q^\alpha P^\mu) + C_5^A(q^2) g^{\alpha\mu} + \frac{C_6^A(q^2)}{M^2} q^\alpha q^\mu \right) \right] u(p), \tag{3.30}$$

where $\psi_\alpha(P)$ is the Rarita-Schwinger spinor for the Δ resonance of momentum P and $u(p)$ is the Dirac spinor for the nucleon of momentum p, $q(= P - p = k - k')$ is the momentum transfer and M is the nucleon mass. $C_i^V(i = 3 - 6)$, $C_i^A(i = 3 - 6)$ are respectively the vector and axial vector transition form factors. The factor of $\sqrt{3}$ in the matrix element is according to the relation in Eq.(3.28). The conservation of vector current hypothesis in momentum space implies that $C_6^V(q^2) = 0$ and the other three vector form factors are given in terms of isovector electromagnetic form factors in the p-Δ^+ electromagnetic transition. The vector transition from factors $C_i^V(i = 3, 4, 5)$ are determined from the analysis of photo-production and electro-production data of Δ resonance, and it is done in terms of the multipole amplitudes.

In the case of axial vector form factors, using partially conserved axial current(PCAC) hypothesis, matrix element given in Eq.(3.30) may be written as

$$\begin{aligned}\langle \Delta^{++}|i\partial_\mu A^\mu|p\rangle &= \sqrt{3}\bar{\Psi}_\alpha(P)q_\mu\left(C_5^A(q^2)g^{\alpha\mu} + \frac{C_6^A(q^2)}{M^2}q^\alpha q^\mu\right)u(p) \\ &= \sqrt{3}\bar{\Psi}_\alpha(P)q^\alpha\left(C_5^A(q^2) + \frac{C_6^A(q^2)}{M^2}q^2\right)u(p) \qquad (3.31)\end{aligned}$$

Pion pole dominance implies that the pseudoscalar form factor C_6^A must have a pion pole [58]:

$$C_6^A(q^2) \approx \frac{g_{\pi N\Delta} f_\pi}{2\sqrt{3}M}\frac{M^2}{m_\pi^2 - q^2}, \qquad (3.32)$$

where $g_{\pi N\Delta} = \frac{f_{\pi N\Delta}}{m_\pi} = 28.6$ is the coupling constant for $\Delta^{++} \to p\pi^+$ and $f_\pi = 0.97 m_\pi$ is the pion decay constant. Using Eq.(3.32) in Eq.(3.31), when $m_\pi = 0$, we find that this pole will give a non-vanishing contribution to the the matrix element of the divergence even for $q^2 \to 0$.

$$\langle \Delta^{++}|i\partial_\mu A^\mu|p\rangle \longrightarrow^{m_\pi=0.}_{q^2\to 0.} \sqrt{3}\,\bar{\psi}_\alpha(P)\,q^\alpha\left(C_5^A(0) - \frac{g_{\pi N\Delta} f_\pi}{2\sqrt{3}M}\right)u(p) \qquad (3.33)$$

Recently, the various parametrization for the N-Δ transition form factors has been discussed in literature [67]-[69]. For example, the parametrization given by Lalakulich et al. [68] for the N-Δ transition form factor is given by

$$C_i^V(Q^2) = C_i^V(0)\left(1 + \frac{Q^2}{M_V^2}\right)^{-2}\mathcal{D}_i \ , \quad i = 3, 4, 5. \qquad (3.34)$$

where

$$\begin{aligned}\mathcal{D}_i &= \left(1 + \frac{Q^2}{4M_V^2}\right)^{-1} \quad \text{for} \quad i = 3, 4 \quad \textit{and} \\ \mathcal{D}_i &= \left(1 + \frac{Q^2}{0.776M_V^2}\right)^{-1} \quad \text{for} \quad i = 5. \qquad (3.35)\end{aligned}$$

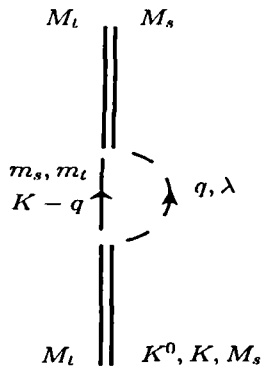

Figure 3.3: Diagrammatic representation of Δ self energy.

The axial vector form factors are parametrized as

$$C_i^A(Q^2) = C_i^A(0) \left(1 + \frac{Q^2}{M_A^2}\right)^{-2} \left(1 + \frac{Q^2}{3M_A^2}\right)^{-1}, \; i = 3, 4, 5 \tag{3.36}$$

where M_A is the axial vector dipole mass and m_π is the pion mass. The Δ decay width Γ is in general 120MeV. Here we have used a P-wave decay width which is given by [70, 71]:

$$\Gamma(W) = \frac{1}{6\pi} \left(\frac{f_{\pi N\Delta}}{m_\pi}\right)^2 \frac{M}{W} |\vec{q}_{cm}|^3 \tag{3.37}$$

where $|q_{cm}|$ is the pion momentum in the rest frame of the resonance given by

$$|\vec{q}_{cm}| = \frac{\sqrt{(W^2 - m_\pi^2 - M^2)^2 - 4m_\pi^2 M^2}}{2W},$$

where M is the nucleon mass and W is the center of mass energy. In the nuclear medium the properties of Δ gets modified like its mass M_Δ is modified by the real part of delta self energy and decay width Γ is modified by the imaginary part of delta self energy. These modifications in the Δ width Γ and mass M_Δ of the delta resonance are given by:

$$\frac{\tilde{\Gamma}}{2} \rightarrow \frac{\tilde{\Gamma}}{2} - Im\Sigma_\Delta \;\; and \;\; \tilde{M}_\Delta \rightarrow M_\Delta + Re\Sigma_\Delta. \tag{3.38}$$

The expressions for the real and the imaginary parts of self energy Σ_Δ which is shown in Fig.-3.3, are [70, 71]:

$$\begin{aligned} Re\Sigma_\Delta &= 40\frac{\rho}{\rho_0} MeV \;\; and \\ -Im\Sigma_\Delta &= C_Q \left(\frac{\rho}{\rho_0}\right)^\alpha + C_{A2} \left(\frac{\rho}{\rho_0}\right)^\beta + C_{A3} \left(\frac{\rho}{\rho_0}\right)^\gamma \end{aligned} \tag{3.39}$$

T_π(MeV)	C_Q(MeV)	C_{A2}(MeV)	C_{A3}(MeV)	α	β	γ
85	9.7	18.9	3.7	0.79	0.72	1.44
125	11.9	17.7	8.6	0.62	0.77	1.54
165	12.0	16.3	15.8	0.42	0.80	1.60
205	13.0	15.2	18.0	0.31	0.83	1.66
245	14.3	14.1	20.2	0.36	0.85	1.70
315	9.8	13.1	14.7	0.42	0.88	1.76

Table 3.1: Coefficients for the calculation of $Im\Sigma_\Delta$ as a function of the energy in the case of pion nuclear scattering.

In the Eq.(3.39), C_Q accounts for $\Delta N \rightarrow \pi NN$ process, C_{A2} for the two body absorption process $\Delta N \rightarrow NN$ and C_{A3} for the three body absorption process $\Delta NN \rightarrow NNN$. The coefficients C_Q, C_{A2}, C_{A3} and α, β and γ(Table-3.1) are taken from Refs. [70, 71]. In the nuclear medium Δ resonance decays through two and three body absorption processes like $\Delta N \rightarrow NN$ and $\Delta NN \rightarrow NNN$ through which Δ disappear in the nuclear medium without producing a pion. While a two body Δ absorption process like $\Delta N \rightarrow \pi NN$ gives rise to some more pions.

The expression for the total cross section for the neutrino induced charged current $1\pi^+$ production in the local density approximation [25] is given by

$$\begin{aligned}\sigma_A(E) &= \frac{1}{(4\pi)^5}\int_{r_{min}}^{r_{max}}(\rho_p(r)+\frac{1}{9}\rho_n(r))d\vec{r}\int_{Q^2_{min}}^{Q^2_{max}}dQ^2\int_{k'_{min}}^{k'_{max}}dk' \\ &\times\int_{-1}^{+1}dcos\theta_\pi\int_0^{2\pi}d\phi_\pi\frac{\pi|\vec{k}'||\vec{k}_\pi|}{ME_\nu^2E_l} \\ &\times\frac{1}{E'_p+E_\pi\left(1-\frac{|\vec{q}|}{|\vec{k}_\pi|}cos\theta_\pi\right)}\bar{\Sigma}\Sigma|\mathcal{M}_{fi}|^2 \end{aligned} \quad (3.40)$$

In Eq.(3.40), a factor of 1/9 comes with ρ_n in the production of π^+ from neutron target ($\nu_l + n \rightarrow l^- + \Delta^+ \rightarrow l^- + \pi^+ + n$) due to Clebsch-Gordan coefficients as compared to the π^+ production from proton target. While in case of $\bar{\nu}_l$ induced $1\pi^-$ production a factor of 1/9 comes with ρ_p i.e. π^- would get produced dominantly from the neutron target.

3.2.2 Results and Conclusions

GENIE Monte Carlo [16] uses Rein–Sehgal model [12] in the resonance region with $W_{cut} < 1.7GeV$ and includes 16 resonances that are tabulated in Table-3.2. The Rein-Sehgal model incorporates the quark model of Feynman-Kislinger-Ravndal(FKR) [72] of baryon resonances. The contribution from resonances are added incoherently. A small fraction

Resonances	M_R(GeV)	J	I	P	$W(GeV)$
$P_{33}(1232)$	1.232	3/2	3/2	+	0.120
$S_{11}(1535)$	1.535	1/2	1/2	-	0.150
$D_{13}(1520)$	1.520	3/2	1/2	-	0.120
$S_{11}(1650)$	1.650	1/2	1/2	-	0.150
$D_{13}(1700)$	1.700	3/2	1/2	-	0.100
$D_{15}(1675)$	1.675	5/2	1/2	-	0.150
$S_{31}(1620)$	1.620	1/2	3/2	-	0.150
$D_{33}(1700)$	1.700	3/2	3/2	-	0.300
$P_{11}(1440)$	1.440	1/2	1/2	+	0.350
$P_{13}(1720)$	1.720	1/2	1/2	+	0.150
$F_{15}(1680)$	1.680	5/2	1/2	+	0.130
$P_{31}(1910)$	1.910	1/2	3/2	+	0.250
$P_{33}(1920)$	1.920	3/2	3/2	+	0.200
$F_{35}(1905)$	1.905	5/2	3/2	+	0.350
$F_{37}(1950)$	1.950	7/2	3/2	+	0.300
$P_{11}(1710)$	1.710	1/2	1/2	+	0.100

Table 3.2: Properties of resonances that may contribute to the π production process in GENIE. Here M_R is Breit-Wigner mass, J is spin, I is isospin, P is parity and W is the Breit-Wigner decay width of the resonances.

of non-resonant background is also included incoherently in DIS cross-section. In GENIE Monte Carlo code [16] nuclear effects which are included are Fermi motion and Pauli blocking at the primary vertex and uses INTRANUKE for final state interaction(FSI) effects [16]. In the model developed by Aligarh group [25] the effect of Pauli blocking, Fermi motion of the nucleon and the renormalization of Δ properties in a nuclear medium are considered. The final state interaction(FSI) is also taken into account.

3.2.3 Differential Scattering Cross Section

In this section, we present the results of Q^2 distribution and pion energy distribution obtained by using Rein-Sehgal model in the GENIE Monte Carlo code [16] and the model developed by Aligarh group [25] for nucleons bound inside the nucleus.

In Fig.-3.4, we show the results of Q^2 distribution obtained by using GENIE Monte Carlo [16] without final state interaction (FSI) and from the model developed by Aligarh group [25] for free case i.e. without medium effect and we find that both the results are in good agreement. With the inclusion of random phase approximation in the case of Q^2 distribution at neutrino energy $E_\nu = 1$ GeV the reduction in the charged current

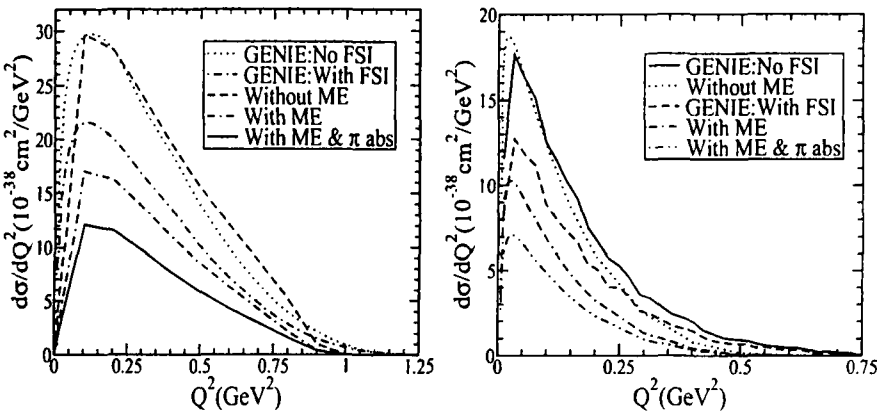

Figure 3.4: $d\sigma/dQ^2$ vs Q^2 for CC1π^+(left panel) production in $\nu_\mu - ^{56}Fe$ reaction and CC1π^-(right panel) production in $\bar{\nu}_\mu - ^{56}Fe$ reaction including all resonances .

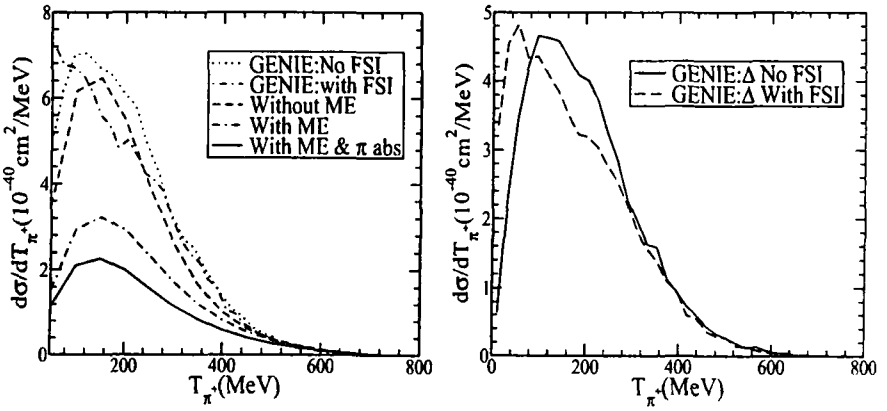

Figure 3.5: $d\sigma/dT_{\pi+}$ vs $T_{\pi+}$ for CC1π^+ production in $\nu_\mu - ^{56}Fe$ reaction including all resonances(left-panel) and only Δ resonance(right-panel) .

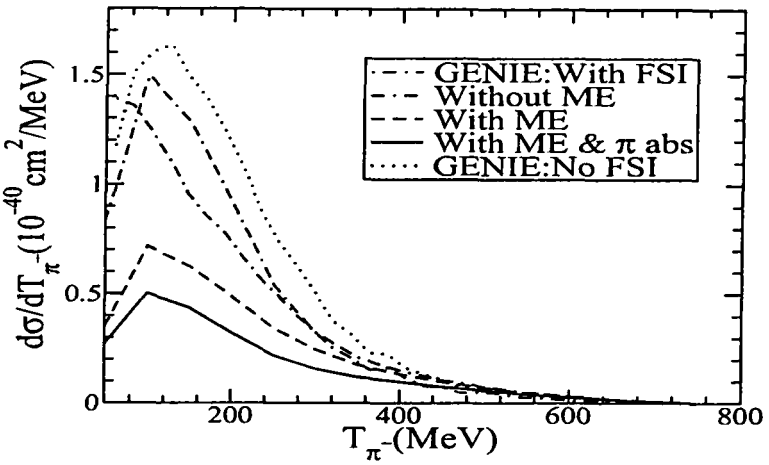

Figure 3.6: $d\sigma/dT_{\pi^-}$ vs T_{π^-} for $CC1\pi^-$ production in $\bar{\nu}_\mu - {}^{56}Fe$ reaction including all resonances.

differential scattering cross section for $\nu_\mu - {}^{56}$Fe is around 20% at $Q^2 = 0.120$ GeV^2 and 45% at $Q^2 = 0.5$ GeV^2 while for the reaction $\bar{\nu}_\mu - {}^{56}$Fe the reduction in the differential scattering cross section is 44% in the peak region at $Q^2 = 0.036$ GeV^2 and 46% at $Q^2 = 0.5$ GeV^2. Furthermore, when final state interaction effects are also taken into account, there is further reduction in the cross section which is around 28% at $Q^2 = 0.120$ GeV^2 and 31% at $Q^2 = 0.5$ GeV^2 for neutrino induced process and in the case of antineutrino the reduction in the cross section is 30% at $Q^2 = 0.036$ GeV^2 and 26% at $Q^2 = 0.5$ GeV^2, respectively.

In Fig.-3.5, the results are shown for the pion energy distribution for the charged current ν_μ and $\bar{\nu}_\mu$ induced π^+ and π^- production processes in ${}^{56}Fe$. Aligarh group [25] found the reduction in the distribution due to the medium effects to be about 52% at $T_{\pi^+} = 100$ MeV, 18% at $T_{\pi^+} = 400$ MeV, when the calculations are performed in the Δ dominance model. When final state interaction effects are also included, then the cross section further reduced around 29% at $T_{\pi^+} = 100$ MeV, 28% at $T_{\pi^+} = 400$ MeV. For antineutrino($\bar{\nu}_\mu$) induced π^- production process in ${}^{56}Fe$ the results are shown in Fig.-3.6, and the reduction in the distribution due to the medium effects is around 52% at $T_{\pi^-} = 100$ MeV and around 11% at $T_{\pi^-} = 400$ MeV and with final state interaction effects there is further reduction in the cross section ~30% at $T_{\pi^-} = 100$ MeV and around 27% at $T_{\pi^-} = 400$ MeV. In Fig.-3.5, we have also shown the results obtained by the GENIE Monte Carlo code [16] without final state interaction(FSI) has also been shown.

3.2.4 Total Scattering Cross Section

Here we study the behaviour of total scattering cross section for ν_l induced charged current single π^+ production and $\bar{\nu}_l$ induced charged current single π^- production using GENIE Monte Carlo code [16] and compare the obtained results with the model developed by Aligarh group [25]. The results of cross section obtained by using GENIE Monte Carlo code [16] without final state interaction and from the model developed by Aligarh group [25] without medium effects, shown in Fig.-3.7, are in good agreement.

For ν_μ induced single π^+ production in ^{56}Fe, the reduction in the total scattering cross section when calculated with Δ renormalization effects is about 48% at E_ν = 0.8 GeV, 42% at E_ν = 1.2 GeV and 35% at E_ν = 2.0 GeV, from the cross section calculated without the medium effects. When final state interaction effects are also taken into account there is further reduction in the cross section which is around 30% at E_ν = 0.8 GeV, 39% at E_ν = 1.2 GeV and 24% at E_ν = 2.0 GeV, respectively. It is clear from the Fig.-3.7 that in the case of incoherent pion production the reduction in the cross section due to the renormalization effects is larger than due to the final state interaction effects.

In Fig.-3.8, we have shown the results for $\bar{\nu}_\mu$ induced single π^- production and the reduction in the total scattering cross section when calculated with Δ renormalization effects is 48% at E_ν = 0.8 GeV, 42% at E_ν = 1.2 GeV and 34% at E_ν = 2.0 GeV, from the cross section calculated without medium effects and when the final state interaction effects are also included the cross section further get reduced around 30% at E_ν = 0.8 GeV, 28% at E_ν = 1.2 GeV and 23% at E_ν = 2.0 GeV, respectively. We have shown the contribution of Δ resonance in total scattering cross section for charged current single π^+ production in Fig.-3.7 and it may be seen that it has the most dominant contribution.

Similarly, we have shown the contribution of Δ resonance for charged current incoherent $\bar{\nu}_\mu$ induced single π^- production in ^{56}Fe obtained by using GENIE Monte Carlo code [16] and from the model developed by Aligarh group [25] in Fig.-3.8. Hence, it is clear that the contribution of higher resonances in the energy region $0 \leq E_\nu \leq 2.5$ is small in comparison to the contribution of Δ resonance. We have also performed the calculation of total scattering cross section for $1\pi^0$ production from neutral current incoherent scattering process with GENIE Monte Carlo code [16].

In this process a neutrino interacts with the nucleus and in the final state we get a π^0 besides the residual nucleus. Neutral current reactions are flavor blind. For the vector form factor and axial vector form factors Eq.(3.34) and Eq.(3.36) are used. In Fig.-3.9, total scattering cross section for neutral current ν_μ induced incoherent process in ^{56}Fe are shown. We have also compared the results obtained by using GENIE Monte Carlo code [16] for Δ resonance only and all 16 resonances tabulated in Table-3.2 for neutral current $\bar{\nu}_\mu$–^{56}Fe in Fig.-3.10 and find that the contribution of Δ resonance is maximum amongst all resonances.

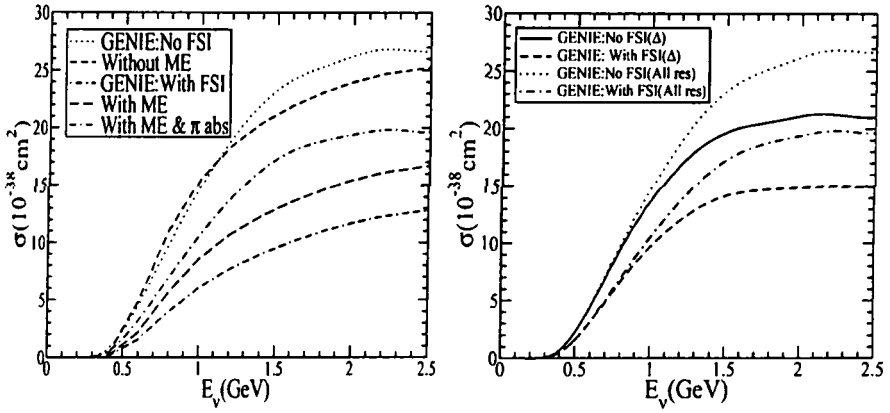

Figure 3.7: σ vs E_ν for CC1π^+ production from all resonances(left panel) and only from Δ resonance(right-panel) in ν_μ $-^{56}$ Fe reaction.

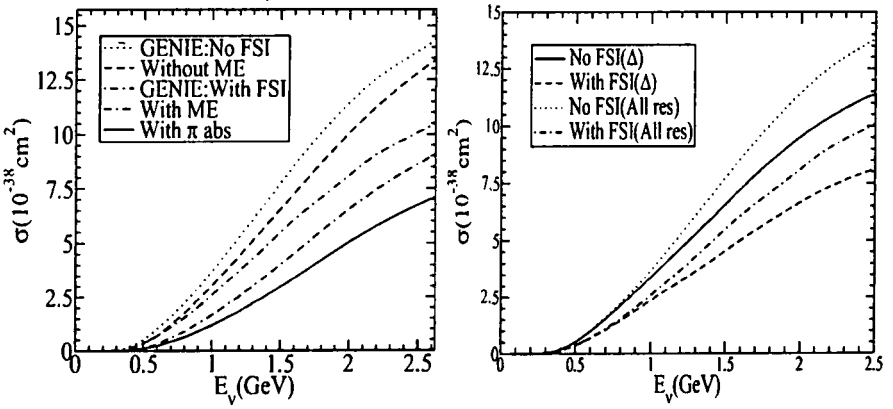

Figure 3.8: σ vs E_ν for CC1π^- production in $\bar{\nu}_\mu$ $-^{56}$ Fe reaction including all resonances(left-panel) and from Δ resonance(right-panel) only.

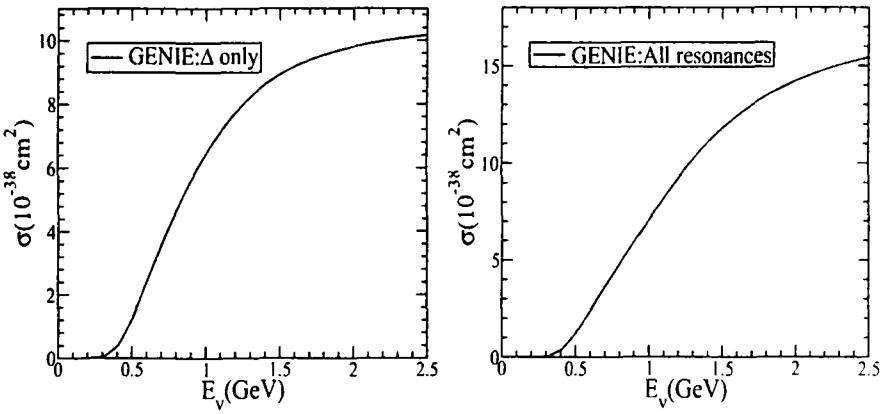

Figure 3.9: σ vs E_ν for NC1π^0 production in ν_μ–^{56}Fe reaction from Δ only(left-panel) and including all resonance(right-panel).

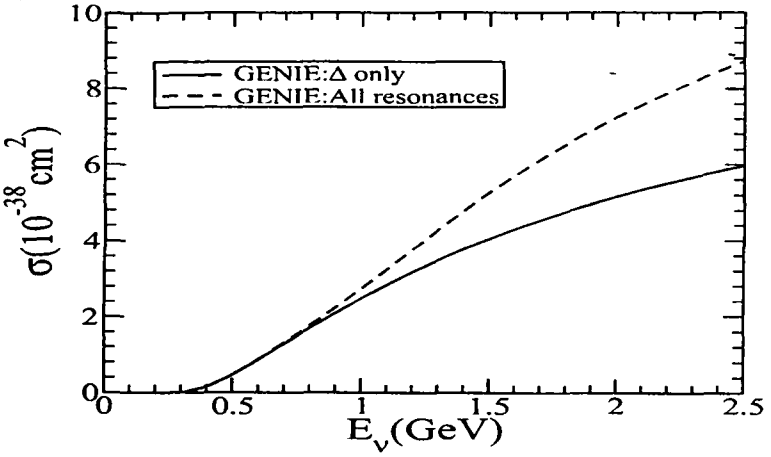

Figure 3.10: σ vs E_ν for NC1π^0 production in $\bar{\nu}_\mu$–^{56}Fe reaction including all resonances and contribution of Δ only.

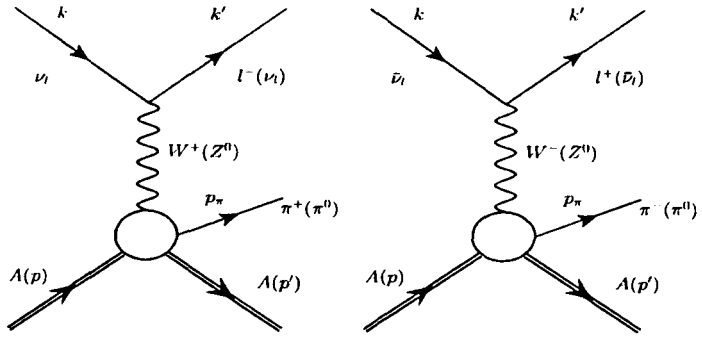

Figure 3.11: Feynman diagram corresponding to neutrino and antineutrino induced charged (neutral) current coherent scattering processes.

3.3 Coherent Scattering

In the coherent scattering process when a neutrino/antineutrino interacts with the nucleus, the nucleus does not change its identity after the interaction i.e. it remains in the ground state.

$$\begin{aligned} \nu_l + A &\rightarrow l^- + A + \pi^+ \\ \nu_l + A &\rightarrow \nu_l + A + \pi^0 \\ \bar{\nu}_l + A &\rightarrow l^+ + A + \pi^- \\ \bar{\nu}_l + A &\rightarrow \bar{\nu}_l + A + \pi^0 \end{aligned} \tag{3.41}$$

Charged(neutral) current coherent scattering process given in the above equation can be easily understood with the help of Feynman diagrams that are shown in Fig.-3.11. In coherent reactions the target nucleus recoils as a whole with very little recoil energy and does not break. The effect of incident wave is approximately same on all the nucleons, otherwise, coherence condition would be violated. Coherent pions are produced in both charged- and neutral-current neutrino-nucleus interactions. In this interaction nucleus remains in its ground state. In general, the coherent π^0 are distinguished from the resonantly produced pions due to their strongly forward peaked angular distribution. However, in atmospheric neutrino experiments, due to a lack of directional information of the incoming neutrinos, it is not possible to distinguish the coherent π^0 events from incoherent pions. In the case of coherent charged pions the forward angle dominance of the cross section leads to a small opening angle between two charged particles μ or e and charged pion in the final state, and these two particles could be detected as one isolated electromagnetic shower. In contrast to incoherent charged pions whose Cerenkov tracks are usually identified as muon

events, the special characteristics of coherent pions may lead to an increase of identified ν_e events and therefore underestimating the ν_μ to ν_e ratio.

Coherent pion production in nuclei is considered to investigate the properties of pion-nucleus interaction and to obtain the information about the behaviour of pion in nuclear medium. Coherent interactions have great importance to neutrino experiments because it provides an important background to the ν_e appearance measurement.

In the following subsection we discuss the calculation of neutrino induced coherent pion production at intermediate neutrino energies for charged and neutral current interactions. The calculation uses the local density approximation to the Δ-hole model. The nuclear medium effects are taken into account in the weak production process as well as in the final state interactions of the outgoing pions with the nucleus.

3.3.1 Formalism

For the coherent pion production induced by neutrino/antineutrino in the intermediate energy region Δ resonance is the most dominant one. The theoretical description and the form factors for higher resonances have larger uncertainties.

The weak interaction vertex contains both vector and axial vector parts while the $\pi N\Delta$ vertex contain only axial vector part contracted with the pion four momentum(k_π). The relativistic expression of matrix element for Δ pole term in u-channel processes is obtained by using the effective form of $\pi N\Delta$ interaction vertices for a $T = 3/2$ particle given by [73], [74]:

$$u^\mu_s(P) = \sqrt{\frac{E_\Delta + M_\Delta}{2M_\Delta}}\, L^{(1)}(P)^\mu_\nu \begin{pmatrix} \vec{I} \\ \frac{\vec{\sigma}.\vec{P}}{E_\Delta + M_\Delta} \end{pmatrix} S^{\nu\dagger}_{\Delta N}\, \chi_s, \tag{3.42}$$

where $L^{(1)}(P)$ is the Lorentz boost operator for spin-1 particle, χ_s is the four components Pauli spinor for spin-3/2 particle and $S^{\nu\dagger}_{\Delta N}$ is the four component transition spin operator. The Rarita-Schwinger spinors obey the completeness relation:

$$\sum_s u^\mu_s(P)\bar{u}^\nu_s(P) = -\frac{\not{P} + m_\Delta}{2M_\Delta}\left(g^{\mu\nu} - \frac{1}{3}\gamma^\mu\gamma^\nu - \frac{2P^\mu P^\nu}{3M^2_\Delta} + \frac{P^\mu\gamma^\nu - \gamma^\mu P^\nu}{3M_\Delta}\right) \tag{3.43}$$

Generally, the spin-3/2 projection operator for Δ is defined as [75]:

$$\begin{aligned}\Lambda^{\mu\nu} &= \sum_{-\frac{3}{2}}^{\frac{3}{2}} u^\mu_s(P)\bar{u}^\nu_s(P) \\ &= -\frac{\not{P} + m_\Delta}{2M_\Delta}\left(g^{\mu\nu} - \frac{1}{3}\gamma^\mu\gamma^\nu - \frac{2P^\mu P^\nu}{3M^2_\Delta} + \frac{P^\mu\gamma^\nu - \gamma^\mu P^\nu}{3M_\Delta}\right)\end{aligned} \tag{3.44}$$

and on mass-shell state the Δ propagator is written as:

$$\Delta^{\mu\nu} = \frac{2M_\Delta\, \Lambda^{\mu\nu}(P)}{P^2 - M^2_\Delta} \tag{3.45}$$

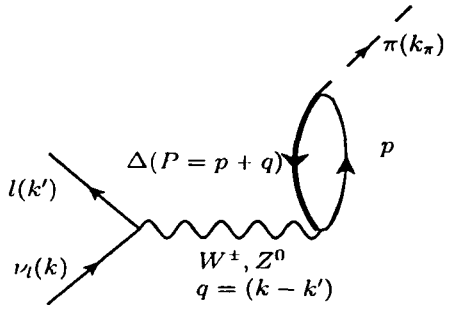

Figure 3.12: Scattering diagram for coherent pion production through Δ-hole excitations.

On introducing the delta width the above expression modifies to

$$\Delta^{\mu\nu} = \sum_{-\frac{3}{2}}^{\frac{3}{2}} u_s^\mu(P)\bar{u}_s^\nu(P) = -\frac{\not{P} + m_\Delta}{P^2 - M_\Delta^2 + i\Gamma M_\Delta}\left(g^{\mu\nu} - \frac{1}{3}\gamma^\mu\gamma^\nu - \frac{2P^\mu P^\nu}{3M_\Delta^2} + \frac{P^\mu\gamma^\nu - \gamma^\mu P^\nu}{3M_\Delta}\right), \tag{3.46}$$

where P and M_Δ are the four momenta and mass of delta and Γ is the decay width of Δ given in Eq.(3.37). The Lagrangian for the $\pi N\Delta$ interaction is given by

$$\mathcal{L}_{\pi N\Delta}^{int} = \frac{f_{\pi N\Delta}}{m_\pi}\bar{\Psi}_\mu \partial^\mu \phi \Psi + h.c. \ , \tag{3.47}$$

where $\frac{f_{\pi N\Delta}}{4\pi} = 0.36$ and it describes the on shell $\pi N\Delta$ interaction. The off-shell effects at the $\pi N\Delta$ vertex has been studied by using:

$$f_{\pi N\Delta}(P^2) = \frac{\Lambda^4}{\Lambda^4 + (P^2 - M_\Delta^2)^2}\, f_{\pi N\Delta} \ , \tag{3.48}$$

where Λ =1 GeV [76]-[77]. The amplitude of the reaction given in Eq.(3.41) for charged current interaction shown in Fig.-3.13 is written as

$$\mathcal{A} = \frac{G_F}{\sqrt{2}}\, b\, l^\mu\, \mathcal{J}_\mu\, \mathcal{F}(\vec{q} - \vec{k}_\pi) \ , \tag{3.49}$$

where $b = \cos\theta_c$ for the charged current interaction, $b = 1$ for the neutral current interaction, $G_F = 1.16 \times 10^{-5} GeV^2$ is the Fermi coupling constant, l^μ is the leptonic current

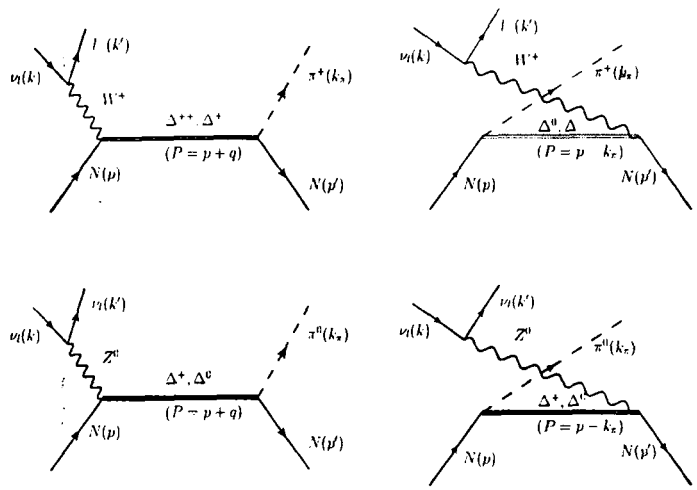

Figure 3.13: Feynman diagrams for neutrino induced weak coherent pion production in charged and neutral current interactions.

given by Eq.(2.7), $\mathcal{J}_\mu$ is the hadronic current and $\mathcal{F}(\vec{q} - \vec{k}_\pi)$ is the nuclear form factor modulated by isospin factors. The hadronic current $\mathcal{J}_\mu$ is the sum of direct and crossed diagrams, given by

$$\begin{aligned} \mathcal{J}_\mu &= J^s_\mu + J^u_\mu \\ &= \sqrt{3}\,\frac{f_{\pi N\Delta}}{m_\pi} \sum_s \bar{\Psi}^s(p') \Big[k_{\pi\sigma}\, \Delta^{\sigma\lambda}\, \mathcal{O}_{\lambda\mu} \\ &\quad + k_{\pi\sigma}\, \mathcal{O}^{\sigma\lambda}\, \Delta_{\lambda\mu} \Big]\, \Psi^s(p), \end{aligned} \tag{3.50}$$

where $\Delta^{\sigma\lambda}$ and $\Delta^{\lambda\mu}$ is the relativistic Δ propagator modified by a phenomenological decay width given in Eq.(3.46) and $\mathcal{O}^{\sigma\lambda}$ or $\mathcal{O}_{\lambda\mu}$ is the weak N-Δ transition vertex given by

$$\begin{aligned} \mathcal{O}^{\mu\alpha} &= \left[\frac{C_3^V}{M}(g^{\mu\alpha}\, \not{q} - q^\mu \gamma^\alpha) + \frac{C_4^V}{M^2}(g^{\mu\alpha} q.P - q^\mu P^\alpha) \right. \\ &+ \left. \frac{C_5^V}{M^2}(g^{\mu\alpha} q.p - q^\mu p^\alpha) \right] \gamma^5 + \left[\frac{C_3^A}{M}(g^{\mu\alpha}\, \not{q} - q^\mu \gamma^\alpha) \right. \\ &+ \left. \frac{C_4^A}{M^2}(g^{\mu\alpha} q.P - q^\mu P^\alpha) + C_5^A g^{\mu\alpha} + \frac{C_6^V}{M^2} q^\mu q^\alpha \right] \end{aligned} \tag{3.51}$$

The first term in the bracket in Eq.(3.50) is for direct(s-channel) diagram term and the second term for the crossed(u-channel) diagram shown in Fig.-3.13. Similarly, the amplitude in neutral current case for the direct(s-channel) and crossed(u-channel) Δ resonance

term is written with zero lepton mass and $\cos\theta_c$ by one along with the isospin factors $\xi_V^{I=1}$ and $\xi_A^{I=1}$ as defined in Eq.(3.16). The weak N-Δ transition vertex in case of neutral current is given by

$$\begin{aligned}\mathcal{O}_{NC}^{\lambda\mu} &= \xi_V^{I=1}\left[\frac{C_3^V}{M}(g^{\lambda\mu}\not{q} - q^\lambda\gamma^\mu) + \frac{C_4^V}{M^2}(g^{\lambda\mu}q.P - q^\lambda P^\mu)\right.\\ &+ \left.\frac{C_5^V}{M^2}(g^{\lambda\mu}q.P - q^\lambda p^\mu)\right]\gamma^5 + \xi_A^{I=1}\left[\frac{C_3^A}{M}(g^{\lambda\mu}\not{q} - q^\lambda\gamma^\mu)\right.\\ &+ \left.\frac{C_4^A}{M^2}(g^{\lambda\mu}q.P - q^\lambda P^\mu) + C_5^A g^{\lambda\mu} + \frac{C_6^V}{M^2}q^\lambda q^\mu\right] \qquad (3.52)\end{aligned}$$

After taking the average over initial spin states and sum over the final spin states the square of the amplitude is written as

$$|\bar{\mathcal{A}}|^2 = \frac{G_F^2}{2}\cos^2\theta_c\,\mathcal{L}^{\mu\nu}\,\mathcal{J}_{\mu\nu}\,|\mathcal{F}(\vec{q}-\vec{k}_\pi)|^2\,, \qquad (3.53)$$

The leptonic tensor is given by

$$\begin{aligned}\mathcal{L}^{\mu\nu} &= Tr\left[(\not{k}' + m_\nu)\gamma^\mu(1-\gamma^5)(\not{k} + m_l)\gamma^\nu(1-\gamma^5)\right]\\ &= 8\left[k^\mu k'^\nu + k'^\mu k^\nu - (k.k')g^{\mu\nu} + i\epsilon^{\mu\nu\rho\sigma}k^\rho k'^\sigma\right] \qquad (3.54)\end{aligned}$$

and hadronic tensor is given by

$$\begin{aligned}\mathcal{J}_{\mu\nu} &= \frac{1}{2}\mathcal{J}_\mu\mathcal{J}_\nu\\ &= \frac{1}{2}\left(J^s_{\mu\nu} + J^u_{\mu\nu} + |J^s_\mu J^{u\dagger}_\nu| + |J^u_\mu J^{s\dagger}_\nu|\right) \qquad (3.55)\end{aligned}$$

The square of the amplitude for the neutrino induced weak charged current coherent pion production from a nucleus is obtained by summing over all the occupied nucleons in the amplitude and considering the s- and u- channel resonant terms, one may write

$$\bar{\sum}\sum|\mathcal{A}_\Delta|^2_{CC} = \bar{\sum}\sum\left(|\mathcal{A}^s_\Delta| + |\mathcal{A}^u_\Delta| + |\mathcal{A}^s_\Delta\mathcal{A}^{u\dagger}_\Delta| + |\mathcal{A}^u_\Delta\mathcal{A}^{s\dagger}_\Delta|\right) \qquad (3.56)$$

The matrix element square in the neutral current process for $\Delta-$ direct and crossed diagrams are directly related with the charged current matrix elements through the isospin factor given in Eq.(3.16). The nucleon form factor in Eq.(3.49) is defined as

$$\mathcal{F}(\vec{q}-\vec{k}_\pi) = \int d^3\vec{r}\;\rho(\vec{r})\;e^{-i(\vec{q}-\vec{k}_\pi).\vec{r}}, \qquad (3.57)$$

where $\rho(\vec{r})$ is the nuclear matter density which is a function of nucleon relative coordinates. When pion absorption effect is taken into account using the Eikonal approximation the

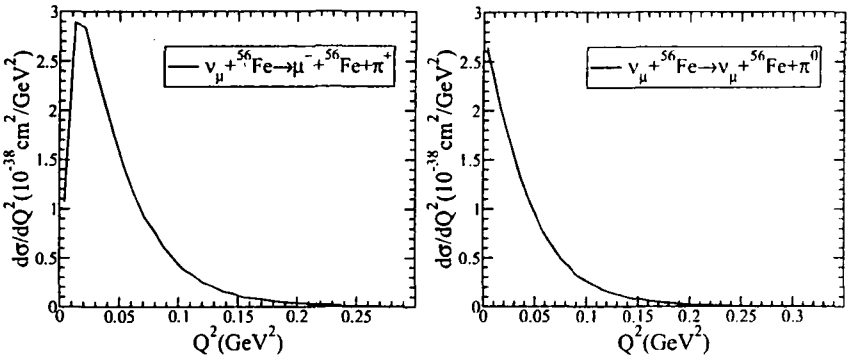

Figure 3.14: $d\sigma/dQ^2$ vs Q^2 in $\nu_\mu - {}^{56}Fe$ reaction from CC(NC) coherent scattering process.

nucleon form factor $\mathcal{F}(\vec{q} - \vec{k_\pi})$ is modified to $\tilde{\mathcal{F}}(\vec{q} - \vec{k_\pi})$ is calculated in Eikonal approximation [78] and is obtained as

$$\tilde{\mathcal{F}}(\vec{q} - \vec{k_\pi}) = 2\pi \int_0^\infty b\ db \int_{-\infty}^\infty dz\ \rho(\vec{b}, z)\ J_0(k_\pi^t b)\ e^{i(|\vec{q}| - k_\pi^l)z} e^{-if(\vec{b},z)} \tag{3.58}$$

where $f(\vec{b}, z) = \int_z^\infty \frac{1}{2|\vec{k_\pi}|} \Pi(\rho(\vec{b}, z'))dz'$, k_π^l and k_π^t are the longitudinal and transverse components of the pion momentum and Π is the self-energy of pion, the expression for which is taken from Ref. [78] and is given by

$$\Pi(\rho(\vec{b}, z')) = \frac{4}{9} \left(\frac{f_{\pi N\Delta}}{m_\pi} \right)^2 \frac{M^2}{W^2} |\vec{k_\pi}|^2\ \rho(\vec{b}, z')\ \frac{1}{W - \tilde{M}_\Delta + \frac{i\tilde{\Gamma}}{2}} \tag{3.59}$$

with W as the center of mass energy in the Δ rest frame.

Using the amplitude given by Eq.(3.49) and the modifications in the Δ mass and width in the nuclear medium we calculate the total scattering cross section σ given in Eq.(3.40).

3.3.2 Results and Conclusions

Coherent neutrino-nucleus interactions are modeled according to Rein and Sehgal model [79] in GENIE Monte Carlo code [16]. PCAC based model seems to be most accurate at a few GeV and above. At lower energies the microscopic Δ dominance models are believed to be more reliable. Since the coherence condition requires a small momentum transfer to the target nucleus, therefore, it is a low Q^2 process which is related via PCAC theorem. We have calculated the differential and total scattering cross section for this process with axial dipole mass M_A =1.05 GeV using GENIE Monte Carlo [16].

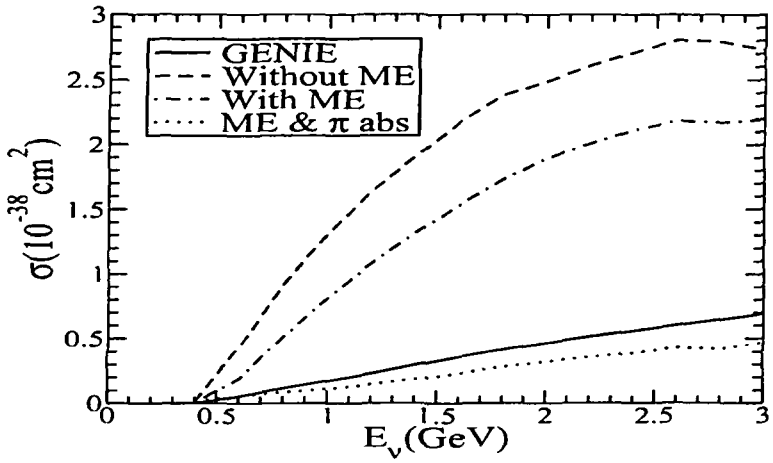

Figure 3.15: σ vs E_ν for single π^+ production in $\nu_\mu - {}^{56}Fe$ reaction from CC coherent scattering process.

3.3.3 Differential Scattering Cross Section

In this section, we show the result for differential cross section $\frac{d\sigma}{dQ^2}$ at neutrino energy $E_\nu = 1$ GeV for charged and neutral current interactions in ^{56}Fe obtained from Rein and Sehgal model by using GENIE Monte Carlo generator [16]. These results are shown in Fig.-3.14 for charged and neutral current respectively. Experimentally, it has been established that the coherent scattering cross section, peaks at very low Q^2 and the cross section rises as a function of neutrino energy and becomes logarithmic at large neutrino energies. Therefore, neutrino induced coherent pion production process has an advantage over other existing reactions to better understand the nuclear excitation mechanism. As well as it allows study of the longitudinal axial current at very small Q^2 values.

3.3.4 Total Scattering Cross Section

In the model developed by Aligarh group [31], for the coherent process, the scattering cross section are the same for both neutrino and antineutrino. We have calculated the total cross section for charged current scattering processes in ^{56}Fe that are shown in Fig.-3.15. The results for $\sigma^{CC}(E_\nu)$ as a function of neutrino energy (E_ν) are shown without nuclear medium effects(dashed line) and with nuclear medium effects(dashed-dotted line). When the pion absorption and nuclear medium effects, are both taken into account the results for $\sigma^{CC}(E_\nu)$ are shown by the dotted lines. We see that the nuclear medium effects lead to a reduction of around 56% for E_ν=0.6 GeV, 38% around E_ν=1.0 GeV, 24% at

E_ν=2.0 GeV and it is about 20% at E_ν=3.0 GeV while the reduction due to final state interaction is quite large. This suppression in the cross section due to the nuclear medium and the pion absorption effects is 86% for E_ν around 1.0 GeV, 83% for E_ν around 2.0 GeV and 78% for E_ν around 3.0 GeV. Thus there is a large reduction in the cross section when nuclear medium effect and final state interaction are taken into account.

It is noticeable that the results obtained from the Rein-Sehgal coherent model used in GENIE Monte Carlo code [16] and from the model developed by Aligarh group [31] without nuclear medium effects are not in agreement.

Chapter 4

Associated Production

4.1 Introduction

After the discovery of pion in 1947, Clifford Butler and George Rochester while studying cosmic rays, discovered particles having strange behaviour [80]. This new particle was found to be heavier than the muon and pion but lighter than the proton, with a mass of about 800 times of electron's mass. In the next few years, with the evolution of cloud chamber and the bubble chamber experiments, researchers found copious examples of such type of strange particles. These evidences indicated that they were created via strong interactions in nuclear matter, however, their life time were much larger than the time involved in the electromagnetic and strong interactions. Because of this strange behaviour they were named as *strange* particles. These strange particles were called Kaons (K^+, K^0, K^-, $\bar{K}^0$). Unlike the charged kaons electrically neutral strange particle, K^0, did not leave any track but decayed into π^+ and π^-, and a V-shaped vertex was left by these particles in the photograph. In subsequent years more strange particles were found which are heavier than the proton like Lambda (Λ^0), Sigma(Σ^+, Σ^-, Σ^0), Cascade(Ξ^0, Ξ^-), etc.

Many theoretical efforts have also been performed in order to understand the properties of these particles. In 1956, Murray Gell-Mann and Nishijima independently proposed a new conservation law, *strangeness*, which is conserved in strong and electromagnetic interactions but not in the weak interaction. A new quantum number corresponding to this conservation law was proposed which is known as "strange quantum number (S)". In the following years, it was found that this quantum number(S) is directly related to the presence of an additional quark, which is in addition to the 'u'and 'd'quarks responsible for the building of (low lying)hadrons, and named as the strange quark 's'. The strange quantum number can be written in terms of the number of strange quarks(n_s) and antiquarks($n_{\bar{s}}$) present in the hadrons and is given by the relation

$$S = -(n_s - n_{\bar{s}}). \tag{4.1}$$

In the strong or electromagnetic processes, S is conserved, i.e. number of particles produced with strangeness quantum number $S = +1$ is/are equal to the number of particles produced with strangeness quantum number $S = -1$. These processes are therefore called Associated Particle Production processes. The charged current neutrino/antineutrino induced associated strange particle production is a topic of great interest. Low energy exclusive reactions can provide much detailed information about the structure of weak interactions.

In the present study, we have considered the associated strange particle production induced by neutrinos/antineutrinos on bound and free nucleon target. The cross sections are calculated by using the GENIE Monte Carlo code [16]. Here we have also presented the results for the charged current neutrino-nucleon process, obtained by the theoretical calculations performed recently by the Aligarh group [34].

4.2 Formalism

A few strangeness conserving $\Delta S = 0$ reactions induced by neutrino and antineutrino where a kaon is produced along with a hyperon are

$$\begin{aligned}
&\nu_\mu + n \to \mu^- + \Sigma^+ + K^0, && \bar{\nu}_\mu + p \to \mu^+ + \Lambda^0 + K^0 \\
&\nu_\mu + n \to \mu^- + \Lambda^0 + K^+, && \bar{\nu}_\mu + p \to \mu^+ + \Sigma^- + K^+ \\
&\nu_\mu + n \to \mu^- + \Sigma^0 + K^+, && \bar{\nu}_\mu + p \to \bar{\nu}_\mu + \Lambda^0 + K^+ \\
&\nu_\mu + p \to \mu^- + \Sigma^+ + K^+, && \bar{\nu}_\mu + n \to \mu^+ + \Sigma^- + K^0 \\
&\nu_\mu + n \to \nu_\mu + \Lambda^0 + K^0, && \bar{\nu}_\mu + n \to \bar{\nu}_\mu + \Lambda^0 + K^0, \\
&\nu_\mu + p \to \nu_\mu + \Sigma^+ + K^0, && \\
&\nu_\mu + p \to \nu_\mu + \Lambda^0 + K^+, && etc.
\end{aligned} \tag{4.2}$$

In Fig.-4.1 and Fig.-4.2 we have shown the Feynman diagrams for the processes like $\nu_\mu + N \to l + K + Y$, where $l = \mu^-$, ν_μ and hence represents the charged and neutral current respectively, N and Y are the nucleons and hyperons(Λ and Σ) respectively and K stands for the kaons.

The basic charge current reaction for the processes under consideration is given by

$$\nu_\mu(k) + N(p) \to \mu^-(k') + K(p_k) + Y(p'), \tag{4.3}$$

where ν_μ and μ^- are incident neutrino and final state lepton with four momenta k and k', respectively. p and p' are the nucleon(N) and hyperon(Y) four momenta and the pseudoscalar strange mesons K is represented with momentum p_k.

The differential cross section for the three body final state in the rest frame of nucleon is given by

$$d^9\sigma = \frac{1}{4ME(2\pi)^5}\frac{d\vec{k}'}{(2E_l)}\frac{d\vec{p}'}{(2E'_Y)}\frac{d\vec{p}_k}{(2E_K)}\delta^4(k + p - k' - p' - p_k)\bar{\Sigma}\Sigma|\mathcal{M}|^2,$$

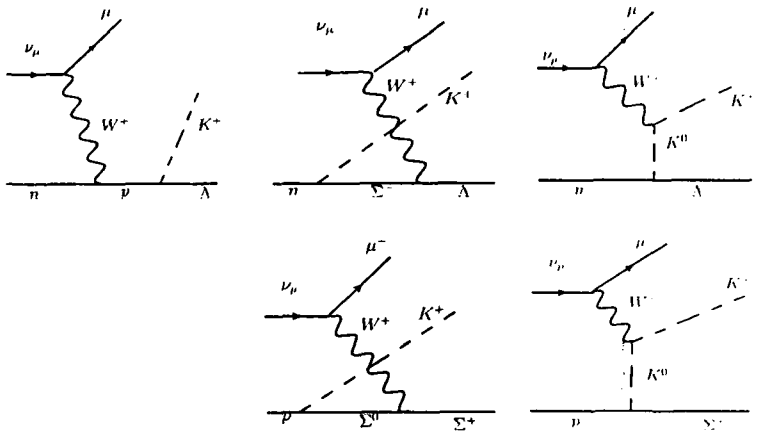

Figure 4.1: Born diagrams for KΛ and KΣ charged current reactions.

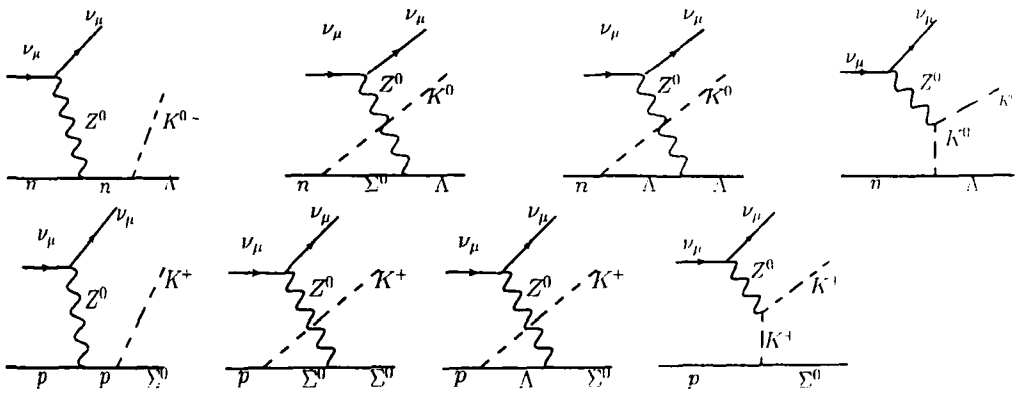

Figure 4.2: Born diagrams for KΛ and KΣ neutral current reactions.

	CC(Δ S=0)	NC
ζ_l	$\frac{-ig}{2\sqrt{2}}$	$\frac{-ig}{4}\frac{M_Z}{M_{W^+}}$
ζ_h	$\frac{-ig}{2\sqrt{2}}\zeta_c$	$\frac{-ig}{4}\frac{M_Z}{M_{W^+}}\zeta_c$

Table 4.1: The parameters ζ_l and ζ_h in terms of weak coupling constant.

where E and E_l are respectively the lepton energy in the initial and final state. M is the nucleon mass and $\bar{\Sigma}\Sigma|\mathcal{M}|^2$ is the square of the transition amplitude matrix element averaged(summed) over the spins of the initial(final) state. At low energies, this amplitude can be written in the usual form as [81]

$$\begin{aligned} -i\mathcal{M} &= \left[\bar{u}_l(k')\ \zeta_l\ \gamma_\mu(I-\gamma_5)\ u_\nu(k)\right]\ iD^{\mu\nu} \\ &\quad \times \left\langle K(p_k)Y(p')|\zeta_h \hat{J}_\nu(q)|N(p)\right\rangle \end{aligned} \tag{4.4}$$

The above expression contains weak leptonic transition current, massive gauge boson propagator, weak hadronic transition current. The weak hadronic transition current is given by

$$\left\langle K(p_k)Y(p')|\zeta_h \hat{J}_\nu(q)|N(p)\right\rangle = \bar{u}_Y(p')\ \zeta_h\ J_\nu(q)\ u_N(p) \tag{4.5}$$

and the form of the gauge propagator $D^{\mu\nu}$ is

$$D^{\mu\nu} = \frac{-g^{\mu\nu} + \frac{q^\mu q^\nu}{M_W^2}}{q^2 - M_W^2}. \tag{4.6}$$

The parameters ζ_l and ζ_h appeared in Eq.(4.4) are tabulated in Table-4.1. While the parameter ζ_c appeared in the above table can be summarized for CC and NC case as,

$$\zeta_c = \begin{cases} \cos\theta_c, & \text{for CC,} \quad \Delta S = 0, \\ 1. & \text{for NC.} \end{cases} \tag{4.7}$$

where the θ_c is the Cabibbo mixing angle. At low and intermediate energies where $q^2 << M_W^2$, the propagator given in Eq.(4.6) reduces to much simplified form as $D^{\mu\nu} = g^{\mu\nu}/M_W^2$. In such energies the coupling can be written in terms of the Fermi coupling constant G_F which further can be related with the gauge coupling g and the mass of weak gauge boson M_W as

$$\frac{G_F}{\sqrt{2}} = \frac{g^2}{8M_W^2} \tag{4.8}$$

The invariant amplitude $\mathcal{M}$ becomes

$$\mathcal{M} = \frac{G_F}{\sqrt{2}}\zeta\left[\bar{u}_l(\vec{k}')\ \gamma_\mu(I-\gamma_5)\ u_\nu(\vec{k})\right]\ \left[\bar{u}_Y(\vec{p}')\ J^\mu(q)\ u_N(\vec{p})\right] \tag{4.9}$$

and the new parameter ζ will be,

$$\zeta = \begin{cases} \zeta_c & \text{for CC,} \\ \\ \frac{\zeta_c}{2} & \text{for NC.} \end{cases} \tag{4.10}$$

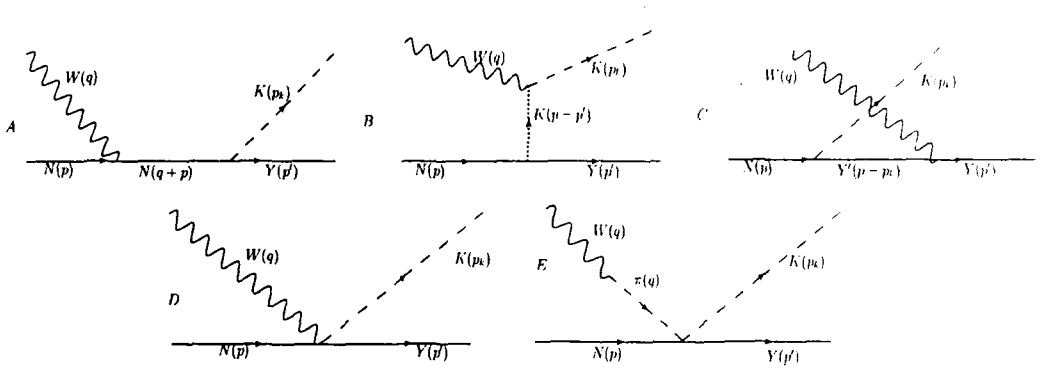

Figure 4.3: Feynman diagrams for the $\nu_\mu/\bar{\nu}_\mu(k) + N(p) \rightarrow L(k') + K(p_k) + Y(p')$, where $L = \mu^-/\mu^+$ and $\nu_\mu/\bar{\nu}_\mu$ for charged and neutral current respectively.

Hence the invariant amplitude square can be written with the help of the Eq.(4.9)

$$|\mathcal{M}|^2 = \frac{G_F^2}{2}\zeta^2 \; L_{\mu\nu} \; W^{\mu\nu}, \tag{4.11}$$

where the leptonic tensor is given by

$$L_{\mu\nu} = \left[\bar{u}_l(\vec{k'}) \; \gamma_\mu(I - \gamma_5) \; u_\nu(\vec{k})\right] \left[\bar{u}_l(\vec{k'}) \; \gamma_\nu(I - \gamma_5) \; u_\nu(\vec{k})\right]^* \tag{4.12}$$

and the hadronic tensor is given by

$$W^{\mu\nu} = \left[\bar{u}_Y(\vec{p'}) \; J^\mu(q) \; u_N(\vec{p})\right] \left[\bar{u}_Y(\vec{p'}) \; J^\nu(q) \; u_N(\vec{p})\right]^* \tag{4.13}$$

Using the trace theorems for Dirac matrices the leptonic tensor given in Eq.(4.12) becomes

$$L_{\mu\nu}^{CC} \propto \left[k_\mu k'_\nu + k_\nu k'_\mu - k.k' g_{\mu\nu} + i\varepsilon_{\mu\nu\alpha\beta} k^\alpha k'^\beta\right], \tag{4.14}$$

where $\epsilon_{\mu\nu\alpha\beta}$ is the four dimensional anti symmetric Levi-Cevita tensor. However, the hadronic tensor will be,

$$W^{\mu\nu} = \frac{1}{2}\mathrm{Tr}\left[J^\mu(q)(\not{p} + M)\tilde{J}^\nu(q)(\not{p}' + M_Y)\right], \tag{4.15}$$

where $\tilde{J}^\mu(q) = \gamma^0 J^{\mu\dagger}(q)\gamma^0$. In literature there are very few works which dealt with the associated production of kaons with hyperons [81]-[83]. Recently Aligarh group [34] has developed a macroscopic model which is based on the SU(3) chiral Lagrangian. The parameters used in the model developed by Aligarh group [34] are the pion decay constant(f_π),

Cabibbo's angle(θ_c), the nucleon magnetic moments and the axial vector coupling constants for the baryons octet, D and F. These parameters are obtained from the analysis of the semileptonic decays of neutron and hyperons.

$$\begin{array}{ll} \nu_\mu\, n \to \mu^-\, \Lambda^0\, K^+\,; & \bar{\nu}_\mu\, p \to \mu^+\, \Lambda^0\, K^0 \\ \nu_\mu\, n \to \mu^-\, \Sigma^0\, K^+\,; & \bar{\nu}_\mu\, p \to \mu^+\, \Sigma^0\, K^0 \\ \nu_\mu\, n \to \mu^-\, \Sigma^+\, K^0\,; & \bar{\nu}_\mu\, p \to \mu^+\, \Sigma^-\, K^+ \\ \nu_\mu\, p \to \mu^-\, \Sigma^+\, K^+\,; & \bar{\nu}_\mu\, n \to \mu^+\, \Sigma^-\, K^0 \end{array} \tag{4.16}$$

Feynman diagrams corresponding to the above reactions are shown in Fig.-4.3. The first row consists of s-channel, t-channel and u-channel diagrams, whereas the next row has the contact and π-pole terms. The hadronic current coupling to the W bosons for Feynman diagrams(Fig.-4.3) are [34],

$$\begin{aligned} j^\mu|_{CT} &= iA_{CT}V_{ud}\frac{\sqrt{2}}{2f_\pi}\bar{u}_Y(p')\,(\gamma^\mu + B_{CT}\,\gamma^\mu\gamma^5)\,u_N(p) \\ j^\mu|_{SY} &= iA_{SY}V_{ud}\frac{\sqrt{2}}{2f_\pi}\bar{u}_Y(p')\not{H}_k\,\gamma_5\frac{\not{p}+\not{q}+M}{(p+q)^2-M^2}\left(\gamma^\mu + i\frac{(\mu_p-\mu_n)}{2M}\sigma^{\mu\nu}q_\nu\right. \\ &\quad \left.-(D+F)\left\{\gamma^\mu - \frac{q^\mu}{q^2-{m_\pi}^2}\not{q}\right\}\gamma^5\right)u_N(p) \\ j^\mu|_{UY} &= iA_{UY'}V_{ud}\frac{\sqrt{2}}{2f_\pi}\bar{u}_Y(p')\,H^\mu_{Y'}\,\frac{\not{p}-\not{H}_k+M_{Y'}}{(p-p_k)^2-M^2_{Y'}}\not{H}_k\,\gamma_5 u_N(p) \\ j^\mu|_{TY} &= iA_{TY}V_{ud}\frac{\sqrt{2}}{2f_\pi}(M+M_Y)\bar{u}_Y(p')\gamma^5\,u_N(p)\frac{q^\mu-2p_k^\mu}{(q-p_k)^2-m_k^2} \\ j^\mu|_{\pi P} &= iA_\pi V_{ud}\frac{\sqrt{2}}{4f_\pi}\bar{u}_Y(p')(\not{q}+\not{H}_k\,)u_N(p)\frac{q^\mu}{q^2-m_\pi^2} \end{aligned}$$

with

$$\begin{aligned} H^\mu_\Lambda &= i\frac{3\mu_n}{4M}\sigma^{\mu\nu}q_\nu + D\left(\gamma^\mu - \frac{\not{q}q^\mu}{q^2-m_\pi^2}\right)\gamma^5 \\ H^\mu_\Sigma &= \gamma^\mu + i\frac{2\mu_p+\mu_n}{4M}\sigma^{\mu\nu}q_\nu - F\left(\gamma^\mu - \frac{\not{q}q^\mu}{q^2-m_\pi^2}\right)\gamma^5, \end{aligned}$$

where $j^\mu|_{CT}$, $j^\mu|_{SY}$, $j^\mu|_{UY}$, $j^\mu|_{TY}$, $j^\mu|_{\pi P}$, are respectively represent the hadronic current for contact term, s-channel, u-channel, t-channel, pion-pole and Y stands for the hyperon in the final state and Y' for the hyperon in the intermediate state in the u-channel diagram. Since dependence of the different terms on the momentum transferred to the nucleon is not well known, therefore, a global dipole form factor $F(q^2) = (1 - q^2/M_A^2)^{-2}$ with a natural value of axial dipole mass $M_A = 1.05$ GeV is taken for the numerical calculations. Effect of this form factor is small at relatively low neutrino energies.

	$\bar{\nu}_L p \to L^+ \Lambda K^0$ $\nu_L n \to L^- \Lambda K^+$	$\bar{\nu}_L p \to L^+ \Sigma^0 K^0$ $\nu_L n \to L^- \Sigma^0 K^+$	$\bar{\nu}_L p \to L^+ \Sigma^- K^+$ $\nu_L n \to L^- \Sigma^+ K^0$	$\bar{\nu}_L n \to L^- \Sigma^- K^0$ $\nu_L p \to L^- \Sigma^+ K^-$
A_{CT}	$-\sqrt{\frac{3}{2}}$	$\mp\frac{1}{\sqrt{2}}$	0	-1
B_{CT}	$-\frac{1}{3}$(D+3F)	(D-F)	0	(D-F)
A_{SY}	$-\frac{1}{\sqrt{6}}$(D+3F)	$\mp\frac{1}{\sqrt{2}}(D-F)$	(D-F)	0
$A_{U\Sigma}$	$-\sqrt{\frac{2}{3}}$(D-F)	$\mp\sqrt{2}(D-F)$	(D-F)	F-D
$A_{U\Lambda}$	0	0	$\frac{1}{3}$(D+3F)	$\frac{1}{3}$(D+3F)
A_{TY}	$-\frac{1}{\sqrt{6}}$(D+3F)	$\pm\frac{1}{\sqrt{2}}$(D-F)	0	(D-F)
A_π	$\sqrt{\frac{3}{2}}$	$\pm\frac{1}{\sqrt{2}}$	0	1

Table 4.2: Constant factors appearing in the hadronic current. The upper(lower) sign corresponds to the processes with $\bar{\nu}(\nu)$ [34].

$\Delta S = 0$ processes are not Cabibbo suppressed. Therefore, these processes are assumed to be dominant even at low energies. Moreover, there may be important resonant contributions to the $\Delta S = 0$ processes, which we have not been considered in the present study. However, it has been pointed out that the inclusion of these resonances, which make the dynamics of these channels more involved, can play a relevant role as is known from associated strangeness photoproduction studies.

4.3 Results and Conclusions

In this section, we have presented the results of total scattering cross section for associated strange particles production. First we are presenting the results obtained from the numerical calculations performed by the Aligarh group [34]. They found that the contri-

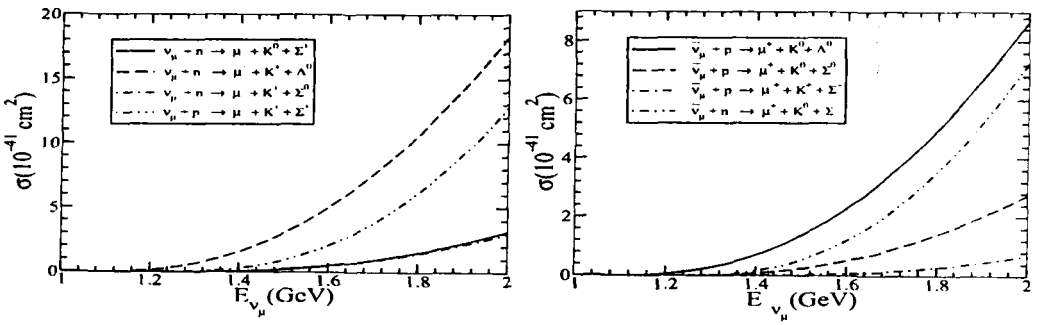

Figure 4.4: Cross section for the $|\Delta S| = 0$ associated kaon production.

Processes	σ ($10^{-41}cm^2$) at E=1.2 GeV	σ ($10^{-41}cm^2$) at E=1.6 GeV	σ ($10^{-41}cm^2$) at E=2.0 GeV
$\sigma(\nu_\mu n \to \mu^- K^+ \Lambda)$	0.14	1.8	5.4
$\sigma(\bar{\nu}_\mu p \to \mu^+ K^0 \Lambda)$	0.12	1.4	4.1
$\sigma(\nu_\mu p \to \nu_\mu K^+ \Lambda)$	3.9×10^{-2}	0.43	1.2
$\sigma(\bar{\nu}_\mu p \to \bar{\nu}_\mu K^+ \Lambda)$	5.5×10^{-2}	0.52	1.4
$\sigma(\nu_\mu n \to \nu_\mu K^0 \Lambda)$	5.4×10^{-2}	0.54	1.5
$\sigma(\bar{\nu}_\mu n \to \bar{\nu}_\mu K^0 \Lambda)$	3.5×10^{-2}	0.37	1.1

Table 4.3: Total scattering cross sections for charged and neutral current $\nu_L N \to LK\Lambda$ and $\bar{\nu}_L N \to \bar{L}K\Lambda$ reactions [82].

Processes	σ Fermilab ($10^{-41}cm^2$)	Processes	σ Fermilab ($10^{-41}cm^2$)
$\nu p \to \mu^- K^+ p$	21.3	$\bar{\nu} p \to \mu^+ \Lambda \pi^0$	24.5
$\bar{\nu} p \to \mu^+ K^0 p$	4.6	$\bar{\nu} p \to \mu^+ \Sigma^0 \pi^0$	1.9
$\nu n \to \mu^- K^0 p$	24.7	$\bar{\nu} n \to \mu^+ \Sigma^- \pi^0$	0.9
$\bar{\nu} n \to \mu^+ K^- n$	12.2	$\bar{\nu} n \to \mu^+ \Sigma^0 \pi^-$	0.8
$\bar{\nu} n \to \mu^+ \Lambda \pi^-$	22.6	$\nu n \to \mu^- K^+ \Lambda$	68.3

Table 4.4: Flux-averaged cross sections for the processes considered [83].

bution of the contact term to be the most dominant one followed by the s- and u- channel diagrams. The results obtained by the Aligarh group [34] for the total scattering cross section as a function of the neutrino/antineutrino energy are shown in Fig.-4.4 for neutrino (left panel) and antineutrino (right panel) induced reactions. For $\nu_\mu n \to \mu^- \Sigma^+ K^0$ and $\bar{\nu}_\mu p \to \mu^+ \Sigma^- K^+$ there is no contribution from the contact term and hence the cross sections are relatively lower. Their work is in progress [34]. Using GENIE Monte Carlo code [16], we have obtained the results of scattering cross section for free nucleon as well as nucleons bound inside the iron(^{56}Fe) in the case of $\nu_\mu(\bar{\nu}_\mu)$ induced charged and neutral current interactions with M_A=1.05 GeV. In GENIE Monte Carlo code [16] for nucleons bound inside the nucleus nuclear medium effects like Fermi motion, Pauli blocking and binding energy correction are taken into account. For the charged and neutral current neutrino/antineutrino induced associated strange particle production on free nucleon target the results, obtained by using the GENIE Monte Carlo code [16], are shown in Fig.-4.5 and Fig.-4.6 for neutrino and in Fig.-4.7 for antineutrino. We have also shown the results for the total scattering cross section for bound nucleons inside the nuclear target iron obtained by using the GENIE Monte Carlo code [16]. These results are shown in figures Fig.-4.8, Fig.-4.9 for neutrino and in Fig.-4.10 for antineutrino.

Previously, Shrock [82] had also obtained the total scattering cross section results

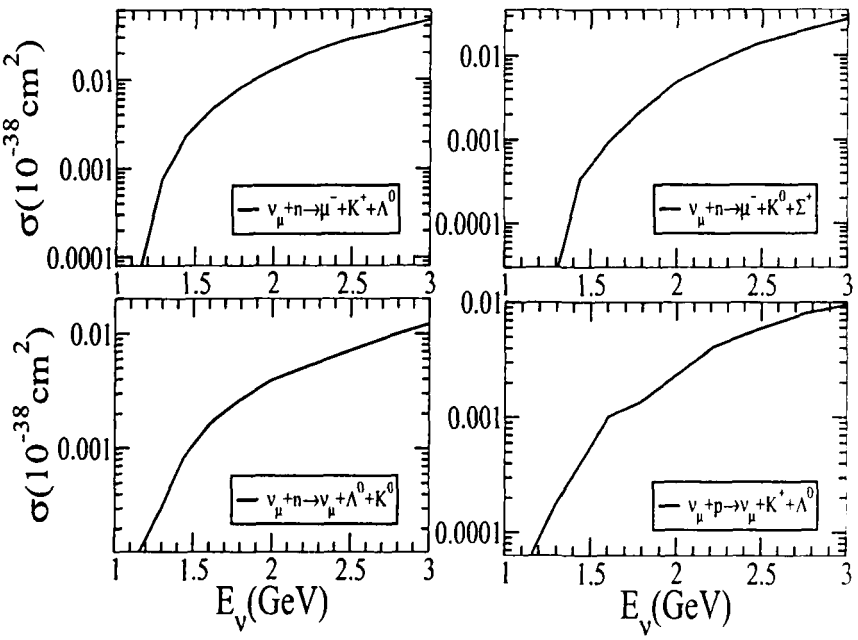

Figure 4.5: σ vs E_ν for associated strange particle production in $\nu_\mu - N(\text{free})$.

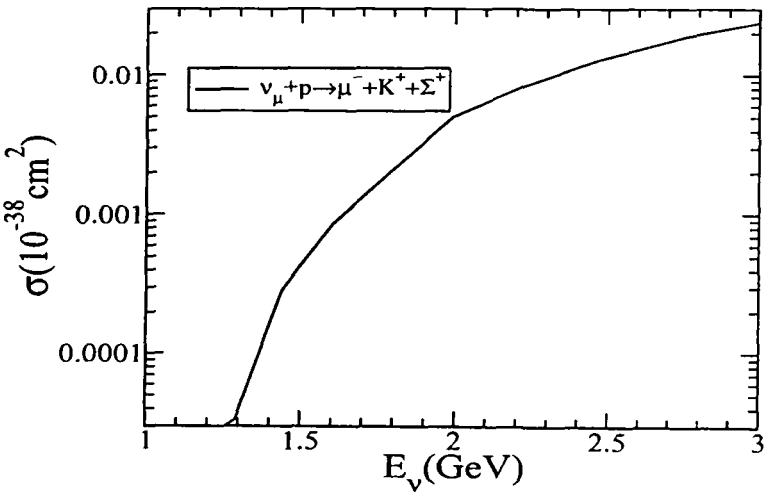

Figure 4.6: σ vs E_ν for associated strange particle production in $\nu_\mu - p(\text{free})$.

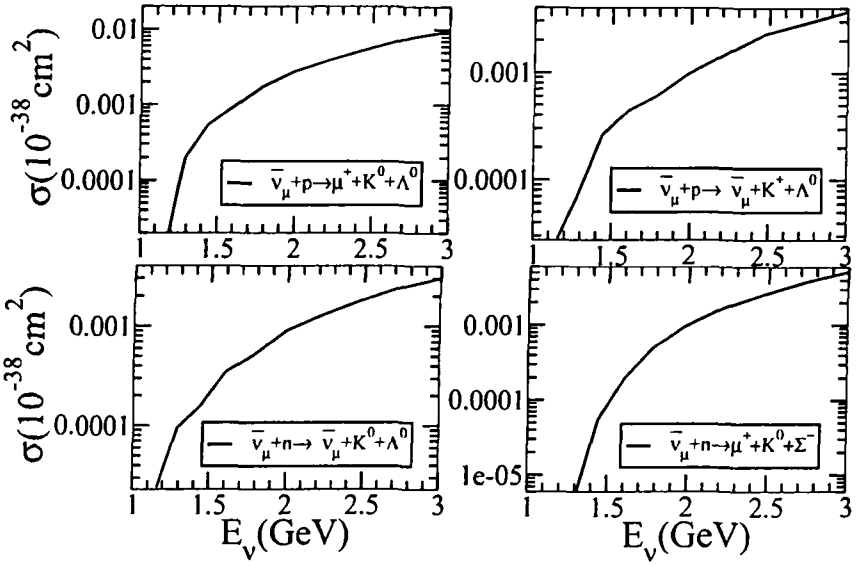

Figure 4.7: σ vs E_ν for associated strange particle production in $\bar{\nu}_\mu - N(free)$.

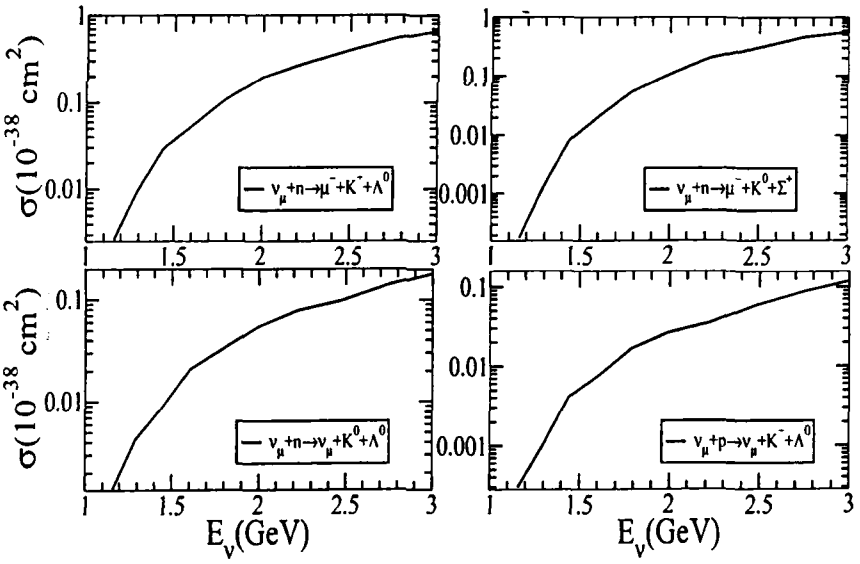

Figure 4.8: σ vs E_ν for associated strange particle production in $\nu_\mu - {}^{56}Fe$.

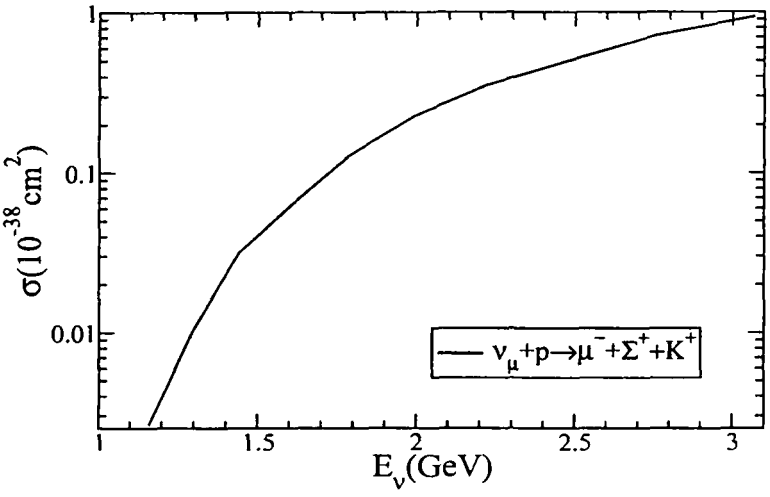

Figure 4.9: σ vs E_ν for associated strange particle production in $\nu_\mu - {}^{56}Fe$.

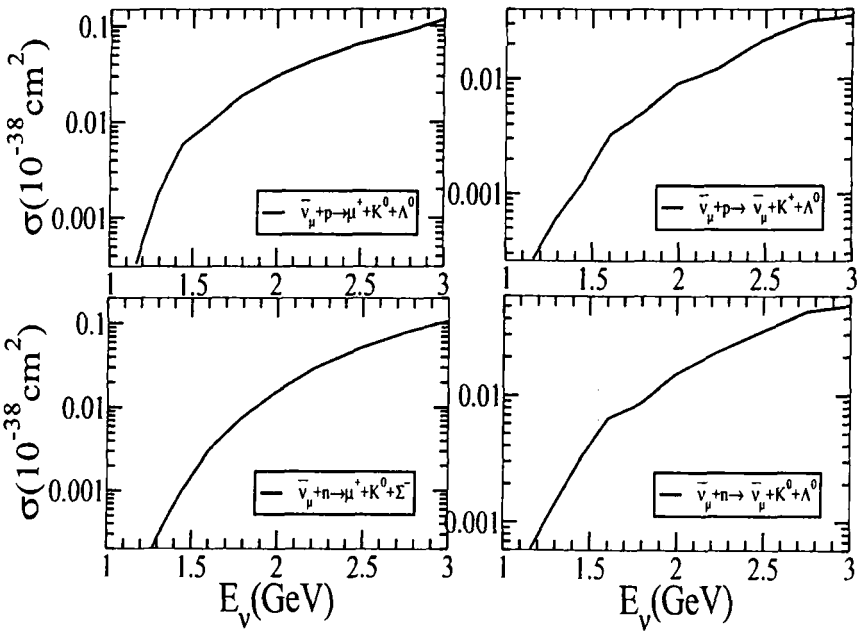

Figure 4.10: σ vs E_ν for associated strange particle production in $\bar{\nu}_\mu - {}^{56}Fe$.

	Processes	$\sigma(10^{-41}\ cm^2)$ at 1.4 GeV	$\sigma(10^{-41}\ cm^2)$ at 1.6 GeV	$\sigma(10^{-41}\ cm^2)$ at 2.0 GeV
GENIE	$\nu_\mu n \rightarrow$	1.73	5.19	13.17
Theoretical	$\mu^- K^+ \Lambda^0$	1.57	4.66	18.26
GENIE	$\nu_\mu p \rightarrow$	0.16	0.84	5.097
Theoretical	$\mu^- K^+ \Sigma^+$	0.28	2.11	12.83
GENIE	$\nu_\mu n \rightarrow$	0.15	0.90	5.0
Theoretical	$\mu^- K^0 \Sigma^+$	0.067	0.51	3.28
GENIE	$\bar{\nu}_\mu p \rightarrow$	0.42	0.97	2.86
Theoretical	$\mu^+ K^0 \Lambda^0$	0.70	2.38	8.67
GENIE	$\bar{\nu}_\mu n \rightarrow$	0.028	0.19	0.99
Theoretical	$\mu^+ K^0 \Sigma^-$	0.15	1.21	7.26

Table 4.5: Total scattering cross section, for associated strange particle production, as a function of E_ν obtained by using the GENIE Monte Carlo code [16] and by the Aligarh group [34].

of associated strange particle production for $\nu_l(\bar{\nu}_l)$ induced charged and neutral current interactions. Shrock [82] considered the associated production reactions $\nu_l N \rightarrow lK\Lambda$ and $\nu_l N \rightarrow lK\Sigma$, where l=μ^-, ν_μ for charged and neutral currents, respectively. The method of generalized Born approximation was used, which includes only tree diagrams. Results obtained by Shrock [82] for the total scattering cross sections for the reactions $\nu_L N \rightarrow LK\Lambda$ and $\bar{\nu}_l N \rightarrow \bar{l}K\Lambda$ are tabulated in Table-4.3. Shrock [82] used axial dipole mass M_A=0.95 GeV. It must be pointed out that Shrock [82] did not consider the contribution of the contact term, which Aligarh group [34] has found out to be significant.

Shrock [82] also calculated the cross section for neutral current reactions in the Weinberg model with $\sin^2\theta_W = \frac{1}{3}$. In the K$\Lambda$ reactions the s-channel was found to have the dominant contribution to the cross section.

Earlier Fermilab [83] had reported that the cross section for the lowest-mass hadronic system is the maximum and the $\Delta S \neq 0$ processes have a cross section larger than the cross section for ΔS=0 process $\nu_\mu n \rightarrow \mu^- K^+ \Lambda$. Their results are presented in Table-4.4.

In this work, we have compared the charged current total scattering cross section results obtained by GENIE Monte Carlo code [16] with the results obtained by the numerical calculation of Aligarh group [34] for the reaction $\nu_\mu(\bar{\nu}_\mu)$-N(free) and the results are tabulated in Table-4.5. We find that total scattering cross section of some processes obtained by the GENIE Monte Carlo code [16] are in good agreement with the theoretical results obtained by the Aligarh group [34]. Thus, we find that more study is required for the weak interaction induced associated particle production processes. Work by the Aligarh group [34] is in progress.

Chapter 5

Deep Inelastic Scattering

5.1 Deep Inelastic Neutrino Nucleon Scattering

In the deep inelastic scattering(DIS) process charged or a neutral lepton when interacts with a nucleon, the nucleon breaks up and loses its identity and a jet of hadrons are produced along with the corresponding lepton in the final state. Deep inelastic scattering is a process by which one can probe the partonic structure of the nucleon. This process occurs at large values of the square of four momentum transfer and the energy transfer to the final state.

In the case of charged and neutral current interactions induced by neutrino/antineutrino the basic reactions are given by:

$$\begin{aligned} &\nu_l(\bar{\nu}_l)(k) + N(p) \rightarrow l^{\mp}(k') + X(p'), \\ &\nu_l(\bar{\nu}_l)(k) + N(p) \rightarrow \nu_l(k') + X(p'), \end{aligned} \tag{5.1}$$

where l stands for e, μ and τ. In the above Eq.(5.1), k , k' are the four momenta of neutrino and the charged lepton respectively. p is the four momenta of target nucleon(N) and p' is the four momenta of the jet of hadrons(X). In the deep inelastic process projectile neutrino scatters off a quark in the hadron via the exchange of intermediate vector bosons($W^{\pm}$ or Z) which is shown in Fig.-5.1.

In a laboratory frame since, target remains at rest, therefore, its three momentum will be zero. Hence four vectors may be written as:

$$k = (E_\nu, \vec{k}),\ p = (M, 0),\ k' = (E', \vec{k}'),\ q = k - k',\ p' = p + q \tag{5.2}$$

where E_ν is the energy of projectile neutrino, $\vec{k}$ is the momentum of the incoming neutrino, E' is the energy of outgoing lepton, and $\vec{k}'$ is the momentum of the outgoing lepton.

The four momentum transfer square(q^2) is defined as:

$$q^2 = k^2 + k'^2 - 2k \cdot k', \tag{5.3}$$

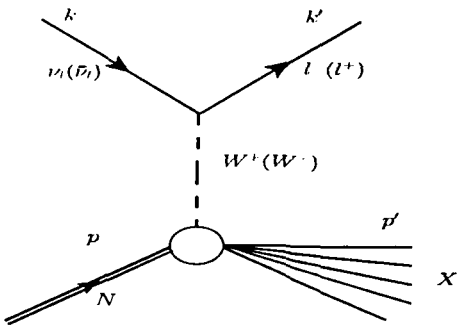

Figure 5.1: Feynman diagram corresponding to the charged current deep inelastic scattering process.

In the DIS limit $k^2 \approx m^2 \approx 0$ and $k'^2 \approx m'^2 \approx 0$.

$$q^2 = -2k \cdot k' \tag{5.4}$$

This q^2 is a negative quantity ($q^2 \leq 0$) and one defines Q^2 ($Q^2 \geq 0$) as:

$$Q^2 = -q^2 = 4E_\nu E' sin^2\left(\frac{\theta}{2}\right) \tag{5.5}$$

and the energy transfer

$$\nu = \frac{p \cdot q}{M} = \frac{p^0 q^0 - p_z q_z}{M}, \tag{5.6}$$

In the DIS process one introduces Bjorken variable x and y which are defined as

$$x = \frac{Q^2}{2p \cdot q} = \frac{Q^2}{2(p^0 q^0 - p_z q_z)}, \; y = \frac{p \cdot q}{p \cdot k} = \frac{\nu}{E} \text{ (in lab frame)} \tag{5.7}$$

For a two body scattering process there are many particles in the final state, the general expression of the cross section is given by

$$\begin{aligned} \sigma \; = \; & \frac{1}{v_{rel}} \frac{2m_\nu}{2E_\nu(\vec{k})} \frac{2M}{2E(\vec{p})} \int \frac{d^3k'}{(2\pi)^3} \frac{2m_l}{2E'(\vec{k}')} \prod_{i=1}^{N} \int \frac{d^3p'_i}{(2\pi)^3} \prod_{l \epsilon f} \left(\frac{2M'_l}{2E'_l}\right) \\ & \times \prod_{j \epsilon b} \left(\frac{1}{2\omega'_j}\right) \bar{\sum} \sum |T|^2 (2\pi)^4 \delta^4 \left(p + k - k' - \sum_{i=1}^{N} p'_i\right), \end{aligned} \tag{5.8}$$

where f stands for fermions and b for bosons in the final state X. The index i splits into indices l and j respectively for fermions and bosons.

T is the invariant matrix element and is written as:

$$-iT = \left(\frac{iG_F}{\sqrt{2}}\right) \bar{u}_l(k')\gamma^\alpha(1-\gamma_5)u_\nu(k) \left(\frac{m_W^2}{q^2 - m_W^2}\right) \langle X|J_\alpha|N\rangle, \tag{5.9}$$

where G_F is the Fermi coupling constant, m_W is the mass of the W boson, $\bar{u}_l(k')$ and $u_\nu(k)$ are the Dirac spinors of outgoing lepton and incoming neutrino, $\bar{u}_l(k')\gamma^\alpha(1-\gamma_5)u_\nu(k)$ is the leptonic current and $\langle X|J_\alpha|N\rangle$ is the hadronic current.

After performing the phase space integration in Eq.(5.8), the double differential scattering cross section evaluated for a nucleon target in its rest frame is expressed by:

$$\frac{d^2\sigma^N_{\nu,\bar{\nu}}}{d\Omega' dE'} = \frac{{G_F}^2}{(2\pi)^2} \frac{|\vec{k}'|}{|\vec{k}|} \left(\frac{m_W^2}{q^2 - m_W^2}\right)^2 L^{\alpha\beta}_{\nu,\bar{\nu}} W^N_{\alpha\beta}, \tag{5.10}$$

where Ω', E' are respectively the solid angle and energy of the outgoing lepton.

The leptonic tensor for neutrino/antineutrino scattering $L^{\alpha\beta}$ is given by:

$$L^{\alpha\beta} = k^\alpha k'^\beta + k^\beta k'^\alpha - k.k' g^{\alpha\beta} \mp i\epsilon^{\alpha\beta\rho\sigma} k_\rho k'_\sigma, \tag{5.11}$$

where -(+) sign is for $\nu(\bar{\nu})$.

The hadronic tensor $W^N_{\alpha\beta}$ is written as:

$$\begin{aligned} W^N_{\alpha\beta} &= \frac{1}{2\pi} \tilde{\sum_{s_N}} \sum_X \sum_{s_i} \prod_{i=1}^n \int \frac{d^3p'_i}{(2\pi)^3} \prod_{l\epsilon f} \left(\frac{2M'_l}{2E'_l}\right) \prod_{j\epsilon b} \left(\frac{1}{2\omega'_j}\right) \\ &\quad \langle X|J_\alpha|N\rangle \langle X|J_\beta|N\rangle^* (2\pi)^4 \delta^4(p + q - \sum_{i=1}^n p'_i), \end{aligned} \tag{5.12}$$

In general, hadronic tensor $W^N_{\alpha\beta}$ is given in terms of structure functions (W^N_i) which are functions of ν and q^2

$$\begin{aligned} W^N_{\alpha\beta} &= \left(\frac{q_\alpha q_\beta}{q^2} - g_{\alpha\beta}\right) W_1^{\nu(\bar{\nu})}(\nu, q^2) + \frac{1}{M^2}\left(p_\alpha - \frac{p.q}{q^2} q_\alpha\right) \times \\ &\quad \left(p_\beta - \frac{p.q}{q^2} q_\beta\right) W_2^{\nu(\bar{\nu})}(\nu, q^2) - \frac{i}{2M^2}\epsilon_{\alpha\beta\rho\sigma} p^\rho q^\sigma W_3^{\nu(\bar{\nu})}(\nu, q^2) \\ &\quad + \frac{1}{M^2} q_\alpha q_\beta W_4^{\nu(\bar{\nu})}(\nu, q^2) + \frac{1}{M^2}(p_\alpha q_\beta + q_\alpha p_\beta) W_5^{\nu(\bar{\nu})}(\nu, q^2) \\ &\quad + \frac{i}{M^2}(p_\alpha q_\beta - q_\alpha p_\beta) W_6^{\nu(\bar{\nu})}(\nu, q^2), \end{aligned} \tag{5.13}$$

where M is the nucleon mass. In the massless limit of leptons the contributions from W_4, W_5 and W_6 are negligible. W^N_i are expressed in terms of dimensionless structure functions $F^N_i(x, Q^2)$, given by the relation

$$\begin{aligned} F_1^{\nu(\bar{\nu})}(x, Q^2) &= M W_1^{\nu(\bar{\nu})}(\nu, Q^2), \quad F_2^{\nu(\bar{\nu})}(x, Q^2) = \nu W_2^{\nu(\bar{\nu})}(\nu, Q^2), \\ F_3^{\nu(\bar{\nu})}(x, Q^2) &= \nu W_3^{\nu(\bar{\nu})}(\nu, Q^2) \end{aligned} \tag{5.14}$$

The structure functions $F_1(x,Q^2)$ and $F_2(x,Q^2)$ are related by the Callan-Gross relation $F_2(x) = 2xF_1(x)$ [84].

We may write the expression for the differential scattering cross section after contracting leptonic tensor and hadronic tensor (in the limit of lepton mass $m_l \to 0$):

$$\frac{d^2\sigma^{\nu(\bar{\nu})}}{dxdy} = \frac{G_F{}^2 M E_\nu}{\pi}\left\{\left(\frac{y^2}{2}+1-y-\frac{xyM}{2E_\nu}\right)F_2^{\nu(\bar{\nu})}(x,Q^2) \pm xy\left(1-\frac{y}{2}\right)F_3^{\nu(\bar{\nu})}(x,Q^2)\right\}, \tag{5.15}$$

where the + (−) sign stands for the neutrino (antineutrino) cross section.

The nucleon structure functions are determined in terms of parton distribution functions(PDFs). Parton distribution functions represent the probability density to find a parton with a fraction x of the original momentum within the hadron. Distribution refers to how the four momentum splits up between each quark. Parton distribution functions are important to determine because the values measured in lepton-nucleon DIS can be used to predict the rates of many other processes. Till now parton distribution functions are experimentally defined and there is no way to predict them theoretically. The parton distribution functions for bound nucleons are experimentally determined in neutrino-nucleon deep inelastic scattering. PDFs are given by the various groups like P. Jimenez Delgado et al. (GRV/GJR) [85], A.D.Martin et al. (MSTW [86]), S. Alekhin et al. (ALEKHIN) [87], Pavel M. Nadolsky et al. (CTEQ6.6) [88], and others. Using these PDFs one writes the structure functions for quarks as:

$$\begin{aligned} F_2^{\nu p} &= 2x[d(x)+s(x)+\bar{u}(x)+\bar{c}(x)], \\ F_2^{\nu n} &= 2x[u(x)+s(x)+\bar{d}(x)+\bar{c}(x)], \\ xF_3^{\nu p} &= 2x[d(x)+s(x)-\bar{u}(x)-\bar{c}(x)], \\ xF_3^{\bar{\nu} p} &= 2x[u(x)+c(x)-\bar{d}(x)-\bar{s}(x)] \end{aligned} \tag{5.16}$$

and for antiquarks

$$\begin{aligned} F_2^{\bar{\nu} p} &= 2x[u(x)+c(x)+\bar{d}(x)+\bar{s}(x)], \\ F_2^{\bar{\nu} n} &= 2x[d(x)+c(x)+\bar{u}(x)+\bar{s}(x)], \\ xF_3^{\nu n} &= 2x[u(x)+s(x)-\bar{d}(x)-\bar{c}(x)], \\ xF_3^{\bar{\nu} n} &= 2x[d(x)+c(x)-\bar{u}(x)-\bar{s}(x)]. \end{aligned} \tag{5.17}$$

5.2 Deep Inelastic Neutrino Nucleus Scattering

When the interactions given by Eq.(5.1), takes place inside a nuclear target, then as these nucleons are not free, medium effects may be important. Earlier, in the Monte Carlo used for generating neutrino/antineutrino event rates, medium corrections were assumed to be very small in the high region of Q^2 and ν, and therefore were not accounted for.

Nuclear medium effects in the deep inelastic scattering processes have been widely discussed after the measurement and comparison of iron and deuterium electromagnetic structure functions $F_2^N(x,Q^2)$ by the European Muon Collaboration at CERN using charged lepton beams [89]. Thereafter studies, both theoretical as well as experimental, have been made in several nuclei. Presently most of the information on nuclear medium effects comes from the charged lepton scattering data. The weak structure functions $F_2^N(x,Q^2)$ and $F_3^N(x,Q^2)$ have also been measured using neutrino/antineutrino beams [90]-[97]. More experiments are planned to obtain data in the deep inelastic region using neutrino/antineutrino beams that will complement the information obtained from the charged lepton scattering. The nuclear effects for the weak structure functions $F_2^A(x,Q^2)$ and $F_3^A(x,Q^2)$ may be in general different. Moreover, the nuclear correction for the weak structure function $F_2^A(x,Q^2)$ may be different from that of the electromagnetic structure function $F_2^{EM,A}(x,Q^2)$. The precise measurement of deep inelastic scattering $\nu(\bar{\nu})$ cross section is also important in providing global fits of the parton distribution functions (PDFs) and due to the fact that most of the $\nu(\bar{\nu})$ experiments are being performed with nuclear targets, the nuclear effects should be properly accounted for before extracting the free nucleon parton distribution function. Furthermore, in the determination of electroweak parameters, a good knowledge of the nuclear medium effects is required.

When we consider the reaction given in Eq.(5.1) taking place inside a nucleus, there are various medium effects and these can be divided into two parts: **(i)** a kinematic effect due the fact that struck nucleon is not at rest but moving with a Fermi momentum in the rest frame of the nucleus, **(ii)** The dynamic effect due to the strong interaction of the initial state nucleon in the nuclear medium.

Recently, Aligarh group [38] has studied nuclear medium effects on the structure functions $F_2(x,Q^2)$ and $F_3(x,Q^2)$ in carbon, iron, and lead nuclear targets. They use a relativistic nucleon spectral function [98] to describe the momentum distribution of nucleons in the nucleus and define everything within a field theoretical approach where nucleon propagators are written in terms of this spectral function. The spectral function has been calculated using the Lehmann's representation for the relativistic nucleon propagator and nuclear many body theory is used for calculating it for an interacting Fermi sea in nuclear matter. A local density approximation is then applied to translate these results to finite nuclei [36, 37, 99]. They have assumed the Callan-Gross relationship for nuclear structure functions $F_2{}^A(x)$ and $F_1{}^A(x)$. The contributions of the pion and rho meson clouds are taken into account in a many body field theoretical approach which is based on Refs. [99, 100]. They have taken into account target mass correction following Ref. [101] which has significant effect at low Q^2, moderate and high Bjorken x. To take into account the shadowing effect which is important at low Q^2 and low x, and modulates the contribution of pion and rho cloud contributions, they have followed the works of Kulagin and Petti [102, 103]. Since they have applied the present formalism at low Q^2 also, hence they have not assumed the Bjorken limit.

The expression of double differential cross section for charged current neutrino/antineutrino interaction with a nucleus is written as [38]:

$$\frac{d^2\sigma^A_{\nu,\bar{\nu}}}{d\Omega' dE'} = \frac{G_F^2}{(2\pi)^2}\frac{|\vec{k}'|}{|\vec{k}|}\left(\frac{m_W^2}{q^2 - m_W^2}\right)^2 L^{\alpha\beta}_{\nu,\bar{\nu}} W^A_{\alpha\beta}, \tag{5.18}$$

In the above expression, $W^A_{\alpha\beta}$ is the nuclear hadronic tensor which can be written in terms of nuclear hadronic structure functions $W_i^A(x, Q^2)$:

$$\begin{aligned} W^A_{\alpha\beta} &= \left(\frac{q_\alpha q_\beta}{q^2} - g_{\alpha\beta}\right) W_1^A + \frac{1}{M_A^2}\left(p_\alpha - \frac{p.q}{q^2}\, q_\alpha\right)\left(p_\beta - \frac{p.q}{q^2}\, q_\beta\right) W_2^A \\ &- \frac{i}{2M_A^2}\epsilon_{\alpha\beta\rho\sigma} p^\rho q^\sigma W_3^A \end{aligned} \tag{5.19}$$

where M_A is the mass of the nucleus. $L^{\alpha\beta}$ is the leptonic tensor and it is given in Eq. 5.11.

The expression of differential scattering cross section for the charged current neutrino nucleus interaction is given in terms of nuclear structure functions W_i^A, as

$$\begin{aligned} \frac{d^2\sigma^{\nu(\bar{\nu})A}_{CC}}{dx_A\, dy_A} &= \frac{G_F^2 M_A E_\nu}{\pi}\left(\frac{m_W^2}{Q^2 + m_W^2}\right)^2 \Bigg(y_A^2 x_A W_1^{\nu(\bar{\nu})A} \\ &+ \left\{1 - y_A - \frac{M_A x_A y_A}{2E_\nu}\right\} W_2^{\nu(\bar{\nu})A} \pm x_A y_A\left(1 - \frac{y_A}{2}\right) W_3^{\nu(\bar{\nu})A}\Bigg) \end{aligned} \tag{5.20}$$

These nuclear structure functions $W_i^A(x, Q^2)$ are redefined in terms of the dimensionless structure functions $F_i^A(x, Q^2)$ as

$$\begin{aligned} M_A W_1^A(\nu, Q^2) &= F_1^A(x, Q^2) \\ \nu W_2^A(\nu, Q^2) &= F_2^A(x, Q^2) \\ \nu W_3^A(\nu, Q^2) &= F_3^A(x, Q^2) \end{aligned} \tag{5.21}$$

The expressions for $F_2^A(x_A, Q^2)$ and $F_3^A(x_A, Q^2)$ in their model are obtained as [38]:

$$\begin{aligned} F_2^A(x_A, Q^2) &= 4\int d^3r \int \frac{d^3p}{(2\pi)^3}\frac{M}{E(\vec{p})}\int_{-\infty}^{\mu} dp^0\, S_h(p^0, \vec{p}, \rho(\vec{r}))\frac{x}{x_N} \times \\ &\left(1 + \frac{2x_N p_x^2}{M\nu_N}\right) F_2^N(x_N, Q^2) \end{aligned} \tag{5.22}$$

$$\begin{aligned} F_3^A(x_A, Q^2) &= 4\int d^3r \int \frac{d^3p}{(2\pi)^3}\frac{M}{E(\vec{p})}\int_{-\infty}^{\mu} dp^0 S_h(p^0, \vec{p}, \rho(\vec{r})) \times \\ &\frac{p^0\gamma - p_z}{(p^0 - p_z\gamma)\gamma} F_3^N(x_N, Q^2) \end{aligned} \tag{5.23}$$

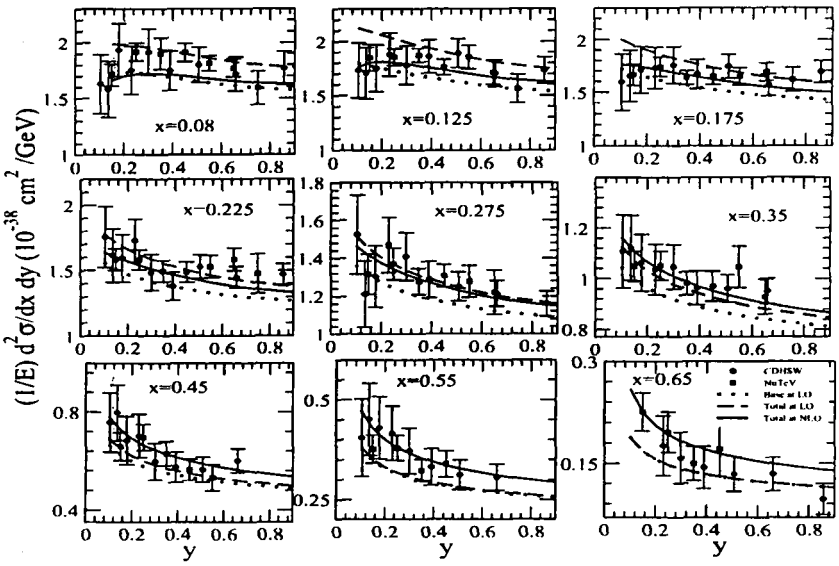

Figure 5.2: Double differential scattering cross section per neutrino energy at 65 GeV for ν_μ induced charged current deep inelastic scattering process.

where S_h (p^0, $\vec{p}$, $\rho(\vec{r})$) is the hole spectral function. Spectral functions of nucleons are the function of local Fermi momentum in local density approximation [104]. Since, spectral functions are the function of density, hence, they are dynamic in nature. All the required nuclear information is hidden in the spectral functions.

In the above Eq.(5.23) γ is given by

$$\gamma = \frac{q_z}{q^0} = \left(1 + \frac{4M^2x^2}{Q^2}\right)^{1/2}, \tag{5.24}$$

and

$$x_N = \frac{Q^2}{2(p^0q^0 - p_zq_z)}$$

Using Eq.(5.22) and Eq.(5.23) in the Eq.(5.20) they have calculated the charged current neutrino/antineutrino differential scattering cross sections on the various nuclear targets [38, 39].

5.3 Results and Conclusions

Here we are presenting the results obtained by the GENIE Monte Carlo code [16]. In the GENIE Monte Carlo code [16], the DIS has been considered using Bodek and Yang

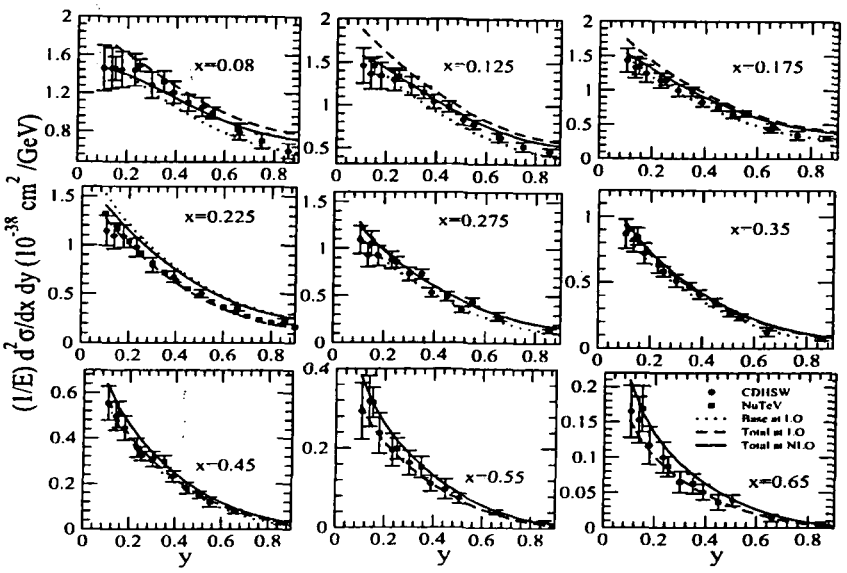

Figure 5.3: Double differential scattering cross section per neutrino energy at 65 GeV for $\bar{\nu}_\mu$ induced charged current deep inelastic scattering process.

prescription [13]. In the present work we have studied the cross sections for the charged current neutrino induced deep inelastic process in ^{56}Fe by using GENIE Monte Carlo code [16] and compared the obtained results with the results obtained by the Aligarh group [38].

Here we are also presenting the results of double differential cross section at E_ν = 65GeV in ^{56}Fe for neutrino and antineutrino obtained by Aligarh group [38] in the local density approximation. They have calculated the double differential cross section at different values of Bjorken variable x for Q^2 >1.0 GeV^2. These results are shown in Fig-5.2 and Fig.-5.3 respectively. We find that the results from the numerical calculation of Aligarh group [38] are in agreement with the experimental results of NuTeV [90] and CDHSW [105] collaborations.

Furthermore, we have also shown the results of total scattering cross section per neutrino energy for charged current interaction for the reaction ν_μ-^{56}Fe obtained using the GENIE Monte Carlo code [16] at Q^2_{min} <1.0 GeV^2 and compared our result with the results obtained from the another Monte Carlo named as, NUANCE [8] and also from the numerical calculation performed by Aligarh group [41]. From Fig.-5.4 we find that the results obtained by Aligarh group [41] and by NUANCE Monte Carlo [8] agrees well and have the advantage that the resonance background can be excluded, but in GENIE Monte

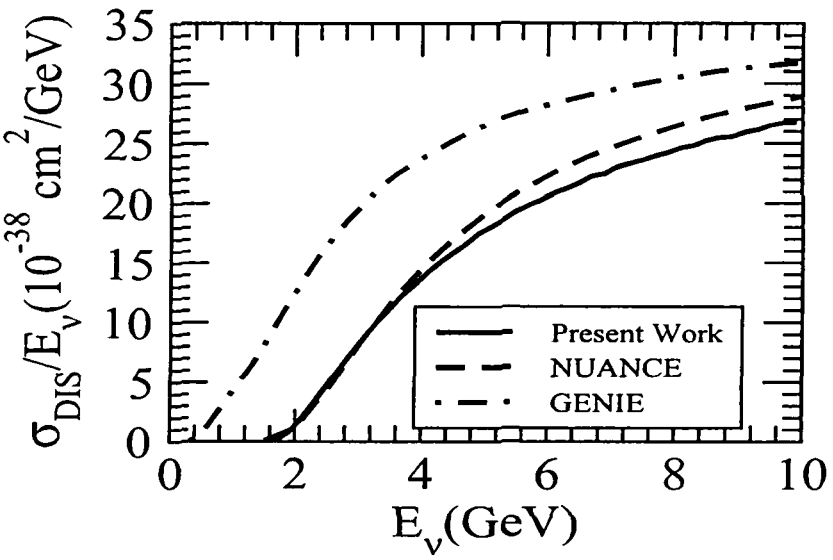

Figure 5.4: σ/E_ν vs E_ν in ν_μ-^{56}Fe for CC deep inelastic scattering.

Carlo code [16] there is background from the resonance in the deep inelastic region and this background is not excluded yet. Therefore, in GENIE Monte Carlo code [16] for the deep inelastic process threshold is very low i.e. of the order of few hundred MeV.

We find that the total scattering cross section obtained by GENIE Monte Carlo code [16] are around 44% higher at E_ν=4 GeV, 16% at E_ν=10 GeV as compared to Aligarh group [41] and around 36% higher at E_ν=4 GeV, 8% at E_ν=10 GeV as compared to the NUANCE Monte Carlo code [8]. This difference in the cross sections is due to the nuclear medium effects.

The Aligarh group [38] strongly feels that there is nuclear medium effects present in the DIS region also, which depend upon the region of x and y, for which the differential cross sections are evaluated.

Chapter 6

Summary and Conclusion

Neutrino physics has travelled a long distance since its discovery due to gargantuan efforts made both experimentally and theoretically, which has resulted in revealing many mysteries about this elusive particle. Nevertheless, there are still more unanswered questions than answers. Being one of the fundamental constituents of matter, scientist are making better efforts while performing or planning experiments using neutrino beam from a very low energy region to very high energy region. In the intermediate energy region of the order of 1 GeV also, there are many experiments going on or proposed with. These experiments are using nuclear targets. To simulate these events there are many neutrino generators like NUANCE, GENIE, etc. In these generators neutrino nucleus cross section is one of the inputs, as the neutrino is interacting with a nucleon bound inside a nuclear target. It has been realised that for getting better understanding of these neutrinos, knowledge of nuclear medium effects are important. Therefore, efforts are being made both theoretically as well as experimentally to understand the dynamics of nucleons in the nuclear medium. In this dissertation, we have performed a comparison between the cross section results being used in the GENIE Monte Carlo version 2.7.1 [16] and the model developed by the Aligarh group [20]-[41]. These studies are made for the charged and neutral current induced quasielastic, inelastic and deep inelastic processes. These comparisons have been performed for the iron nuclear target. Iron has been proposed as the target material at the India-based Neutrino Observatory(INO), to detect atmospheric neutrinos using iron calorimeters. However, this study may also be important for the comparison in other nuclear targets and also for the various Monte Carlo generators.

In chapter 2, we have performed the study for the charged and neutral current neutrino/antineutrino induced total scattering cross section, Q^2-distribution and lepton energy (E_l)-distribution in iron. These calculations are performed for free nucleons as well as bound nucleons inside the nucleus. We find that the results obtained from the models used in the GENIE Monte Carlo code [16], which is Llewellyn-Smith Fermi gas model, and the model developed by Aligarh group, which is a local Fermi gas model [16], the

results are in good agreement both for the total cross section as well as for the various distributions. But when the Aligarh group [23] incorporates the nucleon correlations using random phase approximation, it has been found that there is a significant reduction in the cross section as well as in the various distributions. For example, in the $\nu_\mu - ^{56}Fe$ for the Q^2-distribution, at Q^2=0.05 GeV^2 this reduction is around 36% and at Q^2=0.12 GeV^2 it is ~38%. While for the reaction $\bar{\nu}_\mu - ^{56}$Fe this reduction is about 35% at Q^2=0.07 GeV^2 and 23% at Q^2=0.5 GeV^2.

Similarly, for neutrino induced process in ^{56}Fe the reduction in the lepton energy distribution is about 44% at the peak value of the lepton energy E_l=960 MeV, however, with the increase in the lepton energy this difference becomes gradually smaller and smaller, like it becomes 4% at 700 MeV. While for $\bar{\nu}_\mu - ^{56}$Fe process, this reduction is around 40% at E_l=940 MeV and 28% at E_l=700 MeV. These reductions are reflected in the total scattering cross section(σ) at low neutrino/antineutrino energies. For example, for the neutrino induced process, this reduction is ~30% at E_ν=0.4 GeV, ~17% at E_ν=1.0 GeV, which becomes 15% at E_ν=2.0 GeV.

In chapter 3, we have studied the charged current and neutral current $\nu/\bar{\nu}$ induced total scattering cross section in iron for inelastic single pion production processes. In this chapter, we have also studied Q^2- distribution and pion kinetic energy $T_\pi-$distribution in iron for charged current inelastic single pion production processes. We have presented the results obtained by using GENIE Monte Carlo code [16], which mainly uses Rein and Sehgal model with some factor that takes care of the medium modifications in an ad hoc way, and the model developed by the Aligarh group [25]. We find that the results are in good agreement for the total cross section as well as for various distributions, when the results are obtained without any renormalization effects on the Δ properties and without considering pion absorption effects. However, when the Aligarh group [25] include renormalization effects on the Δ properties and the pion absorption effects, the results are different. Aligarh group [25] finds that when renormalization effects on the Δ properties are included in the calculation the reduction in the total cross section for ν_μ induced single π^+ production at E_ν=0.8 GeV is around 48%, 42% at E_ν=1.2 GeV, and 35% at E_ν=2.0 GeV, respectively. Furthermore, when pion absorption effects are also taken into account there is further reduction in the cross section which is around 30% at E_ν=0.8 GeV, 39% at E_ν=1.2 GeV, and 24% at E_ν=2.0 GeV, respectively.

While in the case of $\bar{\nu}_\mu - ^{56}Fe$ process, the reduction in the cross section when calculated with Δ renormalization effects at E_ν=0.8 GeV is around 48%, 42% at E_ν=1.2 GeV, and 34% at E_ν=2.0 GeV, from the cross section calculated without medium effects. When the pion absorption effects are also accounted for the reduction is around 30% at E_ν=0.8 GeV, 28% at E_ν=1.2 GeV, and 23% at E_ν=2.0 GeV, respectively.

In chapter 4, we have presented the results for the charged and neutral current neutrino/antineutrino induced total scattering cross section for the weak associated particle production processes. Here the results are compared with the results obtained by using

the GENIE Monte Carlo code [16] to the results obtained by the Aligarh group [34]. Aligarh group has developed a microscopic model which is based on SU(3) chiral Lagrangian. This group [34] has also pointed out that contact term has a significant contribution to the cross section. We found that the results obtained by the GENIE Monte Carlo code [16] and by the Aligarh group [34] are in good agreement.

In chapter 5, we have presented the results for the charged current induced deep inelastic scattering process. The results are presented for the double differential scattering cross section $\frac{d^2\sigma^A_{\nu,\bar{\nu}}}{dxdy}$ and the total scattering cross section (σ). We have compared the results of charged current total scattering cross section for the reaction $\nu_\mu - ^{56}Fe$, obtained by using the GENIE Monte Carlo code [16] to the results obtained by the Aligarh group [41] and NUANCE [8] Monte Carlo generator. As deep inelastic scattering process dominates in the high energy region, hence, the Monte Carlo generators do not take care of nuclear medium effects while Aligarh group [38] has taken into account these effects. Aligarh group [38] has found that although deep inelastic scattering is considered a high energy process but nuclear medium effects are also important in the different regions of Bjorken variables x and y.

Thus, in this study we conclude that nuclear medium effects play an important role in determining the neutrino-nucleus cross section. These medium corrections are different in the various processes contributing to the event rates and must be included in the Monte Carlo generators.

Bibliography

[1] Review of Particle Physics, Phys. Rev. D **86**, 1 (2012).

[2] C. Giunti and C. W. Kim, Fundamentals of Neutrino Physics and Astrophysics, Oxford University Press, New York, (2007).

[3] K. Zuber, Neutrino Physics, Second edition, CRC Press, New York, (2012).

[4] W. Winter, hep-ph/0603012.

[5] C. H. Albright *et al.* [Neutrino Factory/Muon Collider Collaboration]. physics/0411123.

[6] A. Bolozdynya, F. Cavanna, Y. Efremenko, G. T. Garvey, V. Gudkov, A. Hatzikoutelis, W. R. Hix and W. C. Louis *et al.*, arXiv:1211.5199 [hep-ex].

[7] P. Lipari, Nucl. Phys. Proc. Suppl. **112**, 274 (2002).

[8] D. Casper, Nucl. Phys. Proc. Suppl. **112**, 161 (2002).

[9] H. Gallagher, Nucl. Phys. Proc. Suppl. **112**, 188 (2002).

[10] Y. Hayato, Nucl. Phys. Proc. Suppl. **112**, 171 (2002).

[11] C. H. Llewellyn Smith, Phys. Rept. **3**, 261 (1972).

[12] D. Rein and L. M. Sehgal, Annals Phys. **133**, 79 (1981).

[13] A. Bodek and U. K. Yang, J. Phys. G **29**, 1899 (2003).

[14] C. Mariani [SciBooNE Collaboration], J. Phys. Conf. Ser. **408**, 012038 (2013).

[15] J. D. Devan [MINERvA Collaboration], J. Phys. Conf. Ser. **408**, 012047 (2013).

[16] C. Andreopoulos, A. Bell, D. Bhattacharya, F. Cavanna, J. Dobson, S. Dytman, H. Gallagher and P. Guzowski *et al.*, Nucl. Instrum. Meth. A **614**, 87 (2010).

[17] S. K. Singh and E. Oset, Phys. Rev. C **48**, 1246 (1993).

[18] S. K. Singh and E. Oset, Nucl. Phys. A **542**, 587 (1992).

[19] S. K. Singh, M. J. Vicente-Vacas and E. Oset, Phys. Lett. B **416**, 23 (1998). [Erratum-ibid. B **423**, 428 (1998)].

[20] M. Sajjad Athar and S. K. Singh, "Atmospheric neutrino absorption cross-sections in Ar-40," Phys. Rev. C **61**, 028501 (2000).

[21] S. K. Singh and M. Sajjad Athar, Nucl. Phys. Proc. Suppl. **112**, 215 (2002).

[22] M. Sajjad Athar, S. Ahmad and S. K. Singh, Eur. Phys. J. A **24**, 459 (2005).

[23] M. Sajjad Athar, S. Ahmad and S. K. Singh, Nucl. Phys. A **764**, 551 (2006).

[24] S. K. Singh, M. Sajjad Athar and S. Ahmad, Phys. Lett. B **641**, 159 (2006).

[25] M. Sajjad Athar, S. Ahmad and S. K. Singh, Phys. Rev. D **75**, 093003 (2007).
S. Ahmad, M. Sajjad Athar and S. K. Singh, Phys. Rev. D **74**, 073008 (2006).

[26] S. Chauhan, M. Sajjad Athar and S. K. Singh, AIP Conf. Proc. **1405**, 337 (2011).

[27] S. K. Singh, M. Sajjad Athar and S. Ahmad, Pramana **66**, 689 (2006).

[28] M. Sajjad Athar, S. Chauhan, S. K. Singh and M. J. Vicente Vacas, Int. J. Mod. Phys. E **18**, 1469 (2009).

[29] M. Sajjad Athar, S. Chauhan and S. K. Singh, Eur. Phys. J. A **43**, 209 (2010).

[30] M. Sajjad Athar, S. Chauhan and S. K. Singh, J. Phys. G **37**, 015005 (2010).

[31] S. K. Singh, M. Sajjad Athar and S. Ahmad, Phys. Rev. Lett. **96**, 241801 (2006).

[32] M. Rafi Alam, I. Ruiz Simo, M. Sajjad Athar and M. J. Vicente Vacas, Phys. Rev. D **82**, 033001 (2010).

[33] M. R. Alam, I. R. Simo, M. Sajjad Athar and M. J. Vicente Vacas, Phys. Rev. D **85**, 013014 (2012).

[34] M. R. Alam, I. R. Simo, M. Sajjad Athar, L. Alvarez-Ruso and M. J. Vicente Vacas, arXiv:1303.5924 [hep-ph] (2013).

[35] M. R. Alam, L. Alvarez-Ruso, M. Sajjad Athar and M. J. Vicente Vacas, arXiv:1303.5951 [hep-ph].

[36] M. Sajjad Athar, S. K. Singh and M. J. Vicente Vacas, Phys. Lett. B **668**, 133 (2008).

[37] M. Sajjad Athar, I. Ruiz Simo and M. J. Vicente Vacas, Nucl. Phys. A **857**, 29 (2011).

[38] H. Haider, I. R. Simo, M. Sajjad Athar and M. J. Vicente Vacas, Phys. Rev. C **84**, 054610 (2011).

[39] H. Haider, I. Ruiz Simo and M. Sajjad Athar, Phys. Rev. C **85**, 055201 (2012).

[40] H. Haider, I. R. Simo and M. Sajjad Athar, Phys. Rev. C **87**, 035502 (2013).

[41] S.Chauhan, F. Zaidi, H. Haider, R. Alam and M. Sajjad Athar, Proceeding of the DAE Symposium on Nucl. Phys.**56**, 1104 (2011).

[42] R. Bradford, A. Bodek, H. S. Budd and J. Arrington, Nucl. Phys. Proc. Suppl. **159**, 127 (2006).

[43] T. Leitner, L. Alvarez-Ruso and U. Mosel, Phys. Rev. C **74**, 065502 (2006).

[44] R. A. Smith and E. J. Moniz, Nucl. Phys. B **43**, 605 (1972). [Erratum-ibid. B **101**, 547 (1975)].

[45] A. C. Hayes, I. S. Towner and , Phys. Rev. C **61**, 044603 (2000) [nucl-th/9907049].

[46] C. Volpe, N. Auerbach, G. Colo, T. Suzuki, N. Van Giai and , Phys. Rev. C **62**, 015501 (2000) [nucl-th/0001050].

[47] J. Engel, E. Kolbe, K. Langanke and P. Vogel, Phys. Rev. D **48**, 3048 (1993).

[48] J. Marteau, Nucl. Phys. Proc. Suppl. **112**, 203 (2002).
J. Marteau, Eur. Phys. J. A **5**, 183 (1999).

[49] L. A. Ahrens, S. H. Aronson, P. L. Connolly, B. G. Gibbard, M. J. Murtagh, S. J. Murtagh, S. Terada and D. H. White *et al.*, Phys. Rev. D **35**, 785 (1987).

[50] E. Oset, in *SERC School in Nuclear Physics*, Ed. by B. K. Jain. World Sceintific, Singapore (1987).

[51] A. L. Fetter and J. D. Walecka, *Quantum Theory of Many Particle Systems*, McGraw Hill (1971).

[52] E. Oset, in *Quarks, Mesons and Isobars*, Ed. by R. Guardiola and A. Polls, World Sceintific, Singapore.

[53] E. Oset and A. Palanques-Mestre, Nucl. Phys. A **359**, 289 (1981).

[54] C. Garcia-Recio, E. Oset and L. L. Salcedo, Phys. Rev. C **37**, 194 (1988).

[55] G. L. Fogli and G. Nardulli, Nucl. Phys. B **160**, 116 (1979).

[56] H. W. Hammer and D. Drechsel, Z. Phys. A **353**, 321 (1995). [nucl-th/9508014].

[57] G. L. Fogli and G. Nardulli, Nucl. Phys. B **165**, 162 (1980).

[58] P. A. Schreiner and F. Von Hippel, Nucl. Phys. B **58**, 333 (1973).

[59] O. Lalakulich and E. A. Paschos, Phys. Rev. D **71**, 074003 (2005).

[60] S. K. Singh, M. J. Vicente-Vacas and E. Oset, Phys. Lett. B **416**, 23 (1998). [Erratum-ibid. B **423**, 428 (1998)].

[61] L. Alvarez-Ruso, S. K. Singh and M. J. Vicente Vacas, Phys. Rev. C **57**, 2693 (1998). L. Alvarez-Ruso,*Excitation of Baryonic Resonances Induced by Nucleons and leptons*, Ph.D. Thesis, Departmento de Fisica Teorica, University de valencia, (1999).

[62] A. W. Thomas and W. Weise, *The Structure of the Nucleon*, Wiley-VCH, Berlin, (2001).

[63] S. J. Barish et al., Phys. Rev. D **19**, 2521 (1979).

[64] G. M. Radecky, V. E. Barnes, D. D. Carmony, A. F. Garfinkel, M. Derrick, E. Fernandez, L. Hyman and G. Levman *et al.*, Phys. Rev. D **25**, 1161 (1982) [Erratum-ibid. D **26**, 3297 (1982)].

[65] S. L. Adler, Annals Phys. **50**, 189 (1968).

[66] D. Rein and L. M. Sehgal, Annals Phys. **133**, 79 (1981).

[67] E. A. Paschos, M. Sakuda, I. Schienbein and J. Y. Yu, Nucl. Phys. (Proc.Suppl. B) **139**, 125 (2005).

[68] O. Lalakulich, E. A. Paschos and G. Piranishvili, Phys. Rev. D **74**, 014009 (2006).

[69] T. Leitner, L. Alvarez-Ruso and U. Mosel, Phys. Rev. C **73**, 065502 (2006).

[70] E. Oset and L. L. Salcedo, Nucl. Phys. A **468**, 631 (1987).

[71] C. Garcia-Recio, E. Oset, L. L. Salcedo, D. Strottman and M. J. Lopez, Nucl. Phys. A **526**, 685 (1991).

[72] R. P. Feynman, M. Kislinger and F. Ravndal, Phys. Rev. D **3**, 2706 (1971).

[73] W. Rarita and J. Schwinger, Phys. Rev. **60**, 61 (1941).

[74] T. Ericson and W. Weise, *Pion and Nuclei*, Claredon Press, Oxfords, (1988).

[75] M. Benmerrouche, R. M. Davidson and N. C. Mukhopadhyay, Phys. Rev. C **39**, 2339 (1989).

[76] M. Post, *Hadronic Spectral Functions in Nuclear Matter*, PhD thesis, Universitat Giessen (2003).

[77] G. Penner and U. Mosel, Phys. Rev. C **66**, 055211 (2002).

[78] R. C. Carrasco, J. Nieves and E. Oset, Nucl. Phys. A **565**, 797 (1993).

[79] D. Rein and L. M. Sehgal, Nucl. Phys. B **223**, 29 (1983).

[80] G. D. Rochester and C. C. Butler, Nature **160**, 855 (1947).

[81] G. B. Adera, B. I. S. Van Der Ventel, D. D. van Niekerk and T. Mart, Phys. Rev. C **82**, 025501 (2010) [arXiv:1112.5748 [nucl-th]].

[82] R. E. Shrock, Phys. Rev. D **12**, 2049 (1975).

[83] H. K. Dewan, Phys. Rev. D **24**, 2369 (1981).

[84] C. G. Callan, Jr. and D. J. Gross, Phys. Rev. Lett. **22**, 156 (1969).

[85] P. Jimenez-Delgado and E. Reya, Phys. Rev. D **80**, 114011 (2009).

[86] A. D. Martin, W. J. Stirling, R. S. Thorne and G. Watt, Eur. Phys. J. C **63**, 189 (2009).

[87] S. Alekhin, J. Blumlein, S. Klein and S. Moch, arXiv:0908.3128 [hep-ph].

[88] P. M. Nadolsky, H. -L. Lai, Q. -H. Cao, J. Huston, J. Pumplin, D. Stump, W. -K. Tung and C. -P. Yuan, Phys. Rev. D **78**, 013004 (2008).

[89] J. J. Aubert *et al.* [European Muon Collaboration], Phys. Lett. B **105**, 322 (1981).

[90] M. Tzanov *et al.* [NuTeV Collaboration], Phys. Rev. D **74**, 012008 (2006).

[91] D. Allasia et al. Zeit. Phys.C **28**, 321 (1991).

[92] J. P. Berge et al. Zeit. Phys. C **49**, 187 (1991).

[93] K. Varvell et al. Zeit. Phys. C **36**, 1 (1991).

[94] E. Oltman et al. Zeit. Phys. C **53**, 51 (1992).

[95] W. G. Seligman et al. Phys. Rev. Lett. **79**, 1213 (1997).

[96] A. V. Sidorov et al. Eur. Phys. J. C **10**, 405 (1999).

[97] Bonnie T. Fleming et al. Phys. Rev. Lett. **86**, 5430 (2001).

[98] P. Fernandez de Cordoba and E. Oset, Phys. Rev. C **46**, 1697 (1992).

[99] E. Marco, E. Oset and P. Fernandez de Cordoba, Nucl. Phys. A **611**, 484 (1996).

[100] C. Garcia-Recio, J. Nieves and E. Oset, Phys. Rev. C **51**, 237 (1995).

[101] I. Schienbein, V. A. Radescu, G. P. Zeller, M. E. Christy, C. E. Keppel, K. S. McFarland, W. Melnitchouk and F. I. Olness *et al.*, J. Phys. G **35**, 053101 (2008).

[102] S. A. Kulagin and R. Petti, Phys. Rev. D **76**, 094023 (2007).

[103] S. A. Kulagin and R. Petti, Nucl. Phys. A **765**, 126 (2006).

[104] E. Marco, E. Oset and P. Fernandez de Cordoba, Nucl. Phys. A **611**, 484 (1996).

[105] J. P. Berge, H. Burkhardt, F. Dydak, R. Hagelberg, M. Krasny, H. J. Meyer, P. Palazzi and F. Ranjard *et al.*, Z. Phys. C **49**, 187 (1991).